

A model of fiber reorientation in fiber-reinforced biological materials combining statistical and configurational mechanics

Alessandro Giammarini¹, Andrea Pastore¹ and Alfio Grillo^{1*}

Monday 15th September, 2025

¹Dip. di Scienze Matematiche “G. L. Lagrange”, Politecnico di Torino, Corso Duca degli Abruzzi 24, 10129, Torino, Italia.

Abstract

We present a mathematical model for the reorientation of fibers in a soft, fiber-reinforced, fluid-saturated porous medium describing a hypothetical biological tissue. We consider two types of remodeling that, at different scales, concur in determining the structural reorganization of the solid phase of the medium: one pertains to the development of plastic-like distortions, which are introduced as the macroscopic manifestation of processes occurring at lower scales, but not resolved explicitly; the other one, originating at the mesoscale, concerns the capability of the fibers of reorienting in the extracellular matrix. This latter form of remodeling is studied as a Langevin-like process in which two main agencies are recognized: a drift term, which is given by the effects that the deformation of the extracellular matrix exerts on the fibers; a noise term, which accounts for the interactions among nearby fibers. We employ the framework of the Principle of Virtual Power to present our model, in which we “free” the kinematics of the system from the constraints of isochoricity of remodeling and incompressibility of the mixture by appending the Chetaev forms of these constraints to the Principle of Virtual Power. Then, we specialize our model to articular cartilage. We do this for comparing our results with some experimental curves describing the distribution of collagen fibers in a sample of articular cartilage, and for studying, through the simulation of a uniaxial compression test, the interplay between fluid flow and the two aforementioned forms of remodeling. Our main result is the establishment of a framework that captures effectively the mechanical coupling between the fiber distribution specific to a given medium and the mechanical stimuli exerted on such distribution. Quite differently from other works on this subject, our framework is capable of accounting for the stochastic effects of the fibers on the overall evolution of the considered tissue.

Keywords: Biological tissues, Remodeling, Fiber reorientation, Inelastic distortions, Anisotropic materials.

1 Introduction

As recently reported in the work by Gunda et al. [1], a rather common praxis in the biomechanics of soft tissues [2] is to describe soft and hydrated biological tissues as biphasic media [3], comprising at least a solid and a fluid phase. The fluid phase essentially consists of water, and plays a relevant role in a number of chemical and mechanical processes that are vital for the nourishment of the tissues themselves [4, 3, 2], whereas the solid phase represents the “summa” of extracellular matrix, nuclei and membranes of the cells, protein networks and, in some cases, collagen fibers [2, 5, 6]. In fact, fibrous constituents are present in a variety of tissues (e.g. articular cartilage [7], aorta walls [8], cornea [9, 10], among others), and have an impact on their overall mechanical properties and on their capability of being permeated by

*Corresponding author: Alfio Grillo, Dipartimento di Scienze Matematiche “G. L. Lagrange”, Politecnico di Torino, Torino, 10129.

Email: alfio.grillo@polito.it

39 a fluid. Such impact is so high that the ability of a tissue to correctly perform its biological functionality
40 can be compromised when its fibrous constituents are damaged.

41 Understanding the role played by the fibers is important also for the design and the manufacturing
42 of bio-compatible materials, since, as put forward by Gentleman et al. in [11], “*The development of*
43 *novel collagen gel/scaffold constructs requires a clear understanding of the mechanical properties of the*
44 *constituent biomaterial*”.

45 In fact, many researchers have undertaken large efforts to provide a mechanical framework able to
46 capture the behavior of fiber-reinforced materials. The first works focused on some phenomenological
47 aspects of this problem (see, e.g., [3] for articular cartilage), and, in doing so, they regarded fiber-
48 reinforced tissues as homogeneous and isotropic in spite of the inhomogeneity and anisotropy introduced
49 by the fibers themselves. Then, the focus shifted onto the study of inhomogeneous and anisotropic media,
50 which are described through one or more families of fibers with structural properties. For instance, the
51 constitutive framework developed in [8] for the mechanical description of arteries has been adapted and
52 generalized to many cases of biological interest [12, 13, 9, 14, 15, 16, 17, 10, 18, 19, 20, 21].

53 To list a few of the many remarkable results in the literature, a class of orthotropic and transversely
54 isotropic strain energy functions satisfying poly-convexity is proposed in [22], whereas transversely
55 isotropic materials are studied by using a different, but equivalent, set of invariants in [15]. Moreover,
56 in [23], the anisotropic part of the Holzapfel–Gasser–Ogden (HGO) model [8] is modified to take into
57 consideration the constitutive response of a material under hydrostatic stress.

58 In the case of a medium featuring statistically oriented fibers, such as articular cartilage, the con-
59 stitutive law describing the tissue is extended to consider a statistical distribution of orientation of the
60 fibers, while taking into account that the preferred direction changes with the depth of the tissue. Hence,
61 the constitutive setting requires the introduction of directional averages [24], which have been employed
62 extensively (see e.g. [25, 26, 10, 27, 28, 29, 30, 31, 32, 33, 34, 35]).

63 In the literature, a line of research of particular relevance in the study of tissues as solid-liquid
64 biphasic media focuses on how the hydraulic properties of a medium change in the presence of fibers
65 [36, 7, 37, 29, 38]. In fact, depending on the direction of orientation, the fibers can favor or hinder the
66 motion of the interstitial fluid permeating a tissue. Such enhancement or inhibition, in turn, may influence
67 the mobility of chemical substances transported by the fluid, thereby affecting their concentration within
68 the tissue. Some consequences of the amount and alignment of collagen fibers on the permeability of
69 cartilaginous tissues were investigated, e.g., by Maroudas and Bullough [39], and more recent studies
70 done in [25, 26, 28, 29] aimed to model their findings.

71 The study of the mechanical properties of fiber-reinforced media is a relevant topic also in many other
72 chapters of the biomechanical research and, more generally, in the characterization of the mechanical
73 properties of materials. In the following, without the intent of being exhaustive, but with the sole purpose
74 of exemplifying a few contributions, we list some relevant works from different fields, and we refer to the
75 references contained therein for further reads. For example, a robust mechanical setting for dealing with
76 damage, growth and remodeling is developed in [40, 41, 4, 42, 43, 44], whereas a theoretical setting for
77 elastic, polar fiber-reinforced materials is discussed in [45, 46]. Computational schemes are developed
78 and studied in [47, 48, 49], and statistical methods to resolve the distribution of the fibers are investigated
79 in [34, 30, 33, 50].

80 In our work, we take off from the line of thought previously put forward in [32]. In [32], the problem of
81 fiber reorientation was studied in conjunction with the isochoric remodeling of the solid phase, described
82 as a porous medium permeated by an interstitial fluid and undergoing large deformations (“isochoric
83 remodeling” was understood as a plastic-like reorganization of the solid phase of the tissue in response
84 to mechanical stress). This setting made it possible to evaluate the influence of fiber reorientation and
85 remodeling on the flow of the medium’s interstitial fluid and, conversely, the influence of the fluid on the
86 overall mechanical behavior of the system. However, in this present work, we introduce two differences:
87 one methodological and one conceptual.

88 From the methodological point of view, we base the formulation of our present work on a revisit
89 [51, 52] of the Principle of Virtual Power (PVP) at the scale of the tissue. Within this approach, we

90 append the constraint of isochoric remodeling and the constraint of incompressibility of the fluid and of
 91 the solid phase to the PVP. The constraints are then addressed with the Lagrange multiplier technique.
 92 As a consequence, we isolate the constitutive contribution of the stress from the one that originates from
 93 the constraint. The former one is also referred to as *active part* of the overall stress, while the latter one
 94 is the *reactive part* of it. Note that the adjective “active” should not be confused with the one sometimes
 95 used to indicate the addend of the additive decomposition of stress that is taken as alternative modeling
 96 option to the one based on the concept of “active strain” (e.g., in muscle mechanics [53, 54, 55]).

97 The conceptual difference with respect to [32] consists in a description of the reorientation of the
 98 fibers that is borrowed from Statistical Mechanics. Accordingly, we assume to “observe” the dynamic
 99 process of the reorientation at the scale of a single fiber, i.e., at the mesoscale, and we characterize it
 100 by a *drift* and a *stochastic* term. By doing so, we aim at recovering the probability density distribution
 101 supplied initially in [13] as the solution of a stochastic process occurring at a lower scale than that of the
 102 tissue as a whole. Hence, instead of speaking of “*target angle*” [47, 56], our aim is to recover a *target*
 103 *probability distribution*, which resembles the one characterizing the material under study.

104 2 Theoretical background and evolution of the fiber angle distribution

105 In this section, we recall the framework for studying the evolution of a fiber-reinforced biphasic material
 106 that undergoes an anelastic process of structural reorganization, as put forward in [40, 41, 4, 57, 43, 44,
 107 31, 32, 51, 52].

108 2.1 Modeling Hypothesis and fundamental notation

109 We turn our attention to fiber-reinforced, soft, and hydrated biological tissues, which comprise, for
 110 example, articular cartilage. We model such tissues as *saturated* porous media permeated by an interstitial
 111 fluid and consisting of a solid composite material, made of extracellular matrix and reinforcing collagen
 112 fibers. A tissue of this type is modeled as a mixture. The interstitial fluid plays a fundamental role in
 113 transport-related phenomena, and contributes significantly to the diffusion of bio-relevant markers. As
 114 shown by numerous studies, if fibers are present, the capability of the fluid of flowing through the tissue
 115 is substantially influenced by the concentration and orientation of the fibers [39, 36, 7, 28, 58, 29, 38, 59,
 116 30, 50].

117 We hypothesize that each phase of the tissue is *intrinsically incompressible* (see e.g.[2]), and, thus,
 118 that the changes of the tissue’s overall volume are due to the variation of the porosity of the solid phase,
 119 which, in turn, equals the volumetric fraction of the fluid phase because of the hypothesis of saturation.
 120 Hence, if, for instance, the porosity of the solid phase diminishes in response to a compressing loading,
 121 the fluid, which occupies entirely the pores of the solid phase, has to flow away from the compressed
 122 zones, thereby allowing for a global change of volume.

123 By denoting by φ_{0s} and φ_{1s} the volumetric fractions of the matrix and of the reinforcing fibers,
 124 respectively, and by indicating with φ_p the *porosity*, i.e., the volumetric fraction associated with the pore
 125 space of the solid phase as a whole, the identity $\varphi_{0s} + \varphi_{1s} + \varphi_p = 1$ holds true (see e.g. [29]). However,
 126 because of the hypothesis of saturation, φ_p must equal the volumetric fraction of the fluid phase, φ_f , i.e.,
 127 $\varphi_p \equiv \varphi_f$, which yields the condition

$$\varphi_{0s} + \varphi_{1s} + \varphi_f = \varphi_s + \varphi_f = 1, \quad (1)$$

128 where $\varphi_s := \varphi_{0s} + \varphi_{1s}$ is the volumetric fraction of the solid phase as a whole.

129 In this work, we do not tackle growth phenomena or inter-phase mass transfer processes, but we
 130 consider the remodeling of the tissue due to the reorganization of the extracellular matrix or due to the
 131 formation of irreversible strains (as is the case for damaged tissues [60, 61]). Moreover, similarly to
 132 what is done in plasticity, we describe remodeling in terms of anelastic distortions through the generally
 133 incompatible tensor \mathbf{F}_γ , introduced by means of the Bilby–Kröner–Lee (BKL) decomposition (see e.g.

$$\mathbf{F} = \mathbf{F}_e \mathbf{F}_\gamma, \quad (2)$$

135 where \mathbf{F}_e characterizes the elastic distortions that take place in the tissue to accommodate for \mathbf{F}_γ . For
 136 future use, we denote by $J := \det \mathbf{F} > 0$, $J_e := \det \mathbf{F}_e > 0$, and $J_\gamma := \det \mathbf{F}_\gamma > 0$ the determinants of \mathbf{F} ,
 137 \mathbf{F}_e , and \mathbf{F}_γ , respectively. In particular, we prescribe the condition $J_\gamma = 1$ since, in our present work and
 138 for the considered time scales, the processes described by \mathbf{F}_γ concern solely the isochoric alteration of
 139 the structural properties of the extracellular matrix. Indeed, we assume here that the fibers do not grow,
 140 are not reabsorbed, and do not undergo internal processes. Clearly, each of these processes does occur,
 141 and are studied elsewhere [4, 44]. In this respect, our modeling choice is dictated solely by simplicity
 142 and has the purpose of focusing on the main point of our work, which is the stochastic description of the
 143 fiber reorientation.

144 Once \mathbf{F}_γ is introduced, it is possible to characterize the “natural —or relaxed— state” of the
 145 biological medium under study as $\mathcal{N}(t) = \cup_{X \in \mathcal{B}} (\{X\} \times \mathcal{N}_X(t))$, where, at a given instant of time t ,
 146 $\mathcal{N}_X(t) := \mathbf{F}_\gamma(X, t) T_X \mathcal{B}$ is the relaxed state of the “material neighborhood” [40] of X (“body element”,
 147 in the terminology of [63]), identified with the tangent space of the body’s reference placement \mathcal{B} at
 148 the point X , i.e., $T_X \mathcal{B}$ (see also [64] for a discussion on this issue). Here, the notation “ $\mathbf{F}_\gamma(X, t) T_X \mathcal{B}$ ”
 149 means that $\mathbf{F}_\gamma(X, t)$ is applied to the whole tangent space $T_X \mathcal{B}$, while the terminology “relaxed state”
 150 indicates that $\mathcal{N}_X(t)$ is free of residual stresses due, e.g., to the formation of geometric incompatibilities.
 151 Here, however, by adhering to the approach developed in [65], we consider the simplified setting in which
 152 $\mathcal{N}_X(t)$ is viewed as the relaxed “version” of $T_X \mathcal{B}$ itself.

153 We complete the geometric setting that acts as background in our work (see e.g. [66]) by introducing
 154 the metric tensors \mathbf{G} , $\boldsymbol{\eta}$, and \mathbf{g} , associated with the reference placement, with the natural state, and with
 155 the current placement, respectively. Although it is often assumed to work within a Cartesian setting,
 156 from a conceptual point of view, the introduction of an underlying geometric setting, along with the
 157 covariant formalism, allows us to “put order” in the presentation of the forthcoming results.

158 For future use, we also introduce the volumetric fractions associated with the matrix, fibers, and
 159 interstitial fluid measured per unit volume of the relaxed state and of the reference placement \mathcal{B} . Hence,
 160 in general, we write $\Phi_{0sv} := J_e \varphi_{0s}$ and $\Phi_{1sv} := J_e \varphi_{1s}$ for the pull-backs of the volumetric fractions of the
 161 matrix and of the fibers to the natural state, and we write $\Phi_{0s} := J \varphi_{0s} = J_\gamma \Phi_{0sv}$ and $\Phi_{1s} := J \varphi_{1s} = J_\gamma \Phi_{1sv}$
 162 for the same quantities expressed per unit volume of the reference placement. For the volumetric fraction
 163 of the fluid, we write $\Phi_f := J \varphi_f$ and $\Phi_{fv} := J_e \varphi_f$, while we set $\Phi_s := J \varphi_s$ and $\Phi_{sv} := J_e \varphi_s$ for the solid.
 164 In fact, since $J_\gamma(X, t)$ is equal to unity at all points $X \in \mathcal{B}$ and at all times, the following identities apply:
 165 $\Phi_{0s} \equiv \Phi_{0sv}$, $\Phi_{1s} \equiv \Phi_{1sv}$, and $\Phi_f \equiv \Phi_{fv}$.

166 2.2 Revisited Principle of Virtual Power

167 In this section, we adhere to the formulation proposed by [51, 52] to revisit the Principle of Virtual Power
 168 (PVP) for the case of the dynamics of a mixture made of intrinsically incompressible phases. For this
 169 purpose, we regard the saturation condition, the mass balance of each phase, and the shared kinematics
 170 of fibers and matrix as constraints. In fact, from here on, the extracellular matrix and the fibers are
 171 assumed to have the same velocity $\mathbf{V}_{0s} = \mathbf{V}_{1s} = \mathbf{V}_s$, which characterizes the homogenized kinematics of
 172 the mixture.

173 Because of incompressibility, the mass balance laws of the constituents of the mixture become balance
 174 equations for the volumetric fractions of the constituents themselves. Furthermore, these balance laws are
 175 viewed as constraints relating the evolution of the volumetric fractions with the velocities of the solid and
 176 of the fluid phase. In particular, such constraints are combined so as to re-obtain the relations $\Phi_{0s} = J \varphi_{0s}$
 177 and $\Phi_{1s} = J \varphi_{1s}$ for the solid constituents, and a relation between \dot{J} and the material divergence of the
 178 material filtration velocity $\mathbf{Q} := \Phi_f (\mathbf{V}_f - \mathbf{V}_s) \mathbf{F}^{-T}$, i.e., $\dot{J} + \text{Div} \mathbf{Q} = 0$.

179 We consider the constraints of saturation, of “shared” kinematics $\mathbf{V}_{0s} = \mathbf{V}_{1s} = \mathbf{V}_s$, and of the mass
 180 balances of the solid constituents in explicit form, so that the constrained quantities are expressed in

181 terms of the “free” ones, whereas the mass balance of the mixture as a whole and the isochoricity of the
 182 remodeling distortions are handled implicitly. With this wording, we mean here that these constraints
 183 are studied by the Lagrange multiplier technique.

184 To this end, we consider the *virtual* velocity fields $(\mathbf{V}_s, \mathbf{V}_f, \mathbf{V}_{v\gamma})$, defined over the medium’s
 185 reference placement and associated with the kinematic descriptors $(\mathbf{V}_s, \mathbf{V}_f, \dot{\mathbf{F}}_\gamma)$. Moreover, by introducing
 186 the generalized forces that are power-conjugate with $(\mathbf{V}_s, \mathbf{V}_f, \mathbf{V}_{v\gamma})$, we write the real-valued functionals
 187 of the internal and external virtual powers (see [67])

$$\mathcal{W}_v^{(\text{int})}(\mathbf{V}_s, \mathbf{V}_f, \mathbf{V}_{v\gamma}) := - \int_{\mathcal{B}} \left\{ \sum_{\alpha} J \mathbf{m}_{\alpha} \mathbf{V}_{v\alpha} + \sum_{\alpha} \mathbf{P}_{\alpha} : \text{Grad} \mathbf{V}_{v\alpha} \right\} - \int_{\mathcal{B}} \mathbf{F}_{\gamma}^{-\text{T}} \mathbf{Y}_u : \mathbf{V}_{v\gamma}, \quad (3a)$$

$$\mathcal{W}_v^{(\text{ext})}(\mathbf{V}_s, \mathbf{V}_f, \mathbf{V}_{v\gamma}) := \int_{\mathcal{B}} \sum_{\alpha} J \rho_{\alpha} \mathbf{f} \mathbf{V}_{v\alpha} + \int_{\partial \mathcal{B}} \sum_{\alpha} \xi_{\alpha} \boldsymbol{\tau} \mathbf{V}_{v\alpha} + \int_{\mathcal{B}} \mathbf{F}_{\gamma}^{-\text{T}} \mathbf{Z} : \mathbf{V}_{v\gamma}, \quad (3b)$$

188 where the sum over the index α must be understood on the set $\{s, f\}$. In Equation (3a), \mathbf{P}_{α} is the active
 189 part of the stress tensor associated with the α th phase; $J \mathbf{m}_{\alpha}$ is the density, per unit volume of the reference
 190 placement, of the linear momentum exchanged between the solid phase as a whole (matrix and fibers)
 191 and the fluid phase; $\mathbf{F}_{\gamma}^{-\text{T}} \mathbf{Y}_u$ is the generalized force that is power-conjugate with $\mathbf{V}_{v\gamma}$. In Equation (3b),
 192 $J \rho_{\alpha} \mathbf{f}$ is the α th contribution, with $\alpha \in \{s, f\}$, of the external body force densities acting on the mixture
 193 and expressed per unit volume of the reference placement, while ρ_{α} is the apparent mass density of the
 194 α th phase, which is defined as the product $\rho_{\alpha} = \varphi_{\alpha} \varrho_{\alpha}$, with ϱ_{α} being the “true”, or intrinsic, mass
 195 density; $\xi_{\alpha} \boldsymbol{\tau}$ is the contact force on the portion of $\partial \mathcal{B}$ with area fraction ξ_{α} of the α th component; $\mathbf{F}_{\gamma}^{-\text{T}} \mathbf{Z}$
 196 is the external generalized force dual to $\mathbf{V}_{v\gamma}$ [68, 63, 51, 52, 69].

197 To study the constraints handled in implicit form, we follow the procedure described in [51, 52], and
 198 we write them in differential form as

$$\hat{\mathcal{C}}_{\text{tot}} \circ (\mathbf{F}, \mathbf{F}_{\gamma}, \mathbf{V}_s, \mathbf{V}_f) = \text{Div} [J_{\gamma} (\Phi_{sv} \mathbf{V}_s + \Phi_{fv} \mathbf{V}_f) \mathbf{F}^{-\text{T}}] = 0, \quad (4a)$$

$$\hat{\mathcal{C}}_{\gamma} \circ (\mathbf{F}_{\gamma}, \dot{\mathbf{F}}_{\gamma}) = \mathbf{F}_{\gamma}^{-\text{T}} : \dot{\mathbf{F}}_{\gamma} = \mathbf{I}^{\text{T}} : \mathbf{F}_{\gamma}^{-1} \dot{\mathbf{F}}_{\gamma} = 0. \quad (4b)$$

199 Note that, since Equations (4a) and (4b) are linear in the velocities, the Chetaev forms [70, 71, 72] of
 200 the constraints (4a) and (4b) can be obtained by replacing \mathbf{V}_s , \mathbf{V}_f , and $\dot{\mathbf{F}}_{\gamma}$ with their virtual counterparts.
 201 Hence, after introducing the Lagrange multipliers P and μ_{γ} associated with the constraints, and by
 202 following the procedure depicted in [51, 52], we write the augmented form of the internal virtual power
 203 as

$$\begin{aligned} & \mathcal{W}_v^{(\text{int,a})}(\mathbf{V}_s, \mathbf{V}_f, \mathbf{V}_{v\gamma}, P_v, \mu_{v\gamma}) \\ & := \mathcal{W}_v^{(\text{int})}(\mathbf{V}_s, \mathbf{V}_f, \mathbf{V}_{v\gamma}) + \int_{\mathcal{B}} \{ P [\hat{\mathcal{C}}_{\text{tot}} \circ (\mathbf{F}, \mathbf{F}_{\gamma}, \mathbf{V}_s, \mathbf{V}_f)] - \mu_{\gamma} [\hat{\mathcal{C}}_{\gamma} \circ (\mathbf{F}_{\gamma}, \mathbf{V}_{v\gamma})] \} \\ & \quad + \int_{\mathcal{B}} \{ P_v [\hat{\mathcal{C}}_{\text{tot}} \circ (\mathbf{F}, \mathbf{F}_{\gamma}, \mathbf{V}_s, \mathbf{V}_f)] - \mu_{v\gamma} [\hat{\mathcal{C}}_{\gamma} \circ (\mathbf{F}_{\gamma}, \dot{\mathbf{F}}_{\gamma})] \}. \end{aligned} \quad (5)$$

204 Next, we impose the Principle of Virtual Power, thereby requiring the total virtual power, obtained as the
 205 sum of the augmented internal virtual power and the external virtual power, to be null for any arbitrary
 206 set of virtual fields $(\mathbf{V}_s, \mathbf{V}_f, \mathbf{V}_{v\gamma}, P_v, \mu_{v\gamma})$, i.e.,

$$\mathcal{W}_v^{(\text{int,a})}(\mathbf{V}_s, \mathbf{V}_f, \mathbf{V}_{v\gamma}, P_v, \mu_{v\gamma}) + \mathcal{W}_v^{(\text{ext})}(\mathbf{V}_s, \mathbf{V}_f, \mathbf{V}_{v\gamma}) = 0. \quad (6)$$

207 Hence, standard arguments permit to write the dynamic equations and the implicit constraints in the
 208 reference placement \mathcal{B} , i.e.,

$$\text{Div} \mathbf{P}_{\alpha} - J \mathbf{m}_{\alpha} - J_{\gamma} \Phi_{\alpha v} \mathbf{F}^{-\text{T}} \text{Grad} P + J_{\gamma} \varrho_{\alpha} \Phi_{\alpha v} \mathbf{f} = \mathbf{0}, \quad \text{with } \alpha \in \{s, f\}, \quad (7a)$$

$$\text{Div} [J_{\gamma} \mathbf{F}^{-1} (\Phi_{sv} \mathbf{V}_s + \Phi_{fv} \mathbf{V}_f)] = 0, \quad (7b)$$

$$\mathbf{Y}_u + \mu_{\gamma} \mathbf{I}^{\text{T}} - \mathbf{Z} = \mathbf{0}, \quad (7c)$$

$$\mathbf{F}_\gamma^{-T} : \dot{\mathbf{F}}_\gamma = 0, \quad (7d)$$

209 which are accompanied by boundary and initial conditions of the type [67]

$$(\mathbf{P}_\alpha - J_\gamma \Phi_{\alpha\nu} P \mathbf{F}^{-T}) \mathbf{N} = \xi_\alpha \boldsymbol{\tau}, \quad \text{with } \alpha \in \{s, f\}, \quad \text{on } \partial_N \mathcal{B}, \quad (8a)$$

$$\chi = \chi_b, \quad \text{on } \partial_D \mathcal{B}, \quad (8b)$$

$$\mathbf{V}_f = \mathbf{V}_{fb}, \quad \text{on } \partial_D \mathcal{B}, \quad (8c)$$

$$\chi(X, t_{in}) = \chi_{in}(X), \quad \text{in } \mathcal{B}, \quad (8d)$$

$$\mathbf{F}_\gamma(X, t_{in}) = \mathbf{F}_{\gamma in}(X), \quad \text{in } \mathcal{B}. \quad (8e)$$

210 These conditions are purely formal at this stage, and have to be specialized for the problems to be solved
 211 (see section 5). Since the mass balance laws for the constituents of the solid phase reduce to the equations
 212 $\dot{\Phi}_{0vs} = 0$ and $\dot{\Phi}_{1vs} = 0$ because of the isochoricity constraint $J_\gamma = 1$, the volumetric fractions in the
 213 natural state read $\Phi_{0sv}(X, t) = \Phi_{0in}(X)$ and $\Phi_{1sv}(X, t) = \Phi_{1in}(X)$ at all times and for all $X \in \mathcal{B}$, where
 214 $\Phi_{0in}(X)$ and $\Phi_{1in}(X)$ define the initial volumetric fractions of the matrix and of the fibers.

215 We notice, in addition, that the volumetric fractions in the reference placement are $\Phi_{0s}(X, t) =$
 216 $\Phi_{0sv}(X, t) = \Phi_{0in}(X)$ and $\Phi_{1s}(X, t) = \Phi_{1sv}(X, t) = \Phi_{1in}(X)$, for all $X \in \mathcal{B}$.

217 We remark that, in Equation (7a), \mathbf{P}_α can be identified with the *constitutive* first Piola–Kirchhoff
 218 stress tensor of the α th phase, whereas \mathbf{m}_α is the dissipative part of the exchange of linear momentum
 219 between the fluid phase and the solid phase as a whole. Moreover, we assume that the mixture is closed
 220 under exchange of linear momentum, so that $\mathbf{m}_s + \mathbf{m}_f = \mathbf{0}$ [73, 74, 75, 76, 7, 77]. Finally, a suitable
 221 constitutive characterization of \mathbf{m}_f extracts Darcy’s Law (see e.g. [2]) from Equation (7a), written for
 222 $\alpha = f$.

223 We notice that we can split Equation (7c) in its spherical and deviatoric parts, the former of which
 224 gives an expression for the *a posteriori* determination of μ_γ [51], i.e.,

$$\mu_\gamma = -\frac{1}{3} \text{tr}(\mathbf{Y}_u) + \frac{1}{3} \text{tr}(\mathbf{Z}), \quad \text{in } \mathcal{B}, \quad (9a)$$

$$\text{dev} \mathbf{Y}_u - \text{dev} \mathbf{Z} = \mathbf{0}, \quad \text{in } \mathcal{B}. \quad (9b)$$

225 By adding together Equation (7a) over $\alpha \in \{s, f\}$, setting $\varrho = \varphi_s \varrho_s + \varphi_f \varrho_f$, and exploiting the relation
 226 $\mathbf{m}_s + \mathbf{m}_f = \mathbf{0}$ as well as Piola’s identity [66], we obtain the set of equations

$$\text{Div}(\mathbf{P}_s + \mathbf{P}_f) - J \mathbf{F}^{-T} \text{Grad} P + J \varrho \mathbf{f} = \mathbf{0}, \quad (10a)$$

$$\text{Div} \mathbf{P}_f - J \mathbf{m}_f - J_\gamma \Phi_{fv} \mathbf{F}^{-T} \text{Grad} P + J_\gamma \varrho_f \Phi_{fv} \mathbf{f} = \mathbf{0}, \quad (10b)$$

$$\text{Div}[J_\gamma \mathbf{F}^{-1}(\Phi_{sv} \mathbf{V}_s + \Phi_{fv} \mathbf{V}_f)] = 0, \quad (10c)$$

$$\text{dev} \mathbf{Y}_u - \text{dev} \mathbf{Z} = \mathbf{0}, \quad (10d)$$

$$\mathbf{F}_\gamma^{-T} : \dot{\mathbf{F}}_\gamma = 0, \quad (10e)$$

227 in which μ_γ does not appear because Equation (9a) allows to determine it after the dynamic equations are
 228 solved. For this reason, μ_γ can be eliminated from the set of the unknowns of the problem. Moreover, since
 229 we are considering explicitly the mass balance of the solid constituents, the volumetric fractions of the
 230 matrix and of the fibers are determined by $\varphi_{0s} = J^{-1} \Phi_{0in}$ and $\varphi_{1s} = J^{-1} \Phi_{1in}$, with $\varphi_s = J^{-1}(\Phi_{0in} + \Phi_{1in})$.
 231 Therefore, also φ_{0s} and φ_{1s} can be removed from the set of unknowns.

232 In conclusion, the unknowns featuring in Equations (10a)–(10e) consists of 46 variables: 3 for the
 233 components of the motion χ ; 3 for the components of the fluid velocity \mathbf{V}_f ; 9 for the components of
 234 \mathbf{P}_s ; 9 for the components of \mathbf{P}_f ; 3 for the components of \mathbf{m}_f ; 9 for the components of \mathbf{F}_γ ; 9 for the
 235 components of \mathbf{Y}_u ; and 1 for the Lagrange multiplier P , associated with the mass balance of the mixture
 236 as a whole. Since \mathbf{f} , $\boldsymbol{\tau}$, and \mathbf{Z} are external forces assigned from the outset, from now on we consider
 237 them as given quantities, with an expression that depends on the case to which the model is specialized.
 238 In the following sections, we supply the constitutive expressions of \mathbf{P}_s , \mathbf{P}_f , \mathbf{m}_f , and \mathbf{Y}_u , thereby adding
 239 30 scalar equations. Hence, the model consists of 46 scalar equations for 46 macroscopic variables.

240 However, at the mesoscopic scale, the biological tissue is characterized by the presence of fibers, and the
 241 mechanical properties of the medium are heavily influenced by their orientations. In this framework, we
 242 will describe the probability distribution that a fiber is aligned along a certain direction as the solution
 243 of a prototype evolutionary law [50], thereby considering it as an additional unknown of the problem,
 244 coupled with the deformation at the macroscale, but determined by its own dynamics.

245 2.3 Stochastic dynamics of the fiber angle distribution

246 Following a standard notation in continuum mechanics [24, 8, 12, 13, 14, 15, 16, 17, 25, 26, 10, 18, 27,
 247 28, 29, 19, 30, 20, 31, 32, 35, 33, 78, 79], for each point $X \in \mathcal{B}$, we define the *set of all directions* in the
 248 reference placement \mathcal{B} as

$$\mathbb{S}_X^2 \mathcal{B} := \{ \mathbf{M}_X \in T_X \mathcal{B} : \|\mathbf{M}_X\| = 1 \}, \quad (11)$$

249 where $T_X \mathcal{B}$ is the tangent space of \mathcal{B} at $X \in \mathcal{B}$ [66]. The tangent bundle of \mathcal{B} is $T\mathcal{B} := \cup_{X \in \mathcal{B}} (\{X\} \times$
 250 $T_X \mathcal{B})$. In the sequel, we denote by $(T_X \mathcal{B})^*$ the cotangent space of \mathcal{B} at X , i.e., the dual space of $T_X \mathcal{B}$,
 251 and by $(T\mathcal{B})^*$ the cotangent bundle. We also define the bundle $\mathbb{S}^2 \mathcal{B} = \cup_{X \in \mathcal{B}} (\{X\} \times \mathbb{S}_X^2 \mathcal{B})$ along with
 252 the field of unit vectors $\mathbf{M} : \mathcal{B} \mapsto \mathbb{S}^2 \mathcal{B}$, such that $\mathbf{M}(X) := (X, \mathbf{M}_X) \in (\{X\} \times \mathbb{S}_X^2 \mathcal{B})$ and $\mathbf{M}_X \in \mathbb{S}_X^2 \mathcal{B}$.
 253 Together with $\mathbb{S}_X^2 \mathcal{B}$ and $\mathbb{S}^2 \mathcal{B}$, we introduce $(\mathbb{S}_X^2 \mathcal{B})^*$ and $(\mathbb{S}^2 \mathcal{B})^*$ as the subsets of $(T_X \mathcal{B})^*$ and $(T\mathcal{B})^*$
 254 generated by all the real-valued linear and bounded maps defined over $\mathbb{S}_X^2 \mathcal{B}$ and $\mathbb{S}^2 \mathcal{B}$, respectively.

255 By employing local spherical coordinates, a generic element $\mathbf{M}_X \in \mathbb{S}_X^2 \mathcal{B}$ can be expressed through
 256 the parameterization

$$\hat{\mathbf{M}}_X : [0, \pi] \times [0, 2\pi[\rightarrow \mathbb{S}_X^2 \mathcal{B}, \quad (12a)$$

$$\mathbf{M}_X = \hat{\mathbf{M}}_X(\Theta, \Phi) = \sin\Theta \cos\Phi \mathbf{E}_1 + \sin\Theta \sin\Phi \mathbf{E}_2 + \cos\Theta \mathbf{E}_3, \quad (12b)$$

257 where $\{\mathbf{E}_1, \mathbf{E}_2, \mathbf{E}_3\} \in T_X \mathcal{B}$ is an orthonormal vector basis of $T_X \mathcal{B}$ (to make the notation lighter, we
 258 omit the subscript “ X ” in the specification of the unit vectors \mathbf{E}_A , for $A = 1, 2, 3$).

259 In the “classical” literature on fiber-reinforced media (see e.g. [24, 8, 12, 13, 14, 15, 16, 17, 25,
 260 26, 10, 18, 27, 28, 29, 19, 30, 20, 31, 32, 35, 33, 78, 79]), the directions of fiber reinforcement \mathbf{M}_X
 261 undergo no evolution in time apart from the passive one $\mathbf{M}_X \mapsto \mathbf{F}(X, t)\mathbf{M}_X$, since each \mathbf{M}_X describes
 262 a preferred direction in the reference placement of the body. Quite differently, however, in some other
 263 works on *remodeling*, the generic \mathbf{M}_X is endowed with its own kinematics (see e.g. [56]). The purpose
 264 of this modeling choice is to capture the capability of the fibers of changing their orientation not only in
 265 response to deformation or to stress, but also as a result of their inherent dynamics. To the best of our
 266 understanding, it is in this sense that one speaks of “active evolution” when referring to the remodeling
 267 of the fibers, since this remodeling is, in fact, a manifestation of the fibers’ intrinsic evolution. In this
 268 respect, we emphasize that, in our work, we have two types of remodeling: the one described by \mathbf{F}_γ , and
 269 the one expressed by the intrinsic capability of the fibers to reorient.

270 Whereas models of the type mentioned above remind of Cosserat media (see e.g. [80]), a different
 271 point of view, suggested in [81] and, later, in [6, 82, 31, 32], applies to fiber-reinforced composite media
 272 with statistical distribution of orientation of the fibers. In these papers, it is assumed that the probability
 273 density distribution of fiber alignment at a given point of the composite medium under study depends on
 274 the most probable direction of orientation, the latter being regarded as an independent kinematic variable
 275 subjected to its own remodeling dynamics (“active” evolution). More specifically, the probability density
 276 distribution is assigned from the outset, while the evolution of the most probable orientation solves an
 277 initial- and boundary-value problem (IBVP) [31, 32] coupled with the deformation and, when considered,
 278 with other forms of remodeling [32]. In the present work, however, we propose another perspective,
 279 which expands the previous ones in that the probability density distribution *is not* given a priori, but is
 280 rather an unknown of the model and is determined by solving a Fokker–Planck equation. In fact, this
 281 idea was suggested in [6], but not developed therein, and it has recently been expanded in [83, 50]. The
 282 main ingredients of this latter perspective can be summarized as follows.

283 To account for the evolution of the preferred direction associated with the generic $\mathbf{M}_X \in \mathbb{S}_X^2 \mathcal{B}$, we
 284 hypothesize that \mathbf{M}_X can be seen as the imagine of a function of time obtained by composition of $\hat{\mathbf{M}}_X$
 285 with the unknown angular functions

$$\theta : [t_{\text{in}}, t_{\text{fin}}] \rightarrow \mathbb{R}, \quad \phi : [t_{\text{in}}, t_{\text{fin}}] \rightarrow \mathbb{R}, \quad (13)$$

286 defined over the time window $[t_{\text{in}}, t_{\text{fin}}]$ over which the considered system is observed, and we write

$$\mathbf{M}_X = \hat{\mathbf{M}}_X(\theta(t), \phi(t)) = \check{\mathbf{M}}_X(t), \quad \check{\mathbf{M}}_X := \hat{\mathbf{M}}_X \circ (\theta, \phi) : [t_{\text{in}}, t_{\text{fin}}] \rightarrow \mathbb{S}_X^2 \mathcal{B}. \quad (14)$$

287 Since the time change of $\check{\mathbf{M}}_X$ is expressed in terms of θ and ϕ through Equation (14), we regard these
 288 two functions as generalized Lagrangian parameters of our theory (see e.g. [56]), and we prescribe that
 289 they evolve in time as dictated by a suitable *local* force balance taking on the form (see [56, 83, 50])

$$\gamma_\Theta \dot{\theta} = \frac{\partial \hat{\mathcal{W}}}{\partial \Theta} \circ (\mathbf{F}, \mathbf{F}_\gamma, \theta, \phi, \mathcal{X}) + \underbrace{\mathcal{F}_\Theta^{\text{ext,det}} + \mathcal{F}_\Theta^{\text{ext,noise}}}_{\equiv \mathcal{F}_\Theta^{\text{ext}}}, \quad (15a)$$

$$\gamma_\Phi \dot{\phi} = \frac{1}{\sin \theta} \frac{\partial \hat{\mathcal{W}}}{\partial \Phi} \circ (\mathbf{F}, \mathbf{F}_\gamma, \theta, \phi, \mathcal{X}) + \underbrace{\mathcal{F}_\Phi^{\text{ext,det}} + \mathcal{F}_\Phi^{\text{ext,noise}}}_{\equiv \mathcal{F}_\Phi^{\text{ext}}}, \quad (15b)$$

290 where γ_Θ and γ_Φ are damping coefficients, with units $\text{N} \cdot \text{s}/\text{m}^2$, here assumed to be strictly positive and
 291 coincident $\gamma_\Theta = \gamma_\Phi = \gamma$, and defining the dissipative nature of the generalized forces $\gamma \dot{\theta}$ and $\gamma \dot{\phi}$; $\hat{\mathcal{W}}$
 292 is the solid medium's strain energy function per unit volume, while $\mathcal{F}_\Theta^{\text{ext}} := \mathcal{F}_\Theta^{\text{ext,det}} + \mathcal{F}_\Theta^{\text{ext,noise}}$ and
 293 $\mathcal{F}_\Phi^{\text{ext}} := \mathcal{F}_\Phi^{\text{ext,det}} + \mathcal{F}_\Phi^{\text{ext,noise}}$ are generalized forces, conceived as external (see the discussion reported in
 294 section 4.2, in which they will be expressed explicitly), that feature both the deterministic terms $\mathcal{F}_\Theta^{\text{ext,det}}$
 295 and $\mathcal{F}_\Phi^{\text{ext,det}}$, and the *stochastic* terms $\mathcal{F}_\Theta^{\text{ext,noise}}$ and $\mathcal{F}_\Phi^{\text{ext,noise}}$. Note that $\hat{\mathcal{W}}$ is composed also with the map
 296 \mathcal{X} , such that $\mathcal{X}(X, t) = X$ for all $(X, t) \in \mathcal{B} \times \mathcal{I}$, where \mathcal{I} is the time line, to highlight that the material
 297 is inhomogeneous in general. Finally, the derivatives of $\hat{\mathcal{W}}$ with respect to Θ and Φ are non-dissipative
 298 contributions to generalized forces power-conjugate with $\dot{\theta}$ and $\dot{\phi}$.

299 Since Equations (15a) and (15b) express the process of reorientation of a fiber embedded in the
 300 extracellular matrix, the non-dissipative contributions due to the interactions with the matrix, given by
 301 the derivatives of $\hat{\mathcal{W}}$ with respect to Θ and Φ , have to be regarded as external generalized forces. In fact,
 302 these terms describe the agency of the extracellular matrix on the fibers embedded in it, and represent a
 303 deterministic drift term guiding the fiber reorientation.

304 We emphasize here that stochastic models of fiber reorientation have been recently proposed in [83]
 305 for a problem of cell reorientation and in [50] within a study on fiber reinforced composite materials.
 306 It is also important to mention that, beyond some “technical” differences between the model presented
 307 in the sequel and the one proposed in [56] (these essentially referring to the way in which $\hat{\mathcal{W}}$ and the
 308 forces $\mathcal{F}_\Theta^{\text{ext}}$ and $\mathcal{F}_\Phi^{\text{ext}}$ are constructed), the most relevant features of the theory discussed in our work are
 309 as follows:

- 310 • On the trail of an idea put forward in [6], and by elaborating the framework presented in [83, 50], we
 311 introduce stochastic sources $\mathcal{F}_\Theta^{\text{ext,noise}}$ and $\mathcal{F}_\Phi^{\text{ext,noise}}$ that drive the dynamics of the angle functions
 312 θ and ϕ , thereby interpreting Equations (15a) and (15b) as Langevin-like evolution laws for θ and
 313 ϕ . Hence, whereas in [56] $\mathcal{F}_\Theta^{\text{ext}}$ and $\mathcal{F}_\Phi^{\text{ext}}$ are related to the deterministic concept of “*target angle*”
 314 [17, 56] only, we *presume* here that the reorientation of the fibers is influenced also by reciprocal
 315 interactions that, understood as the easiest type of “collisions”, may be described through a *white*
 316 *noise*. On the basis of these considerations, and by employing a well-established procedure in the
 317 field of stochastic processes, we replace Equations (15a) and (15b), which are valid at the scale of
 318 a single fiber (or of a family of fibers aligned along the same direction), with the resulting Fokker–
 319 Planck equation in the associated probability density distribution [6, 83, 50]. This distribution,

320 denoted by \hat{f}_R when expressed with respect to the reference placement \mathcal{B} of the composite, must
 321 thus satisfy the Fokker–Planck equation on the boundary of the sphere associated with $\mathbb{S}_X^2 \mathcal{B}$, i.e.,

$$\begin{aligned} \partial_t \hat{f}_R = & - \frac{1}{\sin \Theta} \frac{\partial}{\partial \Theta} \left[\frac{1}{\gamma} \left(\mathcal{F}_\Theta^{\text{ext,det}} + \frac{\partial \hat{\mathcal{W}}}{\partial \Theta} \right) \sin \Theta \hat{f}_R \right] - \frac{1}{\sin \Theta} \frac{\partial}{\partial \Phi} \left[\frac{1}{\gamma} \left(\mathcal{F}_\Phi^{\text{ext,det}} + \frac{1}{\sin \Theta} \frac{\partial \hat{\mathcal{W}}}{\partial \Phi} \right) \hat{f}_R \right] \\ & + D \frac{1}{\sin \Theta} \frac{\partial}{\partial \Theta} \left[\sin \Theta \frac{\partial \hat{f}_R}{\partial \Theta} \right] + D \frac{1}{(\sin \Theta)^2} \frac{\partial^2 \hat{f}_R}{\partial \Phi^2}, \end{aligned} \quad (16)$$

322 where the explicit dependence of $\partial_\Theta \hat{\mathcal{W}}$ and $\partial_\Phi \hat{\mathcal{W}}$ on their arguments has been omitted for the
 323 sake of a lighter notation; $D \in \mathbb{R}^+$ is referred to as *diffusion coefficient* and has units of rad^2/s ;
 324 and \hat{f}_R is defined through the identification $\hat{f}_R(X, \Theta, \Phi, t) \equiv f_R(X, \mathbf{M}_X, t)$, with the probability
 325 density distribution f_R being such that

$$f_R : \mathbb{S}^2 \mathcal{B} \times \mathcal{I} \rightarrow \mathbb{R}^+, \quad (17a)$$

$$(X, \mathbf{M}_X, t) \mapsto f_R(X, \mathbf{M}_X, t) = f_R(X, \hat{\mathbf{M}}_X(\Theta, \Phi), t) \equiv \hat{f}_R(X, \Theta, \Phi, t) \in \mathbb{R}^+. \quad (17b)$$

326 Since f_R is a probability density distribution, it has to be normalized, i.e.,

$$\int_{\mathbb{S}_X^2 \mathcal{B}} f_R(X, \mathbf{M}_X, t) = \int_0^{2\pi} \int_0^\pi \hat{f}_R(X, \Theta, \Phi, t) \sin \Theta \, d\Theta \, d\Phi = 1, \quad (18)$$

327 for all $X \in \mathcal{B}$ and $t \in [t_{\text{in}}, t_{\text{fin}}]$. We emphasize that, in Equation (16), the dependence of \hat{f}_R on
 328 the point X has to be regarded as parametric, since Equation (16) has to be solved at each $X \in \mathcal{B}$
 329 for varying time and with the angular distribution of \hat{f}_R resolved through its dependence on Θ and
 330 Φ . In addition, it should be noticed that, in general, the quantity D may depend on X , while the
 331 energy $\hat{\mathcal{W}}$ and the driving forces $\mathcal{F}_\Theta^{\text{ext,det}}$ and $\mathcal{F}_\Phi^{\text{ext,det}}$ may depend explicitly on X and time.

332 • Although Equation (16) is similar to the one studied in [83], we deviate from the model presented
 333 therein in that our Fokker–Planck equation is formulated in two dimensions (in fact, on the spherical
 334 surface parameterized by Θ and Φ), and because our *drift terms* are defined by $\mathcal{F}_\Theta^{\text{ext,det}} + \partial_\Theta \hat{\mathcal{W}}$
 335 and $\mathcal{F}_\Phi^{\text{ext,det}} + (\sin \Theta)^{-1} \partial_\Phi \hat{\mathcal{W}}$, rather than by the derivatives of the strain energy density, only. The
 336 forces $\mathcal{F}_\Theta^{\text{ext,det}}$ and $\mathcal{F}_\Phi^{\text{ext,det}}$, in turn, will be defined on the basis of the introduction of histological
 337 target angles [17, 56]. Furthermore, our model considers, along with the stochastic reorientation
 338 of the fibers, also the other type of remodeling due to the development of anelastic distortions
 339 in the tissue, described by F_γ . Finally, as will be shown in the forthcoming sections, we study
 340 a fully coupled problem accounting for the influence both of fiber reorientation and of anelastic
 341 distortions on the flow of the tissue’s interstitial fluid.

342 3 Strain energy density and permeability

343 In this section, we briefly recall the procedure for the construction of the strain energy density function
 344 and of the permeability tensor field of the fiber reinforced medium under study. To this end, we will
 345 have recourse to the formulation presented in [31, 32], which, in turn, is largely based on the models
 346 developed in [25, 26, 84, 27, 28, 29]. We emphasize that, although much of the information reported
 347 in this section is known in the literature, we find it important to summarize it here both for the sake of
 348 completeness and in order to highlight some deviations of our present formulation from the previous
 349 ones.

350 The first step is the introduction of the *directional average* [24] of a generic physical quantity \mathfrak{F} .
 351 As done in [31], but with some notational differences from [31], at each instant of time $t \in \mathcal{I}$ and
 352 point $X \in \mathcal{B}$, we evaluate \mathfrak{F} at $\mathbf{M}_X \in \mathbb{S}_X^2 \mathcal{B}$, which identifies the direction along which a single rectified
 353 fiber is aligned. In the most general case, the arguments of \mathfrak{F} are also F, F_γ , and all the model

354 parameters evaluated at X and t . However, to simplify the notation, we shall write $\mathfrak{F}(X, \mathbf{M}_X, t, \dots)$, and,
 355 upon considering the probability density distribution $f_{\mathbb{R}}$ solving Equation (16), we *define* the directional
 356 average of \mathfrak{F} as

$$\begin{aligned} \langle\langle \mathfrak{F} \rangle\rangle(X, t, \dots) &= \int_{\mathbb{S}_X^2 \mathcal{B}} \mathfrak{F}(X, \mathbf{M}_X, t, \dots) f_{\mathbb{R}}(X, \mathbf{M}_X, t) \\ &= \int_0^{2\pi} \int_0^\pi \hat{\mathfrak{F}}(X, \Theta, \Phi, \dots) \hat{f}_{\mathbb{R}}(X, \Theta, \Phi, t) \sin\Theta \, d\Theta \, d\Phi, \end{aligned} \quad (19)$$

357 with $\hat{\mathfrak{F}}(X, \Theta, \Phi, t, \dots) := \mathfrak{F}(X, \mathbf{M}_X, t, \dots)$. Note that $\langle\langle \mathfrak{F} \rangle\rangle$ is a “functional” of $f_{\mathbb{R}}$ (while $\langle\langle \mathfrak{F} \rangle\rangle$ is a true
 358 functional when \mathfrak{F} is scalar-valued, we use this terminology in generalized sense when \mathfrak{F} is a vector or
 359 a tensor field). We also remark that the expression of directional average provided in Equation (19) has
 360 to be understood as a definition, since we do not discuss here the ergodicity of the system under study.

361 As recalled in [85, 86, 31] and in the references therein, $\mathfrak{F}(X, \mathbf{M}_X, t, \dots)$ is assumed to enjoy the
 362 invariance property $\mathfrak{F}(X, -\mathbf{M}_X, t, \dots) = \mathfrak{F}(X, \mathbf{M}_X, t, \dots)$, which has to hold for all $X \in \mathcal{B}$, $t \in \mathcal{I}$, and
 363 $\mathbf{M}_X \in \mathbb{S}_X^2 \mathcal{B}$. In terms of $\hat{\mathfrak{F}}$, this writes $\hat{\mathfrak{F}}(X, \pi - \Theta, \Phi + \pi, t, \dots) = \hat{\mathfrak{F}}(X, \Theta, \Phi, t, \dots)$, for all $(\Theta, \Phi) \in$
 364 $[0, \pi] \times [0, 2\pi[$. In the literature on fiber reinforced composite materials with statistical orientation of the
 365 fibers, the same symmetry property is prescribed to apply also to the fiber probability density distribution
 366 $f_{\mathbb{R}}$, which is thus defined in such a way that it complies with the condition $f_{\mathbb{R}}(X, -\mathbf{M}_X, t) = f_{\mathbb{R}}(X, \mathbf{M}_X, t)$
 367 for all $\mathbf{M}_X \in \mathbb{S}_X^2 \mathcal{B}$ (or, $\hat{f}_{\mathbb{R}}(X, \pi - \Theta, \Phi + \pi, t) = \hat{f}_{\mathbb{R}}(X, \Theta, \Phi, t)$, for all $(\Theta, \Phi) \in [0, \pi] \times [0, 2\pi[$),
 368 uniformly with respect to $X \in \mathcal{B}$ and $t \in \mathcal{I}$. In our approach, however, this property is not imposed
 369 from the outset. Rather, it should be inherited from the drift terms featuring in the Fokker–Planck
 370 equation (16), when they are defined in such a way that $f_{\mathbb{R}}$ solving Equation (16) fulfills the requirement
 371 $f_{\mathbb{R}}(X, -\mathbf{M}_X, t) = f_{\mathbb{R}}(X, \mathbf{M}_X, t)$.

372 The physical quantity \mathfrak{F} must also reflect the material symmetries of the composite material under
 373 study. If, as done in [86, 31], the matrix of the composite is isotropic, and the fiber parallel to \mathbf{M}_X
 374 is transversely isotropic with respect to this direction, then the material is transversely isotropic at X
 375 with respect to the same direction. Then, by denoting by Orth^+ the group of all proper rotations, and
 376 by $\mathcal{G}_X(\mathbf{M}_X) := \{\mathbf{H} \in \text{Orth}^+ : \mathbf{H}\mathbf{M}_X = \mathbf{M}_X\}$ the group of all proper rotations about \mathbf{M}_X , for all
 377 $\mathbf{H} \in \mathcal{G}_X(\mathbf{M}_X)$ it must hold true that¹

$$\mathfrak{F}(X, \mathbf{H}\mathbf{M}_X, t, \mathbf{F}(X, t)\mathbf{H}, \mathbf{F}_\gamma(X, t)\mathbf{H}, \dots) = \mathfrak{F}(X, \mathbf{M}_X, t, \mathbf{F}(X, t), \mathbf{F}_\gamma(X, t), \dots). \quad (20)$$

378 3.1 Strain energy density

379 The considerations discussed so far are now applied to the definition of the strain energy density function
 380 of the composite material. Following [26, 27, 28, 86, 31, 87, 61], we write the strain energy density
 381 function of the solid phase associated with the single family of fibers aligned along \mathbf{M}_X at $X \in \mathcal{B}$, and
 382 written per unit volume of the reference placement \mathcal{B} , as

$$\begin{aligned} \mathcal{W} &= \check{\mathcal{W}}(X, \mathbf{M}_X, \mathbf{F}, \mathbf{F}_\gamma) \\ &= \Phi_s \hat{\mathcal{U}}(X, J, J_\gamma) + \Phi_{0s} \hat{\mathcal{W}}_0(X, \mathbf{F}, \mathbf{F}_\gamma) + \Phi_{1s} [\hat{\mathcal{W}}_{1i}(X, \mathbf{F}, \mathbf{F}_\gamma) + \check{\mathcal{W}}_{1a}(X, \mathbf{M}_X, \mathbf{F}, \mathbf{F}_\gamma)] \\ &= \Phi_s \hat{\mathcal{U}}(X, J, J_\gamma) + \Phi_{0s} \hat{\mathcal{W}}_0(X, \mathbf{F}, \mathbf{F}_\gamma) + \Phi_{1s} [\hat{\mathcal{W}}_{1i}(X, \mathbf{F}, \mathbf{F}_\gamma) + \hat{\mathcal{W}}_{1a}(X, \Theta, \Phi, \mathbf{F}, \mathbf{F}_\gamma)], \end{aligned} \quad (21)$$

383 where the volumetric fractions are expressed as $\Phi_s = J_\gamma \Phi_{sv}$, $\Phi_{0s} = J_\gamma \Phi_{0sv}$, and $\Phi_{1s} = J_\gamma \Phi_{1sv}$, with
 384 Φ_{sv} , Φ_{0sv} , and Φ_{1sv} evaluated at $X \in \mathcal{B}$; \mathbf{F} , \mathbf{F}_γ , J , and J_γ are evaluated in the pair $(X, t) \in \mathcal{B} \times \mathcal{I}$,
 385 although this dependence has been omitted for the sake of brevity; the term $\hat{\mathcal{W}}_0$ is the strain energy

¹We would like to rephrase here the way in which this statement was given in [31], where the invariance property in Equation (20) was formulated as “[...] the symmetry condition $\mathfrak{F}_X(\mathbf{H}\mathbf{M}_X) = \mathfrak{F}_X(\mathbf{M}_X)$, for all proper rotation tensors \mathbf{H} such that $\mathbf{H}\mathbf{M}_X = \pm\mathbf{M}_X$.” [31].

386 density of the matrix; $\hat{\mathcal{W}}_{1i}$ and $\hat{\mathcal{W}}_{1a}$ are the isotropic and anisotropic contributions of the fibers to the
 387 overall strain energy density, respectively; and $\hat{\mathcal{U}}$ is defined by [28]

$$\hat{\mathcal{U}}(X, J, J_\gamma) = \alpha_0(X) \mathcal{H}_-(J_{cr}(X) - J_e) \frac{[J_e - J_{cr}(X)]^{2q}}{[J_e - \Phi_{sv}(X)]^r}, \quad \text{with } J_e = \frac{J}{J_\gamma}. \quad (22)$$

388 The function $\hat{\mathcal{U}}$ plays the role of a “penalty” [86, 31] that prevents compaction by diverging in the limit
 389 in which $J_e(X, t)$ approaches $\Phi_{sv}(X)$ from above. Moreover, $\alpha_0(X)$ is a point-dependent elastic property
 390 of the composite; $J_{cr}(X)$ represents a “critical value” [28, 88] of J_e , below which $\hat{\mathcal{U}}$ is activated by
 391 the Heaviside function $\mathcal{H}_-(J_{cr}(X) - J_e(X, t))^2$; q is a strictly positive integer³, taken to be $q \geq 2$, and
 392 $r \in]0, 1]$; and the inequality $J_e(X, t) > \Phi_{sv}(X)$ must be respected at all times and at all points. Finally,
 393 following [27, 28, 29, 86, 31, 32, 61], $\hat{\mathcal{W}}_0$, $\hat{\mathcal{W}}_{1i}$, and $\hat{\mathcal{W}}_{1a}$ are given by

$$\hat{\mathcal{W}}_0(X, \mathbf{F}, \mathbf{F}_\gamma) = \alpha_0(X) \left[\frac{\exp(\alpha_1(X)[I_{1e} - 3] + \alpha_2(X)[I_{2e} - 3])}{[I_{3e}]^{\alpha_3(X)}} - 1 \right], \quad (23a)$$

$$\hat{\mathcal{W}}_{1i}(X, \mathbf{F}, \mathbf{F}_\gamma) = \alpha_{0i}(X) \left[\frac{\exp(\alpha_{1i}(X)[I_{1e} - 3] + \alpha_{2i}(X)[I_{2e} - 3])}{[I_{3e}]^{\alpha_{3i}(X)}} - 1 \right], \quad (23b)$$

$$\hat{\mathcal{W}}_{1a}(X, \Theta, \Phi, \mathbf{F}, \mathbf{F}_\gamma) = \mathcal{H}_-(I_{4e} - 1) \frac{k_1}{2k_2} \left[\exp\left(k_2[I_{4e} - 1]^2\right) - 1 \right]. \quad (23c)$$

394 The quantities $I_{\alpha e}$, with $\alpha = 1, 2, 3$, are the three principal invariants of the *elastic* right Cauchy–Green
 395 stretch tensor $\mathbf{C}_e = \mathbf{F}_e^T \mathbf{g} \mathbf{F}_e = \mathbf{F}_\gamma^{-T} \mathbf{C} \mathbf{F}_\gamma^{-1}$ ($\mathbf{C} = \mathbf{F}^T \mathbf{g} \mathbf{F}$ being the right Cauchy–Green stretch tensor) [62],
 396 and are defined as

$$I_{1e} := \text{tr} \mathbf{C}_e = \text{tr}(\mathbf{C} \mathbf{B}_\gamma), \quad (24a)$$

$$I_{2e} := \frac{1}{2} \{I_{1e}^2 - \text{tr}(\mathbf{C}_e^2)\} = \frac{1}{2} \{\text{tr}(\mathbf{C} \mathbf{B}_\gamma)^2 - \text{tr}(\mathbf{C} \mathbf{B}_\gamma \mathbf{C} \mathbf{B}_\gamma)\}, \quad (24b)$$

$$I_{3e} := \det \mathbf{C}_e = J_\gamma^{-2} \det \mathbf{C}, \quad (24c)$$

397 where $\mathbf{B}_\gamma = \mathbf{C}_\gamma^{-1}$ is the inverse of the *anelastic* right Cauchy–Green stretch tensor $\mathbf{C}_\gamma = \mathbf{F}_\gamma^T \boldsymbol{\eta} \mathbf{F}_\gamma$.
 398 Moreover, $\alpha_1(X)$, $\alpha_2(X)$, and $\alpha_3(X) \equiv \alpha_1(X) + 2\alpha_2(X)$ are the non-dimensional elastic parameters
 399 characterizing the isotropic material response of the matrix, together with $\alpha_0(X)$ (which, however,
 400 has the physical dimension of a volumetric energy density). Similarly, $\alpha_{0i}(X)$, $\alpha_{1i}(X)$, $\alpha_{2i}(X)$, and
 401 $\alpha_{3i}(X) \equiv \alpha_{1i}(X) + 2\alpha_{2i}(X)$ determine the elastic properties of the isotropic contribution of the fibers to
 402 the overall strain energy density. As in [3, 29], we set $\alpha_3(X) = 1$ and $\alpha_{3i}(X) = 1$. Finally, the elastic
 403 parameters k_1 and k_2 featuring in $\hat{\mathcal{W}}_{1a}$ are assumed here to be constant for the sake of simplicity, and,
 404 following [8, 56], $\hat{\mathcal{W}}_{1a}$ is prescribed as a function of the invariant I_{4e} , which can be written here as

$$I_{4e} = \mathbf{C}_e : \frac{\mathbf{F}_\gamma \mathbf{M}_X}{\|\mathbf{F}_\gamma \mathbf{M}_X\|} \otimes \frac{\mathbf{F}_\gamma \mathbf{M}_X}{\|\mathbf{F}_\gamma \mathbf{M}_X\|} = \frac{\mathbf{C} : \mathbf{M}_X \otimes \mathbf{M}_X}{\mathbf{C}_\gamma : \mathbf{M}_X \otimes \mathbf{M}_X} \equiv \frac{I_4}{I_{4\gamma}} =: \hat{I}_{4e}(\mathbf{C}, \mathbf{C}_\gamma, \Theta, \Phi), \quad (25)$$

405 where $I_4 := \mathbf{C} : \mathbf{M}_X \otimes \mathbf{M}_X$ is the fourth invariant of \mathbf{C} , and $I_{4\gamma} := \mathbf{C}_\gamma : \mathbf{M}_X \otimes \mathbf{M}_X$ the fourth invariant of
 406 \mathbf{C}_γ . Both I_4 and $I_{4\gamma}$ are defined with respect to the direction \mathbf{M}_X associated with the reference placement
 407 of the composite material.

408 It is important to notice that, although a more detailed and realistic description of transverse isotropy
 409 would require making $\hat{\mathcal{W}}_{1a}$ to depend also on the fifth invariant I_{5e} [89, 90], we neglect it for this study.
 410 However, we notice that, if written in terms of \mathbf{C} and \mathbf{C}_γ , I_{5e} reads

$$I_{5e} = \mathbf{C}_e^2 : \frac{\mathbf{F}_\gamma \mathbf{M}_X}{\|\mathbf{F}_\gamma \mathbf{M}_X\|} \otimes \frac{\mathbf{F}_\gamma \mathbf{M}_X}{\|\mathbf{F}_\gamma \mathbf{M}_X\|} = \frac{\mathbf{C} \mathbf{C}_\gamma^{-1} \mathbf{C} : \mathbf{M}_X \otimes \mathbf{M}_X}{\mathbf{C}_\gamma : \mathbf{M}_X \otimes \mathbf{M}_X} \equiv \frac{\tilde{I}_5}{I_{4\gamma}} =: \hat{I}_{5e}(\mathbf{C}, \mathbf{C}_\gamma, \Theta, \Phi), \quad (26)$$

²Here, the Heaviside function is defined as $\mathcal{H}_-(y) = 1$, for $y > 0$, and $\mathcal{H}_-(y) = 0$, for $y \leq 0$.

³In [86, 31], it has been omitted to specify that q is an integer, although it must be so in order for the numerator $[J_e - J_{cr}(X)]^{2q}$ in Equation (22) to be well-defined.

411 where we introduced the notation $\tilde{I}_5 := \mathbf{C}\mathbf{C}_\gamma^{-1}\mathbf{C} : \mathbf{M}_X \otimes \mathbf{M}_X$. For a discussion on a peculiar definition of
412 functions of the invariants I_1, \dots, I_5 , which are particularly suitable for modeling transversely isotropic
413 composite materials, the reader is referred, e.g., to [15]. As remarked in [91] referring to [92], the
414 expressions obtained for I_{4e} and I_{5e} in Equations (25) and (26) allow to write each of these quantities
415 as a function of \mathbf{C} and \mathbf{C}_γ , thereby making it possible to re-define $\hat{\mathcal{W}}_{1a}$ as a function of the same
416 tensor variables as well as of the material points X and of the direction of fiber alignment through
417 $\mathbf{M}_X = \hat{\mathbf{M}}_X(\Theta, \Phi)$.

418 As long as the Fokker–Planck equation is concerned, the derivatives of the strain energy density
419 function with respect to the angles determining the point-wise direction of fiber alignment involve only
420 the anisotropic contribution $\hat{\mathcal{W}}_{1a}$ to \mathcal{W} , as defined in Equation (21). However, to study the mechanical
421 response of the tissue, one has to account for the fact that the strain energy density function of the
422 composite material is the directional average of \mathcal{W} . Thus, since the terms $\hat{\mathcal{U}}$, $\hat{\mathcal{W}}_0$, and $\hat{\mathcal{W}}_{1i}$ do not
423 depend on the fiber direction \mathbf{M}_X , only $\hat{\mathcal{W}}_{1a}$ is effectively averaged. Hence, using Equation (19) and the
424 normalization condition (18), we obtain

$$\langle\langle \mathcal{W} \rangle\rangle = \Phi_s \hat{\mathcal{U}} + \Phi_{0s} \hat{\mathcal{W}}_0 + \Phi_{1s} \hat{\mathcal{W}}_{1i} + \Phi_{1s} \langle\langle \hat{\mathcal{W}}_{1a} \rangle\rangle, \quad (27)$$

425 where we omitted to specify the arguments of each addend for the sake of a lighter notation.

426 3.2 Permeability

427 In this work, the macroscopic permeability tensor \mathbf{K} in the reference placement of a porous, fiber-
428 reinforced material is given by [25, 84, 28]

$$\mathbf{K} = \hat{\mathbf{K}}(X, \mathbf{C}) = \hat{k}_0(J) \frac{(J - \Phi_{1s})^2}{J} \mathbf{C}^{-1} + \hat{k}_0(J) \frac{(J - \Phi_{1s})\Phi_{1s}}{J} \left\langle\left\langle \frac{\mathbf{M}_X \otimes \mathbf{M}_X}{\mathbf{C} : \mathbf{M}_X \otimes \mathbf{M}_X} \right\rangle\right\rangle, \quad (28)$$

429 and the scalar quantity $\hat{k}_0(J)$ is expressed constitutively as [3]

$$\hat{k}_0(X, J) = k_{0R}(X) \left[\frac{J - \Phi_s}{1 - \Phi_s} \right]^{m_0} \exp\left(\frac{m_1}{2}[J^2 - 1]\right), \quad (29)$$

430 where m_0, m_1 are material parameters and k_{0R} is a reference permeability (for other permeability laws
431 see, e.g., [7]). Note that in Equations (28) and (29) the dependence on X is also through the volumetric
432 fractions and, when needed, through the material coefficients, although it has not been explicitly reported
433 for the sake of conciseness. Moreover, in the case of articular cartilage, k_{0R} exhibits a dependence on the
434 material points that is given, for example, in [93]. We emphasize that, throughout this thesis, the term
435 “permeability” is understood as a synonym of “hydraulic conductivity”.

436 We identify the anisotropic contribution to the macroscopic permeability tensor with

$$\mathbf{K}_a = \hat{\mathbf{K}}_a(X, \mathbf{C}) = \hat{k}_0(J) \frac{(J - \Phi_{1s})\Phi_{1s}}{J} \left\langle\left\langle \frac{\mathbf{M}_X \otimes \mathbf{M}_X}{\mathbf{C} : \mathbf{M}_X \otimes \mathbf{M}_X} \right\rangle\right\rangle. \quad (30)$$

437 4 Constitutive assignments and remodeling laws

438 In this section, we recall the usual constitutive assignments in the framework of porous, fluid-saturated,
439 fiber-reinforced media, and the remodeling law for the plastic distortions obtained from the Dissipation
440 inequality [74, 76, 94, 6, 31], which is recalled but not discussed.

441 In Section 2.22, we have identified the first Piola–Kirchhoff stress tensor of a given phase with its
442 constitutive characterization, which we provide in accordance with the residual dissipation. In particular,
443 the behavior of the solid phase is that of a fiber-reinforced, elasto-plastic material (where “plastic” refers
444 to the anelastic distortions due to remodeling); the fluid phase is assumed to bear only equilibrium
445 hydrostatic stresses, while \mathbf{m}_f plays a relevant role in the dissipative processes concerning the fluid. The

446 residual dissipation, as studied in [74, 76, 94, 32], is satisfied with the following constitutive assignments
 447 [27, 28, 29, 32]

$$\mathbf{P}_s := J_\gamma \frac{\partial \langle \langle \mathcal{W} \rangle \rangle}{\partial \mathbf{F}_e} \mathbf{F}_\gamma^{-\text{T}}, \quad (31a)$$

$$\mathbf{P}_f := \mathbf{O}, \quad (31b)$$

$$J\mathbf{m}_f := J_\gamma \Phi_{fv} \mathbf{F}^{-\text{T}} \mathbf{K}^{-1} \mathbf{Q}, \quad (31c)$$

448 where \mathbf{Q} is the material filtration velocity and \mathbf{K} is the material permeability tensor in Equation (28).

449 As customary in this framework, neglecting gravity (which amounts to dropping \mathbf{f} from Equations
 450 (10a) and (10b)), and substituting Equations (31b) and (31c) into Equation (10b) lead to Darcy's Law in
 451 the form $\mathbf{Q} = -\mathbf{K}\text{Grad}P$, while Equations (10a)–(10e) can be “condensed” in the system

$$\text{Div} \mathbf{P}_s - J \mathbf{F}^{-\text{T}} \text{Grad} P = \mathbf{0}, \quad (32a)$$

$$J - \text{Div}(\mathbf{K}\text{Grad}P) = 0, \quad (32b)$$

$$\text{dev} \mathbf{Y}_u - \text{dev} \mathbf{Z} = \mathbf{0}, \quad (32c)$$

$$\mathbf{F}_\gamma^{-\text{T}} : \dot{\mathbf{F}}_\gamma = 0, \quad (32d)$$

452 where we have combined Equations (10b) and (10c) to obtain Equation (32b).

453 By considering the strain energy density function expressed in Equation (27) for a case in which $\hat{\mathcal{U}}$
 454 is not activated, i.e., whenever the porous medium is not approaching compaction, the constitutive first
 455 Piola–Kirchhoff stress tensor can be expressed as

$$\mathbf{P}_s = 2\Phi_s \left[(b_1 + b_2 I_{1e}) \mathbf{g} \mathbf{F} \mathbf{B}_\gamma - b_2 \mathbf{g} \mathbf{F} \mathbf{B}_\gamma \mathbf{C} \mathbf{B}_\gamma + b_3 I_{3e} \mathbf{F}^{-\text{T}} \right] + 2\Phi_{1s} \mathbf{g} \mathbf{F} \left\langle \left\langle \frac{b_4}{I_{4\gamma}} (\mathbf{M}_X \otimes \mathbf{M}_X) \right\rangle \right\rangle, \quad (33)$$

456 where $\zeta_i b_i = \frac{\partial \hat{\mathcal{W}}}{\partial I_{ie}}$, $i = 1, \dots, 4$, are constitutive functions of the invariants of \mathbf{C}_e ; $\zeta_k = \Phi_s$ and $b_k =$
 457 $\partial \mathcal{W}_0 / \partial I_{ke}$ for $k = 1, 2, 3$; $\zeta_4 = \Phi_{1s}$ and $b_4 = \partial \mathcal{W}_{1a} / \partial I_{4e}$ (note that these definitions of ζ_k descend
 458 from taking in our model $\alpha_0 \equiv \alpha_{0i}$, $\alpha_1 \equiv \alpha_{1i}$, and $\alpha_2 \equiv \alpha_{2i}$). It is worth noticing that the Heaviside
 459 function that appears in Equation (23c) is contained within b_4 . In particular, we identify the anisotropic
 460 contribution to the constitutive first Piola–Kirchhoff stress tensor associated with the solid phase as

$$\mathbf{P}_{sa} = 2\Phi_{1s} \mathbf{g} \mathbf{F} \left\langle \left\langle \frac{b_4}{I_{4\gamma}} (\mathbf{M}_X \otimes \mathbf{M}_X) \right\rangle \right\rangle. \quad (34)$$

461 4.1 Remodeling law

462 Following the study of the dissipation inequality conducted in [51, 95], and adapting it to the case of
 463 isochoric inelastic distortions developed in our present work, we provide the following identification for
 464 the deviatoric part of the stress-like tensor \mathbf{Y}_u , power-conjugate with the traceless anelastic rate $\mathbf{F}_\gamma^{-1} \dot{\mathbf{F}}_\gamma$:

$$\text{dev} \mathbf{Y}_u = -\text{dev} \boldsymbol{\Sigma}_s(\mathbf{F}, \mathbf{F}_\gamma) + \text{dev} \mathbf{Y}_{u,d}, \quad (35)$$

465 with $\boldsymbol{\Sigma}_s = \mathbf{F}^{\text{T}} \mathbf{P}_s$ being the constitutive Mandel stress tensor associated with the solid phase and $\mathbf{Y}_{u,d} \equiv$
 466 $\text{dev} \mathbf{Y}_{u,d}$ representing the *dissipative* part of $\text{dev} \mathbf{Y}_u$. In particular, following the study of the residual
 467 dissipation [51, 95], $\text{dev} \mathbf{Y}_{u,d}$ can be prescribed as

$$\text{dev} \mathbf{Y}_{u,d} = \mathbb{A}(\mathbf{F}, \mathbf{F}_\gamma) : \mathbf{F}_\gamma^{-1} \dot{\mathbf{F}}_\gamma, \quad (36)$$

468 where \mathbb{A} is a positive semi-definite fourth-order tensor.

469 From here on we make the strong hypothesis that remodeling is “confined” to the matrix of the
 470 medium under study (we recall that the matrix is isotropic) and that it is independent of the local
 471 direction of fiber alignment. In short, we shall say that remodeling is isotropic in the sense that Equation

472 (36) is covariant under transformations of the type $F \mapsto FH$ and $F_\gamma \mapsto F_\gamma H$, for any proper rotation
473 tensor H , which yield $F_\gamma^{-1} \dot{F}_\gamma \mapsto H^{-1} (F_\gamma^{-1} \dot{F}_\gamma) H$, $\mathbb{A}(FH, F_\gamma H) = H^T \underline{\mathbb{A}} H^{-1} : \mathbb{A}(F, F_\gamma) : H \underline{\mathbb{A}} H^{-T}$, and
474 $\text{dev} Y_{u,d} \mapsto H^T (\text{dev} Y_{u,d}) H^{-T}$. Hence, we prescribe \mathbb{A} in such a way that the preceding transformation
475 laws are satisfied and, for this purpose, we adapt the definition in [96] to our case (see also [51, 95]), that
476 is

$$\mathbb{A}(F, F_\gamma) = J_\gamma \mathfrak{b}_v [C \otimes C^{-1} + I^T \bar{\otimes} I] + J_\gamma \mathfrak{c}_v [C \otimes C^{-1} - I^T \bar{\otimes} I], \quad (37)$$

477 where \mathfrak{b}_v and \mathfrak{c}_v are material parameters such that $\mathfrak{b}_v \geq 0$ and $\mathfrak{c}_v \geq 0$ (we recall that, in all these
478 expressions above, J_γ is equal to unity). We remark that \mathbb{A} only gives rise to an isotropic contribution
479 in the remodeling law, whereas the fiber-reinforced composite is regarded at least as a transversely
480 isotropic material, if not orthotropic [97]. In this regard, an enriched description of remodeling should
481 take into account two separate contributions, one from the matrix and one from the fibers themselves.
482 The latter form of remodeling could be framed as put forward in [6], i.e., by taking \mathbb{A} in the space of
483 the transversely isotropic tensors, the basis of which is identified with a combination of tensor products
484 between $A_X = M_X \otimes M_X$ and $B_X = I - M_X \otimes M_X$. However, in this work we resort to the characterization
485 of \mathbb{A} expressed in Equation (37) of isotropic remodeling, while we set the goal of studying anisotropic
486 remodeling in future works.

487 By enforcing Equations (35) and (37), we can rewrite Equation (32c) and extract its skew-symmetric
488 and symmetric part. Moreover, by assuming $Z = O$, we can write the equations for the evolution of F_γ
489 as

$$2J_\gamma \mathfrak{b}_v \text{Dev}_C \text{Sym}(F_\gamma^{-1} \dot{F}_\gamma C^{-1}) - \text{Dev}_C(C^{-1} \Sigma_s) = O, \quad (38a)$$

$$2J_\gamma \mathfrak{c}_v \text{Skew}(F_\gamma^{-1} \dot{F}_\gamma C^{-1}) = O, \quad (38b)$$

490 where, for any second-order tensor T with contravariant material indices, the notation $\text{Dev}_C T$ means
491 $\text{Dev}_C T := T - \frac{1}{3} \text{tr}(CT) C^{-1}$ [51].

492 Equations (38a) and (38b) are understood as the dynamic equations that drive the onset and evolution
493 of the remodeling distortions. In particular, Equation (38b) retrieves the condition of null plastic spin as
494 a consequence of the model, rather than imposing it, as often done in the literature.

495 4.2 “Target angle” and fiber reorientation

496 Following [47, 81, 17, 56, 32], we introduce the concept of “target” angle, i.e., the angle corresponding
497 to the most probable direction along which fibers tend to align themselves. Various approaches are
498 present in the literature to couple the evolution of the target angle with the mechanical state of the tissue.
499 For example, the evolution of the target angle is driven by the mechanical stress in [17, 56], while it
500 depends on the deformation in [47, 81]. A similar approach is followed also in [31, 32], in which the
501 most probable fiber angle is driven by the target angle, the target angle is treated as a kinematic variable
502 and its evolution is described in terms of external remodeling forces.

503 In this work, we adhere to the conceptual framework put forward in [32], and, by considering the
504 Fokker–Planck equation (16), we expand the approach of Crevacore et al. [32] to describe the time
505 evolution of the probability density distribution f_R . Hence, even though we speak of “target angle”,
506 we search for the identification of a *target probability distribution*, in which the most probable angle
507 of orientation defines the “target angle” of our model. That being said, we follow the same conceptual
508 trail of [31, 32], and we consider $\mathcal{F}_\Theta^{\text{ext,det}}$ and $\mathcal{F}_\Phi^{\text{ext,det}}$ as the driving generalized forces associated with
509 a potential $\Pi = \hat{\Pi}(X, \Theta, \Phi)$. In particular, we assume that all the information regarding the preferred
510 directions along which the fibers align in the absence of elastic and anelastic distortions is stored in Π , and
511 that Π does not vary during the tissue’s evolution. In this setting, Π may represent biochemical, genetic,
512 and/or epigenetic factors that can play a relevant role in shaping the tissue’s mesoscopic structure.

513 Notice that, if we assume the existence of Π and that no other external action is exerted on $f_{\mathbb{R}}$, the
 514 external forces $\mathcal{F}_{\Theta}^{\text{ext,det}}$ and $\mathcal{F}_{\Phi}^{\text{ext,det}}$ consist only of the contributions that read

$$\mathcal{F}_{\Theta}^{\text{ext,det}} = [\text{Grad}\hat{\Pi}]_{\Theta} = \frac{\partial\hat{\Pi}}{\partial\Theta}, \quad \mathcal{F}_{\Phi}^{\text{ext,det}} = [\text{Grad}\hat{\Pi}]_{\Phi} = \frac{1}{\sin\Theta} \frac{\partial\hat{\Pi}}{\partial\Phi}, \quad (39)$$

515 and Equation (16) becomes

$$\partial_t \hat{f}_{\mathbb{R}} = -\frac{1}{\sin\Theta} \frac{\partial}{\partial\Theta} \left[\sin\Theta \left(\frac{1}{\gamma} \frac{\partial(\hat{\Pi} + \hat{\mathcal{W}})}{\partial\Theta} \hat{f}_{\mathbb{R}} - D \frac{\partial\hat{f}_{\mathbb{R}}}{\partial\Theta} \right) \right] - \frac{1}{(\sin\Theta)^2} \frac{\partial}{\partial\Phi} \left[\frac{1}{\gamma} \frac{\partial(\hat{\Pi} + \hat{\mathcal{W}})}{\partial\Phi} \hat{f}_{\mathbb{R}} - D \frac{\partial\hat{f}_{\mathbb{R}}}{\partial\Phi} \right]. \quad (40)$$

516 Hence, we can identify the components of a flux vector $\mathbf{J} = \hat{\mathbf{j}}(X, \Theta, \Phi, F, F_{\gamma})$ as

$$[\hat{\mathbf{j}}]_{\Theta} = \frac{1}{\gamma} \frac{\partial(\hat{\Pi} + \hat{\mathcal{W}})}{\partial\Theta} \hat{f}_{\mathbb{R}} - D \frac{\partial\hat{f}_{\mathbb{R}}}{\partial\Theta}, \quad [\hat{\mathbf{j}}]_{\Phi} = \frac{1}{\sin\Theta} \left(\frac{1}{\gamma} \frac{\partial(\hat{\Pi} + \hat{\mathcal{W}})}{\partial\Phi} \hat{f}_{\mathbb{R}} - D \frac{\partial\hat{f}_{\mathbb{R}}}{\partial\Phi} \right), \quad (41)$$

517 so that Equation (40) becomes

$$\partial_t \hat{f}_{\mathbb{R}} = -\text{Div}_{\mathbb{S}^2} \hat{\mathbf{j}}, \quad (42)$$

518 with $\text{Div}_{\mathbb{S}^2}$ being the divergence operator on the sphere, returning the right-hand side of Equation (40).

519 It is well known that Equation (40) admits a unique stationary solution [98, 99], that is

$$\hat{f}_{\text{SR}} := \frac{1}{\mathcal{Z}} \exp(\beta\hat{\Pi} + \beta\hat{\mathcal{W}}), \quad \mathcal{Z} := \int_0^{2\pi} \int_0^{\pi} \exp(\beta\hat{\Pi} + \beta\hat{\mathcal{W}}) \sin\Theta \, d\Theta d\Phi, \quad (43)$$

520 where $\beta := (D\gamma)^{-1} > 0$ is the inverse of a characteristic energy density. Out of this result for the
 521 stationary solution, we make the following remarks. Equation (43) defines our target probability density
 522 distribution.

523 *Remark 1* ((The spherical von Mises distribution as a particular solution of the Fokker–Planck equation)).
 524 In the absence of deformation and plastic-like distortions, we consider the case in which Π is given by
 525 $\Pi = \Pi_0 \mu_{\mathbf{X}} \mathbf{M}_{\mathbf{X}}$, where $\Pi_0 > 0$ is a coefficient independent of the angles Θ and Φ , and having the units
 526 of energy per unit volume, $\mathbf{M}_{\mathbf{X}} \in \mathbb{S}_{\mathbf{X}}^2 \mathcal{B}$ is a generic direction along which a rectified fiber is aligned,
 527 $\mu_{\mathbf{X}} \in (\mathbb{S}_{\mathbf{X}}^2 \mathcal{B})^*$ is a *constant* linear map (i.e., a covector), and the juxtaposition $\mu_{\mathbf{X}} \mathbf{M}_{\mathbf{X}}$ is a shorthand
 528 notation for expressing the duality product $\langle \mu_{\mathbf{X}} | \mathbf{M}_{\mathbf{X}} \rangle \equiv \mu_{\mathbf{X}} \mathbf{M}_{\mathbf{X}}$. Hence, the stationary solution reads

$$f_{\text{VM}} := \frac{1}{\mathcal{Z}_0} \exp(\beta \Pi_0 \mu_{\mathbf{X}} \mathbf{M}_{\mathbf{X}}), \quad \mathcal{Z}_0 := \int_{\mathbb{S}_{\mathbf{X}}^2 \mathcal{B}} \exp(\beta \Pi_0 \mu_{\mathbf{X}} \mathbf{M}_{\mathbf{X}}), \quad (44)$$

529 which coincides with the von Mises distribution on the sphere. In particular, if $\mu_{\mathbf{X}}$ is taken as the
 530 covector associated with the specific unit vector $\bar{\mathbf{M}}_{\mathbf{X}} = \sin\bar{\Theta} \cos\Phi \mathbf{E}_1 + \sin\bar{\Theta} \sin\Phi \mathbf{E}_2 + \cos\bar{\Theta} \mathbf{E}_3$, where
 531 $\bar{\Theta} \in [0, \pi]$ is a preferred value of the colatitude, then Equation (44) becomes

$$\hat{f}_{\text{VM}} := \frac{1}{\mathcal{Z}_0} \exp(\beta \Pi_0 \cos(\Theta - \bar{\Theta})), \quad \mathcal{Z}_0 := 2\pi \int_0^{\pi} \exp(\beta \Pi_0 \cos(\Theta - \bar{\Theta})) \sin\Theta \, d\Theta. \quad (45)$$

532 However, the distribution in Equation (44) does not satisfy the condition $f_{\mathbb{R}}(X, -\mathbf{M}_{\mathbf{X}}, t) = f_{\mathbb{R}}(X, \mathbf{M}_{\mathbf{X}}, t)$
 533 for all $\mathbf{M}_{\mathbf{X}} \in \mathbb{S}_{\mathbf{X}}^2 \mathcal{B}$ and fixed $\mu_{\mathbf{X}}$, which was discussed at the beginning of Section 3, when introducing
 534 the directional average of a generic physical quantity \mathfrak{F} .

535 The most immediate way to obtain this invariance is to require Π to depend on $\mathbf{M}_{\mathbf{X}}$ through the
 536 structure tensor $\mathbf{A}_{\mathbf{X}} := \mathbf{M}_{\mathbf{X}} \otimes \mathbf{M}_{\mathbf{X}}$, which is invariant under the transformation $\mathbf{M}_{\mathbf{X}} \mapsto -\mathbf{M}_{\mathbf{X}}$. We provide,
 537 thus, the following form for the potential Π :

$$\Pi = \Pi_0 [\mu_{\mathbf{X}} \otimes \mu_{\mathbf{X}}] (\mathbf{M}_{\mathbf{X}} \otimes \mathbf{M}_{\mathbf{X}}) = \Pi_0 (\mu_{\mathbf{X}} \mathbf{M}_{\mathbf{X}})^2, \quad (46)$$

538 so that the stationary solution associated with Equation (46) is

$$f_{\text{SVM}} := \frac{1}{\mathcal{Z}_0} \exp(\beta \Pi_0 (\boldsymbol{\mu}_X \mathbf{M}_X)^2), \quad \mathcal{Z}_0 := \int_{\mathbb{S}_X^2} \exp(\beta \Pi_0 (\boldsymbol{\mu}_X \mathbf{M}_X)^2). \quad (47)$$

539 Therefore, we recover a symmetric, bimodal von Mises distribution as the stationary probability density
 540 distribution associated with the reorientation process described by Equations (15a) and (15b) (see, e.g.,
 541 the comparison in Figure 1). In particular, if, as before, $\boldsymbol{\mu}_X$ is associated with the specific unit vector
 542 $\bar{\mathbf{M}}_X = \sin \bar{\Theta} \cos \Phi \mathbf{E}_1 + \sin \bar{\Theta} \sin \Phi \mathbf{E}_2 + \cos \bar{\Theta} \mathbf{E}_3$, then Equation (46) yields

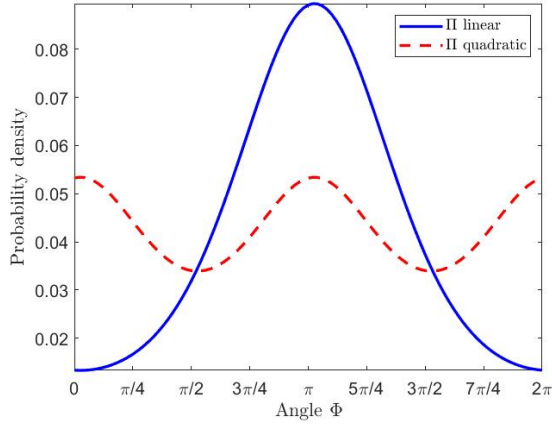
$$\hat{\Pi}(\Theta) = \Pi_0 [\cos(\Theta - \bar{\Theta})]^2 = \Pi_0 \frac{\cos(2[\Theta - \bar{\Theta}]) + 1}{2} = \frac{\Pi_0}{2} \{ \cos(2[\Theta - \bar{\Theta}]) + 1 \}. \quad (48)$$

543 Accordingly, Equation (47) becomes

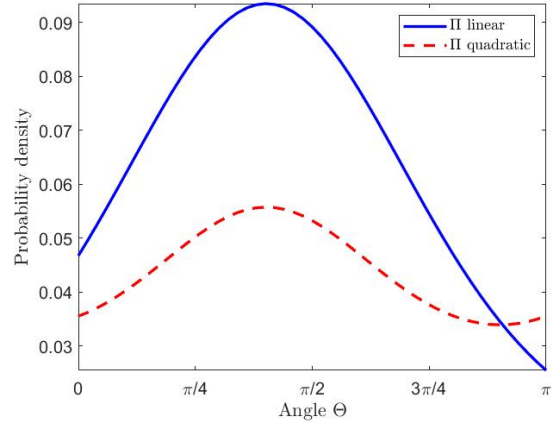
$$f_{\text{SVM}} := \frac{1}{\mathcal{Z}_0} \exp\left(\beta \Pi_0 [\cos(\Theta - \bar{\Theta})]^2\right) = \frac{1}{\mathcal{Z}_0} \exp\left(\frac{\beta \Pi_0}{2} \{ \cos(2[\Theta - \bar{\Theta}]) + 1 \}\right), \quad (49a)$$

$$\begin{aligned} \mathcal{Z}_0 &:= 2\pi \int_0^\pi \exp\left(\beta \Pi_0 [\cos(\Theta - \bar{\Theta})]^2\right) \sin \Theta \, d\Theta \\ &= \frac{2\pi\sqrt{\pi} \cos \bar{\Theta}}{\sqrt{\beta \Pi_0}} \operatorname{erfi}(\sqrt{\beta \Pi_0} \cos \bar{\Theta}) + \frac{2\pi\sqrt{\pi} \sin \bar{\Theta}}{\sqrt{\beta \Pi_0}} e^{\beta \Pi_0} \operatorname{erf}(\sqrt{\beta \Pi_0} \sin \bar{\Theta}), \end{aligned} \quad (49b)$$

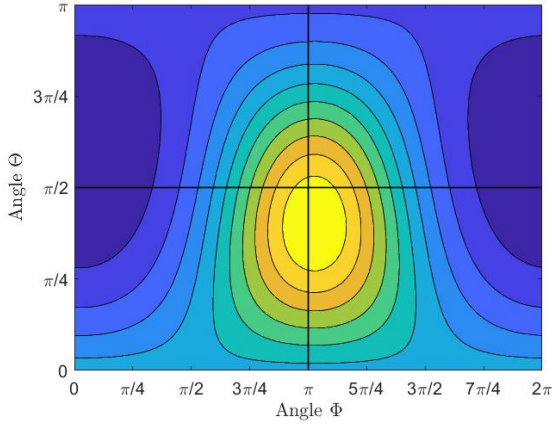
544 where $\operatorname{erfi}(\kappa)$ is the imaginary Error function, defined by $\operatorname{erfi}(\kappa) = -i \operatorname{erf}(i\kappa)$, with $\kappa \in \mathbb{C}$ and i being the
 545 imaginary unit. Before proceeding, it is worth noticing that $\bar{\mathbf{M}}_X$ has been defined for a fixed $\bar{\Theta}$ and variable
 546 Φ (thereby identifying a half cone). Thus, $\bar{\mathbf{M}}_X$ and $\hat{\mathbf{M}}_X$ are parameterized by different angles $\bar{\Theta}$ and Θ ,
 547 but by the same angle Φ . This is the reason why the potential Π prescribed in Equation (46) takes on the
 548 functional form given in Equation (48). Consequently, neither the potential $\hat{\Pi}$ nor the probability density
 549 distribution f_{SVM} in Equation (49a) are symmetric under the transformation $(\Theta, \Phi) \mapsto (\pi - \Theta, \Phi + \pi)$.
 550 Indeed, given $\boldsymbol{\mu}_X \mathbf{M}_X = \bar{\mathbf{M}}_X(\bar{\Theta}, \Phi) \cdot \hat{\mathbf{M}}_X(\Theta, \Phi)$, the expression $\bar{\mathbf{M}}_X(\bar{\Theta}, \Phi + \pi) \cdot \hat{\mathbf{M}}_X(\pi - \Theta, \Phi + \pi) =$
 551 $-\cos(\Theta + \bar{\Theta})$ is not equivalent to $\bar{\mathbf{M}}_X(\bar{\Theta}, \Phi) \cdot \hat{\mathbf{M}}_X(\pi - \Theta, \Phi + \pi) = -\cos(\Theta - \bar{\Theta})$. Rather, both
 552 the potential and the distribution are symmetric with respect to the transformation $(\Theta - \bar{\Theta}, \Phi) \mapsto$
 553 $(\pi - (\Theta - \bar{\Theta}), \Phi + \pi)$. This transformation, in turn, becomes trivially identical to the previous one for
 554 $\bar{\Theta} = 0$ and for $\bar{\Theta} = \pi$, since $\bar{\mathbf{M}}_X$ coincides with \mathbf{E}_3 and $-\mathbf{E}_3$, respectively. However, if $\bar{\mathbf{M}}_X$ is taken as
 555 $\bar{\mathbf{M}}_X = \sin \bar{\Theta} \cos \bar{\Phi} \mathbf{E}_1 + \sin \bar{\Theta} \sin \bar{\Phi} \mathbf{E}_2 + \cos \bar{\Theta} \mathbf{E}_3$, i.e., with fixed $\bar{\Theta}$ and $\bar{\Phi}$, then the potential Π becomes
 556 $\Pi = \Pi_0 (\boldsymbol{\mu}_X \mathbf{M}_X)^2 = \Pi_0 (\bar{\mathbf{M}}_X \cdot \mathbf{M}_X)^2 = \Pi_0 [\sin \bar{\Theta} \sin \Theta \cos(\Phi - \bar{\Phi}) + \cos \bar{\Theta} \cos \Theta]^2$. Then, it is invariant
 557 under the transformation $(\Theta, \Phi) \mapsto (\pi - \Theta, \Phi + \pi)$, and so is also f_{SVM} (see Figure 1). In particular,
 558 for $\bar{\Theta} = 0$ and $\bar{\Theta} = \pi$, one obtains $\Pi = \Pi_0 [\cos \Theta]^2$, and f_{SVM} equals the more ‘‘familiar’’ von Mises
 559 distribution used, e.g., in [27].



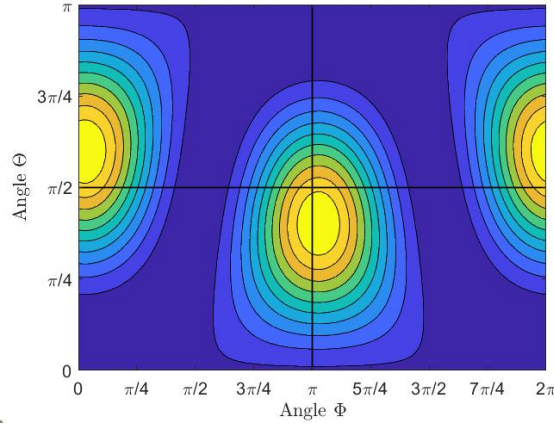
(a) Comparison between f_{VM} and f_{SVM} for $\Theta = \pi/2$.



(b) Comparison between f_{VM} and f_{SVM} for $\Phi = 0$.



(c) Plot of f_{VM} over $[0, 2\pi] \times [0, \pi]$.



(d) Plot of f_{SVM} over $[0, 2\pi] \times [0, \pi]$.

Figure 1: Comparison between the stationary solutions of Equation (42) for a linear and a quadratic potential Π in M_X (see Equations (44) and (47), respectively), with $\beta = 1$, $\Pi_0 = 1$ and $\mu_X = -0.9495E^1 - 0.0792E^2 + 0.3036E^3$ (here, the coefficients of μ_X are taken randomly with respect to the unit covectors E^A , with $A = 1, 2, 3$, of the canonical basis of $(T_X\mathcal{B})^*$). Figures 1a and 1b show f_{VM} and f_{SVM} evaluated for $\Theta = \pi/2$ and for $\Phi = 0$. Figures 1c and 1d show ten level sets of f_{VM} and f_{SVM} plotted on the domain $[0, 2\pi] \times [0, \pi]$. As expected, f_{SVM} respects the symmetry condition $\hat{f}_{SVM}(X, \pi - \Theta, \Phi + \pi) = \hat{f}_{SVM}(X, \Theta, \Phi)$, while f_{VM} does not.

560 *Remark 2* ((Fibers orientation in articular cartilage)).

561 In the absence of deformation, articular cartilage shows a very clear histological pattern in the distribution
562 of the fibers [100, 101, 102, 14]. To see how this histological information can be used to construct the
563 stationary probability density distribution through the potential Π , we consider a cylindrical specimen
564 of cartilage, and we assume it to be “*transversely isotropic and transversely homogeneous*” [14] with
565 respect to the geometric symmetry axis of the specimen itself. Then, by choosing a global reference
566 frame with the E_3 -axis coincident with the specimen’s symmetry axis, the probability density distribution
567 is taken independent of the longitude, i.e., independent of the angle Φ , and dependent on the co-latitude,
568 i.e., on the angle Θ . The histological orientation of the fibers is characterized by the *histological* angle
569 Θ_{hi} , which determines the most probable angle that the collagen fibers form with E_3 . The histological
570 angle Θ_{hi} varies with the axial coordinate of the specimen, but remains constant in each transverse section
571 of the specimen. More specifically, it can be observed that Θ_{hi} ranges from $\Theta_{hi} = 0$ at the bottom of
572 the specimen to $\Theta_{hi} = \pi/2$ at the upper surface of the specimen. Note that, in this description, the
573 bottom surface represents the interface between cartilage and bone, while the upper surface corresponds

574 to the articular surface, i.e., the surface that is in contact with the cartilage covering the extremity of the
575 opposing bone in a synovial joint [103]. In the middle, or transitional, region of the specimen, the fibers
576 exhibit greater variance in the histological angle Θ_{hi} . It is worth noticing that, in spite of the description
577 given so far, some works in the literature relax the hypothesis of transverse isotropy and assume the
578 probability density distribution to be a bi-variate, spherical von Mises distribution, depending both on Θ
579 and on Φ [19, 30, 33].

580 In our framework, we encode the fiber histological pattern described by Θ_{hi} in the target probability
581 density distribution of the tissue, and, by recurring to Equation (43), we couple it with the body's strain
582 energy density per unit volume of the reference placement. However, only the anisotropic term (23c)
583 concurs to shaping f_{SR} , whereas the other energetic contributions do not, since they are independent of
584 Θ and Φ .

585 To proceed with the target probability density distribution, we prescribe the potential Π as

$$\hat{\Pi}(\Theta; \Theta_{\text{hi}}, \omega) = \hat{\Pi}_0(\omega) [\cos(\Theta - \Theta_{\text{hi}})]^2 = \frac{\Pi_c}{\omega^2} [\cos(\Theta - \Theta_{\text{hi}})]^2, \quad \hat{\Pi}_0(\omega) := \frac{\Pi_c}{\omega^2}, \quad (50)$$

586 where the histological fibers' angle Θ_{hi} depends solely on the coordinate X^3 , ω is a dimensionless strictly
587 positive quantity associated with the variance of the fiber distribution and depending only on X^3 , and Π_c
588 is a constant, strictly positive referential value of the potential. Note that, with respect to the potential
589 introduced in Equation (48), the new definition of $\hat{\Pi}$ in Equation (50) is given to rescale the amplitude
590 of the potential with ω^2 . Clearly, this requires reformulating the normalization factor \mathcal{Z}_0 through the
591 substitution $\Pi_0 \mapsto \hat{\Pi}_0(\omega) = \Pi_c/\omega^2$, which, in the absence of deformation, yields

$$\hat{f}_{\text{SR}}(\Theta, \Phi; \Theta_{\text{hi}}, \omega) = \hat{f}_{\text{SVM}}(\Theta; \Theta_{\text{hi}}, \omega) = \frac{1}{\mathcal{Z}_0} \exp\left(\frac{\beta \Pi_c}{\omega^2} [\cos(\Theta - \Theta_{\text{hi}})]^2\right), \quad (51a)$$

$$\begin{aligned} \mathcal{Z}_0 &:= 2\pi \int_0^\pi \exp\left(\frac{\beta \Pi_c}{\omega^2} [\cos(\Theta - \Theta_{\text{hi}})]^2\right) \sin\Theta \, d\Theta \\ &= \frac{2\pi\sqrt{\pi}\omega \cos\Theta_{\text{hi}}}{\sqrt{\beta\Pi_c}} \operatorname{erfi}\left(\frac{\sqrt{\beta\Pi_c}}{\omega} \cos\Theta_{\text{hi}}\right) + \frac{2\pi\sqrt{\pi}\omega \sin\Theta_{\text{hi}}}{\sqrt{\beta\Pi_c}} e^{\beta\Pi_c/\omega^2} \operatorname{erf}\left(\frac{\sqrt{\beta\Pi_c}}{\omega} \sin\Theta_{\text{hi}}\right). \end{aligned} \quad (51b)$$

592 In particular, following [14], we take:

$$\Theta_{\text{hi}}(X^3) := \frac{\pi}{2} \left\{ 1 - \cos\left(\frac{\pi}{2} \left[-\frac{2}{3} \left(\frac{X^3}{H}\right)^2 + \frac{5}{3} \frac{X^3}{H} \right] \right) \right\}, \quad (52a)$$

$$\omega(X^3) := 10^3 \left[\left(1 - \frac{X^3}{H} \right) \frac{X^3}{H} \right]^4 + 0.03, \quad (52b)$$

593 where H is the height of the cartilage sample. Note that, according to Equation (50), Π is defined as
594 a function of Θ parameterized by Θ_{hi} and ω . We prefer this definition instead of expressing Π as a
595 function of Θ and X^3 in order to highlight that the dependence of Π on X^3 is through the parameters Θ_{hi}
596 and ω that characterize the model of tissue under investigation. It is also important to emphasize that,
597 differently from the expression of Π given in Equation (48), ω^2 plays a modulating role on the strength
598 of the drift exerted by Π on the probability density distribution.

599 Also the volumetric fractions of the extracellular matrix and of the fibers depend on X^3 , and are
600 obtained by means of a polynomial fit of experimental data. For example, following [104, 105, 94], we
601 use

$$\Phi_{0s}(X^3) = 0.046 + 0.038 \frac{X^3}{H} - 0.062 \left(\frac{X^3}{H}\right)^2, \quad (53a)$$

$$\Phi_{1s}(X^3) = 0.204 - 0.138 \frac{X^3}{H} + 0.062 \left(\frac{X^3}{H}\right)^2. \quad (53b)$$

602 Therefore, for articular cartilage, we obtain the following stationary probability density distribution

$$\begin{aligned}\hat{f}_{\text{SR}}(\Theta, \Phi; \mathbf{F}, \mathbf{F}_\gamma, \Theta_{\text{hi}}, \omega, \Phi_{1s}) &:= \frac{1}{\mathcal{Z}} \exp(\beta \hat{\Pi} + \beta \hat{\mathcal{W}}) \\ &= \frac{1}{\mathcal{Z}_a} \exp\left(\frac{\beta \Pi_c}{\omega^2} [\cos(\Theta - \Theta_{\text{hi}})]^2 + \beta \Phi_{1s} \hat{\mathcal{W}}_{1a}(\Theta, \Phi, \mathbf{F}, \mathbf{F}_\gamma)\right),\end{aligned}\quad (54)$$

603 in which \mathcal{Z}_a is the normalization constant associated with the sole anisotropic terms of the model, i.e.,

$$\begin{aligned}\mathcal{Z}_a &:= \int_{\mathbb{S}_X^2 \times \mathcal{B}} \exp(\beta \Pi + \beta \Phi_{1s} \mathcal{W}_{1a}) \\ &= \int_0^{2\pi} \int_0^\pi \exp\left(\frac{\beta \Pi_c}{\omega^2} [\cos(\Theta - \Theta_{\text{hi}})]^2\right) \exp\left(\beta \Phi_{1s} \hat{\mathcal{W}}_{1a}(\Theta, \Phi, \mathbf{F}, \mathbf{F}_\gamma)\right) \sin\Theta \, d\Theta d\Phi,\end{aligned}\quad (55)$$

604 where the quantities ω , Θ_{hi} , and Φ_{1s} are functions of the axial coordinate $X^3 \in [0, H]$, the dependence
605 of $\hat{\mathcal{W}}_{1a}$ on X has been suppressed, since its material coefficients are assumed to be homogeneous, and
606 \hat{f}_{SR} is made dependent parametrically also on Φ_{1s} .

607 *Remark 3* ((Change of measure)).

608 Equation (54) permits to introduce the equivalent expression of \hat{f}_{SR} given by

$$\hat{f}_{\text{SR}}(\Theta, \Phi; \mathbf{F}, \mathbf{F}_\gamma, \Theta_{\text{hi}}, \omega, \Phi_{1s}) := \frac{1}{\mathcal{Z}_f} \hat{f}_{1a}(\Theta, \Phi; \mathbf{F}, \mathbf{F}_\gamma, \Phi_{1s}) \hat{f}_{\text{SVM}}(\Theta; \Theta_{\text{hi}}, \omega),\quad (56)$$

609 where the new distribution \hat{f}_{1a} and the new normalization factors \mathcal{Z}_f and \mathcal{Z}_{1a} are defined by

$$\hat{f}_{1a}(\Theta, \Phi; \mathbf{F}, \mathbf{F}_\gamma, \Phi_{1s}) := \frac{1}{\mathcal{Z}_{1a}} \exp(\beta \Phi_{1s} \hat{\mathcal{W}}_{1a}(\Theta, \Phi, \mathbf{F}, \mathbf{F}_\gamma)),\quad (57a)$$

$$\mathcal{Z}_f := \int_0^{2\pi} \int_0^\pi \hat{f}_{1a}(\Theta, \Phi; \mathbf{F}, \mathbf{F}_\gamma, \Phi_{1s}) \hat{f}_{\text{SVM}}(\Theta; \Theta_{\text{hi}}, \omega) \sin\Theta \, d\Theta d\Phi,\quad (57b)$$

$$\mathcal{Z}_{1a} := \int_0^{2\pi} \int_0^\pi \exp(\beta \Phi_{1s} \hat{\mathcal{W}}_{1a}(\Theta, \Phi, \mathbf{F}, \mathbf{F}_\gamma)) \sin\Theta \, d\Theta d\Phi.\quad (57c)$$

610 We remark that the identity $\mathcal{Z}_a = \mathcal{Z}_0 \mathcal{Z}_{1a} \mathcal{Z}_f$ applies, where \mathcal{Z}_0 and \mathcal{Z}_a are defined in Equations (51b) and
611 (55), respectively. Therefore, when the directional average of a given physical quantity g is performed,
612 one can write

$$\begin{aligned}\langle\langle g \rangle\rangle &= \int_0^{2\pi} \int_0^\pi g(X, \Theta, \Phi, \dots) \hat{f}_{\text{SR}}(\Theta, \Phi; \mathbf{F}, \mathbf{F}_\gamma, \Theta_{\text{hi}}, \omega, \Phi_{1s}) \sin\Theta \, d\Theta d\Phi \\ &= \frac{1}{\mathcal{Z}_f} \int_0^{2\pi} \int_0^\pi g(X, \Theta, \Phi, \dots) \hat{f}_{1a}(\Theta, \Phi; \mathbf{F}, \mathbf{F}_\gamma, \Phi_{1s}) \hat{f}_{\text{SVM}}(\Theta; \Theta_{\text{hi}}, \omega) \sin\Theta \, d\Theta d\Phi,\end{aligned}\quad (58)$$

613 and $\langle\langle g \rangle\rangle$ can be rephrased either as the average of g with respect to the distribution \hat{f}_{1a} and the Von Mises
614 measure $dm_{\text{SVM}} := (\mathcal{Z}_f)^{-1} \hat{f}_{\text{SVM}}(\Theta; \Theta_{\text{hi}}, \omega) \sin\Theta \, d\Theta d\Phi$ or, equivalently, as the average of g with respect
615 to the distribution \hat{f}_{SVM} and the deformational measure $dm_{1a} := (\mathcal{Z}_f)^{-1} \hat{f}_{1a}(\Theta, \Phi; \mathbf{F}, \mathbf{F}_\gamma, \Phi_{1s}) \sin\Theta \, d\Theta d\Phi$.
616 In the first case, \hat{f}_{SVM} does not change in time, and encompasses the histological information associated
617 with Θ_{hi} and ω ; in the second case, \hat{f}_{1a} depends on the constitutive representation of the anisotropic part
618 of the material's strain energy density, evolves in time through \mathbf{F} and \mathbf{F}_γ , and is modulated by Φ_{1s} .

619 To conclude this section, we examine the inverse problem, i.e., a procedure to find Π when a given
620 stationary probability density distribution of the fibers is known either by experimental evidence or
621 because it is assigned from the outset. For instance, one can select the probability density distribution
622 at the time conventionally taken as initial for a given benchmark problem. If, in addition, one assumes
623 that neither deformations nor anelastic distortions have occurred at this initial time (in our setting, this

624 amounts to taking $\mathcal{W} = 0$), then, upon identifying the stationary probability density distribution f_{SR}
625 with the initial one $f_{\text{R,in}}$, i.e., $f_{\text{SR}} \equiv f_{\text{R,in}}$, Equation (43)₁ yields

$$f_{\text{SR}} \equiv f_{\text{R,in}} = \frac{1}{\mathcal{Z}_0} \exp(\beta\Pi) \quad \Longrightarrow \quad \Pi = \frac{1}{\beta} \log(\mathcal{Z}_0 f_{\text{SR}}). \quad (59)$$

626 Hence, the deterministic external forces $\mathcal{F}_\Theta^{\text{ext,det}}$ and $\mathcal{F}_\Phi^{\text{ext,det}}$ can be interpreted as the driving forces that
627 lead the system's probability density distribution towards f_{SR} , and that can be written as

$$\mathcal{F}_\Theta^{\text{ext,det}} = \frac{\partial \hat{\Pi}}{\partial \Theta} = \frac{1}{\beta \hat{f}_{\text{SR}}} \frac{\partial \hat{f}_{\text{SR}}}{\partial \Theta}, \quad \mathcal{F}_\Phi^{\text{ext,det}} = \frac{1}{\sin \Theta} \frac{\partial \hat{\Pi}}{\partial \Phi} = \frac{1}{\sin \Theta} \frac{1}{\beta \hat{f}_{\text{SR}}} \frac{\partial \hat{f}_{\text{SR}}}{\partial \Phi}. \quad (60)$$

628 Let us assume now that a mechanical action is applied from the outset in such a way that the system
629 remains in elastic regime (i.e., F_γ remains equal to the identity tensor). Then, the probability density
630 distribution evolves in time and deviates from the initial one, $\hat{f}_{\text{R,in}}$. However, if the system is (elastically)
631 unloaded and brought back to the initial state, then the probability density distribution attained at the end
632 of the unloading phase will be equal to $\hat{f}_{\text{SR}} \equiv \hat{f}_{\text{R,in}}$, and the terms $\mathcal{F}_\Theta^{\text{ext,det}}$ and $\mathcal{F}_\Phi^{\text{ext,det}}$ in Equation (60)
633 can be interpreted as the forces that maintain the original probability density distribution.

634 If anelastic distortions are present at the instant of time taken as initial, then the body is not stress-free
635 in this initial state [106], and the energetic contribution featuring in Equation (43)₁, which we indicate
636 as $\hat{\mathcal{W}}_{1a,\text{in}}(X, \Theta, \Phi) = \hat{\mathcal{W}}_{1a}(\Theta, \Phi; \mathbf{F}_{\text{in}}(X), \mathbf{F}_{\gamma\text{in}}(X))$, is not null in general. Consequently, the initial
637 probability density distribution and its associated potential would read

$$f_{\text{SR}} \equiv f_{\text{R,in}} = \frac{1}{\mathcal{Z}_a} \exp(\beta\Pi + \beta\Phi_{1s} \mathcal{W}_{1a,\text{in}}) \quad \Longrightarrow \quad \Pi = \frac{1}{\beta} \log(\mathcal{Z}_a f_{\text{SR}}) - \Phi_{1s} \mathcal{W}_{1a,\text{in}}. \quad (61)$$

638 Hence, the deterministic external forces would be characterized by the expressions

$$\mathcal{F}_\Theta^{\text{ext,det}}(X, \Theta, \Phi) = \frac{1}{\beta \hat{f}_{\text{SR}}(X, \Theta, \Phi)} \frac{\partial \hat{f}_{\text{SR}}}{\partial \Theta}(X, \Theta, \Phi) - \Phi_{1s}(X) \frac{\partial \hat{\mathcal{W}}_{1a,\text{in}}}{\partial \Theta}(X, \Theta, \Phi), \quad (62a)$$

$$\mathcal{F}_\Phi^{\text{ext,det}}(X, \Theta, \Phi) = \frac{1}{\sin \Theta} \left(\frac{1}{\beta \hat{f}_{\text{SR}}(X, \Theta, \Phi)} \frac{\partial \hat{f}_{\text{SR}}}{\partial \Phi}(X, \Theta, \Phi) - \Phi_{1s}(X) \frac{\partial \hat{\mathcal{W}}_{1a,\text{in}}}{\partial \Phi}(X, \Theta, \Phi) \right). \quad (62b)$$

639 5 Summary of the model and description of the benchmarks

640 In this section, we describe two initial- and boundary-value problems that we simulate with the aid of
641 the software COMSOL Multiphysics[®], version 5.3. To compute the directional averages, we recur to the
642 Spherical Design Algorithm [107, 27], suitably implemented in COMSOL [87]. With these numerical
643 experiments we aim at investigating the capabilities of the model presented in the previous sections. In
644 particular, we are interested in showing how the mesoscopic description of the reorientation of the fibers,
645 accounted for by means of the Fokker–Planck Equation (40), influences the behavior of the tissue at the
646 macroscale. For these purposes, we examine our model for the following two benchmarks:

- 647 1) Uni-axial stretch test of a slice of articular cartilage, taken from the surface region, i.e., the region
648 in which the fibers most likely lie on the transverse plane of the tissue's considered specimen (this
649 corresponds to $\Theta_{\text{hi}}(H) = \pi/2$, where H is the specimen's thickness);
- 650 2) Uni-axial compression-maintenance test of a cylindrical specimen of a hypothetical fiber-reinforced
651 tissue that borrows its properties from articular cartilage.

652 In both of these benchmarks, we consider a *quasi-stationary* evolution of the Fokker–Planck equation
653 for the fibers' probability density distribution, thereby directly employing Equation (54) to describe the
654 fibers' reorientation, instead of enforcing a pseudo-Gaussian or a symmetrized, bi-variate von Mises
655 distribution [19, 32, 33] from the outset. While this approach is justified for the first benchmark, since

656 it aims at recovering some experimental curves in stationary conditions, for the second benchmark the
657 hypothesis of a quasi-stationary evolution of the fibers is a simplifying assumption. However, in spite of
658 this simplification, our procedure yields results similar to the non-stationary Fokker–Planck equation, and
659 requires less computational resources. To be more specific, we are using the general result, based on the
660 spectral analysis of linear operators, according to which the solution of the Fokker–Planck equation with
661 a drift term generated by a potential converges exponentially to the stationary solution [108]. Clearly,
662 the *quasi-stationary* approach reduces significantly the computational burden when the Fokker–Planck
663 equation has to be solved together with Equations (32a)–(32d). Indeed, solving the non-stationary
664 Fokker–Planck Equation (40) would require finding, for each point $X \in \mathcal{B}$, and at each time t , the
665 probability density distribution \hat{f}_R as a function of Θ and Φ . In other words, this approach would require
666 solving, at each time $t \in [t_{\text{in}}, t_{\text{fin}}]$, the Fokker–Planck equation, coupled with the full system (32a)–(32d),
667 for each triplet of coordinates identifying a point $X \in \mathcal{B}$, and for each pair of spherical coordinates
668 (Φ, Θ) identifying a direction $\mathbf{M}_X \in \mathbb{S}_X^2$. Instead, directly using Equation (54), i.e., invoking the
669 quasi-stationary solution of the Fokker–Planck equation, partially decouples the remodeling of the fibers
670 (described through the evolution of their probability density distribution) from the determination of the
671 deformation and anelastic distortions of the extracellular matrix and from the pressure of the interstitial
672 fluid. The decoupling is only partial for the following reason: on the one hand, the probability density
673 distribution is needed, at each time, to evaluate the directional averages of the strain energy density and
674 of the permeability, which are necessary for solving the “macroscopic” problem described by Equations
675 (32a)–(32d); on the other hand, the strain energy density—in particular $\hat{\mathcal{W}}_{1a}$ —is needed, at each time,
676 to determine the quasi-stationary probability density distribution through Equation (54).

677 5.1 Uni-axial stretch test of a slice of articular cartilage

678 We specialize the model to portray the experimental setting used in the work of Mansfield et al. [109].
679 In the aforementioned paper, the harvested articular cartilage is sliced at various depths, and, in each
680 sample, the reorientation of the fibers under mechanical load is studied by imposing uni-axial stretch.
681 Each slice can be thought of as a parallelepiped with thickness much smaller than the other characteristic
682 lengths. Two opposing sides of the lateral boundary of the cuboid are clamped to the experimental
683 apparatus. The experiment is conducted in displacement control, and the orientation of the fibers in a
684 specific zone at the center of the sample itself is measured by studying the scattering of light after the
685 sample reaches the mechanical equilibrium. Under these conditions, the problem can be considered
686 static for each of the imposed displacements assigned in the aforementioned paper [109].

687 We specialize our model to a purely elastic case, i.e., by assuming *no remodeling*, and we neglect the
688 dynamic contribution of the fluid, which, for sufficiently long times (after relaxation), is characterized
689 by a uniformly null pressure field. Thus, we solve the dynamic equation

$$\text{Div} \mathbf{P}_s = \mathbf{0} \quad \text{in } \mathcal{B}. \quad (63)$$

690 The boundary is partitioned as $\partial \mathcal{B} = \Gamma_1 \cup \Gamma_2 \cup \Gamma_3 \cup \Gamma_4 \cup \Gamma_5 \cup \Gamma_6$, where, for $i = 1, 2, 3, 4, 5, 6$, each
691 Γ_i represents a face of the parallelepiped. We select a Cartesian basis $\{\mathbf{E}_1, \mathbf{E}_2, \mathbf{E}_3\}$ such that the unit
692 vector \mathbf{E}_1 is perpendicular to the faces Γ_1 and Γ_4 ; \mathbf{E}_2 is perpendicular to the faces Γ_2 and Γ_5 ; and \mathbf{E}_3
693 is perpendicular to the faces Γ_3 and Γ_6 (see Figure 2a). For simulations, we employ a parallelepiped of
694 length $L = 1.5$ mm, width $W = 1.0$ mm, and thickness $H = 0.1$ mm. Thus, we prescribe the boundary
695 conditions

$$\chi(X, t) = X, \quad \text{on } \Gamma_1, \quad (64a)$$

$$\chi^1(X, t) = (1 + \varepsilon)L, \quad \chi^2(X, t) = X^2, \quad \chi^3(X, t) = X^3, \quad \text{on } \Gamma_4, \quad (64b)$$

$$\mathbf{P}_s \mathbf{N}_2 = \mathbf{0}, \quad \text{on } \Gamma_2, \quad (64c)$$

$$\mathbf{P}_s \mathbf{N}_5 = \mathbf{0}, \quad \text{on } \Gamma_5, \quad (64d)$$

$$\mathbf{P}_s \mathbf{N}_3 = \mathbf{0}, \quad \text{on } \Gamma_3, \quad (64e)$$

$$P_s N_6 = \mathbf{0}, \quad \text{on } \Gamma_6, \quad (64f)$$

696 where $\varepsilon \in \{0.00, 0.04, 0.08, 0.12, 0.16\}$ is the imposed strain.

697 Since the slice is taken from the superficial zone of the tissue, we consider that all the fibers have
 698 the same orientation $\Theta = \pi/2$. This amounts to imposing that the probability density distribution is a
 699 Dirac Delta centered at $\Theta_{hi} = \pi/2$, as can be recovered from the expressions of the initial probability
 700 density distribution $\hat{f}_{R,in}$ and of the normalization factor \mathcal{Z}_0 supplied in Equations (51a) and (51b) by
 701 setting $\Theta_{hi} = \pi/2$ and $\omega \rightarrow 0^+$ (this limit, in fact, is approximated by the value $\omega(H) = 0.03$, assumed in
 702 Equation (52b) consistently with [14]). Indeed, for $\Theta_{hi} = \pi/2$, and ω in a (right) neighborhood of zero,
 703 \mathcal{Z}_0 becomes

$$\mathcal{Z}_0 = \frac{2\pi\sqrt{\pi}\omega}{\sqrt{\beta\Pi_c}} e^{\beta\Pi_c/\omega^2} \operatorname{erf}\left(\frac{\sqrt{\beta\Pi_c}}{\omega}\right), \quad (65)$$

704 and the probability density distribution takes on the form

$$\hat{f}_{R,in}(\Theta; \pi/2, \omega) = \frac{1}{2\pi\sqrt{\pi} \frac{\omega}{\sqrt{\beta\Pi_c}} \operatorname{erf}\left(\frac{\sqrt{\beta\Pi_c}}{\omega}\right)} \exp\left(-\frac{\beta\Pi_c}{\omega^2} [\sin(\Theta - \pi/2)]^2\right). \quad (66)$$

705 Thus, in the limit $\omega \rightarrow 0^+$, $\hat{f}_{R,in}(\Theta; \pi/2, \omega)$ converges towards zero whenever Θ is different from $\pi/2$,
 706 while it diverges positively for $\Theta = \pi/2$. In conclusion, for $\omega \rightarrow 0^+$, $\hat{f}_{R,in}(\Theta; \pi/2, \omega)$ converges, in
 707 distributional sense, to the Dirac Delta distribution divided by 2π , i.e., to $\frac{1}{2\pi}\delta(\Theta - \pi/2)$.

708 Lastly, in the experiments by Mansfield et al. [109], the initial distribution of the fibers is not uniform
 709 with respect to Φ (i.e., the slices are not transversely isotropic). However, since we do not possess enough
 710 information on the whole tissue, we approximate this initial datum with a uniform distribution in Φ
 711 (i.e., the Dirac Delta centered in $\Theta = \pi/2$ and normalized by 2π) in order to calculate the deformations.
 712 Afterwards, we use the calculated deformations in conjunction with the initial distribution of the fibers,
 713 as shown in section 4.2, to reconstruct the experimental data collected in [109].

714 For what concerns the numerical implementation, we used quadratic Lagrange elements for solving
 715 the displacement and the pressure field, whereas no remodeling is accounted for in this benchmark. The
 716 overall system consists of 14937 degrees of freedom, with 5106 internal.

717 5.2 Uni-axial compression test of a cylindrical specimen

718 We consider the case of the uni-axial compression test of a cylindrical sample of cartilage of radius
 719 $R = 1.5$ mm and height $H = 1$ mm, modeled as a saturated, soft, fiber-reinforced material undergoing
 720 a stress-driven remodeling process and reorientation of the fibers. The experimental setup consists of
 721 a chamber, filled with warm water to maintain temperature at about 20°C , in the interior of which the
 722 sample is confined at the top and at the bottom by two non-adhesive, impermeable plates characterized by
 723 a stiffness much higher than that of cartilage. The experiment is in displacement control by prescribing
 724 the compressive ramp [29, 86, 110]

$$\chi_U^3(X^1, X^2, t) \equiv \chi^3(X^1, X^2, H, t) := \begin{cases} H - u_T \frac{t - t_{in}}{t_{ramp} - t_{in}}, & t \in [t_{in}, t_{ramp}], \\ H - u_T, & t \in]t_{ramp}, t_{fin}], \end{cases} \quad (67)$$

725 where, for $t > t_{ramp}$, the apparatus keeps fixed the imposed displacement on the sample. For our study,
 726 we consider $t_{in} = 0$ s, $t_{ramp} = 20$ s and $t_{fin} = 30$ s.

727 For the simulations, rather of speaking of articular cartilage, we speak of a hypothetical tissue
 728 ‘‘borrowing’’ some material properties from articular cartilage, including the histological profile of the
 729 fibers, because we aim at describing a broader class of tissues that may be of interest from the point of
 730 view of bio-engineered materials. For instance, as done for other studies on cartilage (see, e.g., [29]), we

731 assume the referential permeability of the tissue to be a function of X^3 , normalized with respect to the
 732 height H of the sample [93], and we prescribe it to be

$$k_{\text{OR}} \equiv k_{\text{OR}}^{(0)} \left[\frac{e_{\text{R}}(X^3/H)}{e_{\text{R}}^{(0)}} \right]^{m_0} \exp \left\{ \frac{m_1}{2} \left[\left(\frac{1 + e_{\text{R}}(X^3/H)}{1 + e_{\text{R}}^{(0)}} \right)^2 - 1 \right] \right\}, \quad (68)$$

733 with $e_{\text{R}} = (1 - \Phi_{\text{s}})/\Phi_{\text{s}}$ being the void ratio, and $e_{\text{R}}^{(0)}$ being the referential void ratio (we recall that the
 734 hypothesis of isochoric remodeling implies $J_{\gamma} = 1$, and, thus, $\Phi_{\text{sv}} = \Phi_{\text{s}}$).

735 We perform the simulations by solving the equations

$$\text{Div} \mathbf{P}_{\text{s}} - J \mathbf{F}^{-\text{T}} \text{Grad} P = \mathbf{0} \quad \text{in } \mathcal{B}, \quad (69\text{a})$$

$$\dot{J} - \text{Div}(\mathbf{K} \text{Grad} P) = 0 \quad \text{in } \mathcal{B}, \quad (69\text{b})$$

$$2\mathbf{b}_{\gamma} \text{DevSym}(\mathbf{F}_{\gamma}^{-1} \dot{\mathbf{F}}_{\gamma} \mathbf{C}^{-1}) - \text{Dev}(\mathbf{C}^{-1} \boldsymbol{\Sigma}_{\text{s}}) = \mathbf{0} \quad \text{in } \mathcal{B}, \quad (69\text{c})$$

$$\text{Skew}(\mathbf{F}_{\gamma}^{-1} \dot{\mathbf{F}}_{\gamma} \mathbf{C}^{-1}) = \mathbf{0} \quad \text{in } \mathcal{B}, \quad (69\text{d})$$

$$\mathbf{F}_{\gamma}^{-\text{T}} : \dot{\mathbf{F}}_{\gamma} = 0 \quad \text{in } \mathcal{B}, \quad (69\text{e})$$

736 in a cylindrical domain \mathcal{B} , with symmetry axis aligned along \mathbf{E}_3 . We partition the boundary $\partial \mathcal{B}$ as
 737 $\partial \mathcal{B} = \Gamma_{\text{U}} \cup \Gamma_{\text{L}} \cup \Gamma_{\text{B}}$, where Γ_{U} is the upper surface, Γ_{L} is the lateral surface, and Γ_{B} is the bottom
 738 surface. The co-normal of a given surface is indicated by adopting the same subscript, so that \mathbf{N}_{U} , \mathbf{N}_{L} ,
 739 and \mathbf{N}_{B} are the fields of co-normals associated with Γ_{U} , Γ_{L} and Γ_{B} , respectively (see Figure 2b). Hence,
 740 for every time $t \in [t_{\text{in}}, t_{\text{fin}}]$, we prescribe the boundary conditions as

$$\chi^3(X, t) = \chi_{\text{U}}^3(X_1, X_2, t), \quad [(\mathbf{P}_{\text{s}} - J P \mathbf{F}^{-\text{T}}) \mathbf{N}_{\text{U}}] \mathbf{E}_1 = 0, \quad [(\mathbf{P}_{\text{s}} - J P \mathbf{F}^{-\text{T}}) \mathbf{N}_{\text{U}}] \mathbf{E}_2 = 0, \quad \text{on } \Gamma_{\text{U}}, \quad (70\text{a})$$

$$\mathbf{Q} \mathbf{N}_{\text{U}} = 0, \quad \text{on } \Gamma_{\text{U}}, \quad (70\text{b})$$

$$(\mathbf{P}_{\text{s}} - J P \mathbf{F}^{-\text{T}}) \mathbf{N}_{\text{L}} = \mathbf{0}, \quad \text{on } \Gamma_{\text{L}}, \quad (70\text{c})$$

$$P = 0, \quad \text{on } \Gamma_{\text{L}}, \quad (70\text{d})$$

$$\chi(X, t) = (X^1, X^2, 0), \quad \text{on } \Gamma_{\text{B}}, \quad (70\text{e})$$

$$\mathbf{Q} \mathbf{N}_{\text{B}} = 0, \quad \text{on } \Gamma_{\text{B}}. \quad (70\text{f})$$

741 Finally, the initial conditions for the IBVP are

$$\chi(X, t_{\text{in}}) = \chi_{\text{in}}(X), \quad \text{in } \mathcal{B}, \quad (71\text{a})$$

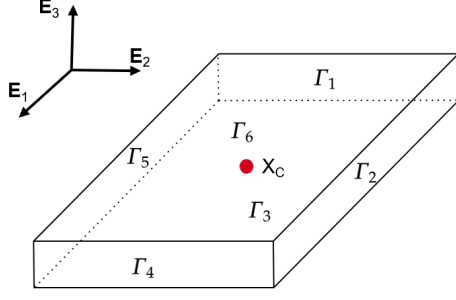
$$P(X, t_{\text{in}}) = 0, \quad \text{in } \mathcal{B}, \quad (71\text{b})$$

$$\mathbf{F}_{\gamma}(X, t_{\text{in}}) = \mathbf{I}, \quad \text{in } \mathcal{B}, \quad (71\text{c})$$

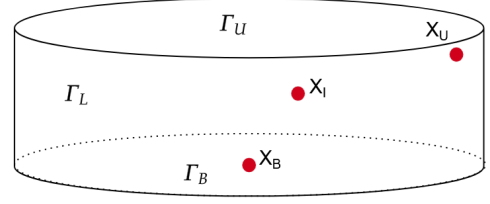
$$\hat{f}_{\text{R}, \text{in}}(\Theta; \Theta_{\text{hi}}, \omega) = \frac{1}{\mathcal{Z}_0} \exp \left(\frac{\beta \Pi_{\text{c}}}{\omega^2} [\cos(\Theta - \Theta_{\text{hi}})]^2 \right), \quad \text{in } \mathbb{S}^2 \mathcal{B}, \quad (71\text{d})$$

742 where we set $\chi_{\text{in}}(X) = (X^1, X^2, X^3)$, \mathbf{I} is the identity tensor in the reference placement, and \mathcal{Z}_0 is
 743 defined in Equation (47). Note that the dependence of $\hat{f}_{\text{R}, \text{in}}$ on X —in fact, on X^3 — is through Θ_{hi} and
 744 ω according to the expressions (52a) and (52b), respectively. Consequently, also \mathcal{Z}_0 depends on X^3
 745 through these quantities, as can be deduced from Equation (51b). Moreover, because of lack of better
 746 information, and to fall within an already established framework [27], we set $\Pi_{\text{c}} = 1/\beta$ in Equation
 747 (71d). By doing so, the quantity $1/\omega^2$ in the argument of the exponential function in Equation (71d) can
 748 be identified with $1/\omega^2 \equiv 2b$, where b is the parameter of the von Mises distribution used for the “Model
 749 B” of Federico and Gasser [27].

750 Also for this benchmark we used quadratic Lagrange elements for solving the displacement and the
 751 pressure field, whereas the remodeling variable is solved in the Gauss points used for integration. In the
 752 case of the cylinder, the overall system consists of 34580 degrees of freedom (plus 7128 internal degrees
 753 of freedom introduced by COMSOL).



(a) Geometry of the cuboid sample for benchmark 1.



(b) Geometry of the cylindrical sample for benchmark 2.

Figure 2: Geometries of the two benchmarks. The point X_C in the first geometry is taken in the middle of the cuboid, at Cartesian coordinates $(0.5, 0.75, 0.05)$, expressed in millimeters. The points X_U , X_I and X_B in the second geometry are taken at Cartesian coordinates $(0.0, 1.35, 0.9)$, $(0.0, 0.375, 0.5)$ and $(0.0, 0.0, 0.0)$, respectively, expressed in millimeters.

6 Results and discussion

In this section, we report and discuss the results of the two benchmarks described previously, and we examine the influence of the fibers on the overall behavior of the medium.

6.1 Fiber orientation under uni-axial stretch of a slice of cartilage

By following the procedure depicted at the end of section 4.2, and by approximating the deformation as written in section 5.1, we aim to recover some experimental curves presented in the work of Mansfield et al. [109]. In particular, we simulate the evolution of the probability density distribution in the cases of uni-axial stretch of superficial slices of cartilage for the two initial data

$$\hat{f}_{R,\text{in}}^{(i)}(\Theta, \Phi) = \frac{1}{2\pi} \delta\left(\Theta - \frac{\pi}{2}\right) \frac{1}{C_0^{(i)}} \hat{h}^{(i)}(\Phi), \quad i \in \{1, 2\}, \quad (72)$$

where $\hat{h}^{(1)}(\Phi)$ and $\hat{h}^{(2)}(\Phi)$ are given by

$$\hat{h}^{(1)}(\Phi) = \exp\left(3.4 \left[\cos\left(\Phi - \frac{\pi}{12}\right)\right]^2\right), \quad (73a)$$

$$\hat{h}^{(2)}(\Phi) = \exp\left(6.4 \left[\cos\left(\Phi - \frac{11}{24}\pi\right)\right]^2\right) + 0.5 \exp\left(6.2 \left[\cos\left(\Phi - \frac{\pi}{18}\right)\right]^2\right), \quad (73b)$$

and the normalizing constants $C_0^{(i)}$ coincide with their averages over $[0, 2\pi]$, i.e.,

$$C_0^{(i)} = \frac{1}{2\pi} \int_0^{2\pi} h^{(i)}(\Phi) d\Phi, \quad i \in \{1, 2\}. \quad (74)$$

For $i = 1, 2$, $\hat{f}_{R,\text{in}}^{(i)}$ fits the experimental curves for the distribution of the fiber orientation without applied stretch [109], and the overall normalization constants are identified by the equalities $\mathcal{Z}_0^{(i)} = 2\pi C_0^{(i)}$.

We are able to predict the evolution of the probability density distributions obtained as solutions of the Fokker–Planck Equation (40) starting from $\hat{f}_{R,\text{in}}^{(1)}$ and $\hat{f}_{R,\text{in}}^{(2)}$. In particular, for these initial distributions, the corresponding potentials $\Pi^{(1)}$ and $\Pi^{(2)}$ are assigned in such a way that $\hat{f}_{R,\text{in}}^{(1)}$ and $\hat{f}_{R,\text{in}}^{(2)}$ coincide with the stationary solutions of the Fokker–Planck equation in the absence of deformation (see Equation (59)₂). After stretching, the stationary solutions can be recast in the form

$$\hat{f}_{\text{SR}}^{(i)}(\Theta, \Phi) = \frac{\mathcal{Z}_0^{(i)}}{\mathcal{Z}_a^{(i)}} \hat{f}_{R,\text{in}}^{(i)}(\Theta, \Phi) e^{\beta \Phi_{1s}(H)} \mathcal{W}_{1a}(\Theta, \Phi, \mathbf{F}(H)), \quad (75a)$$

Parameter	Symbol	Numerical value	Unit of measure	Reference
Density fluid phase	ϱ_f	$1 \cdot 10^3$	kg/m ³	[111]
Density solid phase	ϱ_s	$1 \cdot 10^3$	kg/m ³	[111]
Critical J	J_{cr}	$0.1 + \Phi_{sv}$	-	[32]
Coefficient of \mathcal{U}	q	2	-	[32]
Coefficient of \mathcal{U}	r	0.5	-	[32]
Elastic property	$\alpha_0 = \alpha_{0i}$	0.125	MPa	[29]
Elastic property	$\alpha_1 = \alpha_{1i}$	0.778	-	[29]
Elastic property	$\alpha_2 = \alpha_{2i}$	0.111	-	[29]
Elastic property	k_1	7.5	MPa	[112, 29]
Elastic property	k_2	0.5	-	-
Characteristic energy density	β	$2.71 \cdot 10^{-4}$	Pa ⁻¹	-
Reference hydraulic conductivity	$k_{0R}^{(0)}$	$3.7729 \cdot 10^{-3}$	mm ⁴ /(N · s)	[86]
Material parameter	m_0	0.0848	-	[113]
Material parameter	m_1	4.6380	-	[113]
Referential void ratio	$e_R^{(0)}$	4.0	-	[29]
Remodeling rate	b_γ	25.0	N · s/mm ²	-

Table 1: Values of the material parameters used for the numerical simulations.

$$\begin{aligned}
\frac{\mathcal{Z}_a^{(i)}}{\mathcal{Z}_0^{(i)}} &= \int_0^{2\pi} \int_0^\pi \hat{f}_{R,in}^{(i)}(\Theta, \Phi) e^{\beta \Phi_{1s}(H)} \hat{\mathcal{W}}_{1a}(\Theta, \Phi, \mathbf{F}(H)) \sin\Theta \, d\Theta d\Phi \\
&= \frac{1}{2\pi C^{(i)}} \int_0^{2\pi} \hat{h}^{(i)}(\Phi) e^{\beta \Phi_{1s}(H)} \hat{\mathcal{W}}_{1a}(\pi/2, \Phi, \mathbf{F}(H)) \, d\Phi,
\end{aligned} \tag{75b}$$

771 where the explicit dependence of $\hat{\mathcal{W}}_{1a}$ on \mathbf{F}_γ and on X has been suppressed because, for this benchmark
772 test, no remodeling is considered, and because the parameters k_1 and k_2 are assumed to be constant (see
773 Table 1).

774 In particular, the parameters k_2 and β are assigned by fitting the experimental findings. It is
775 worth noticing that the last integral in Equation (75b) amounts to performing the change of measure
776 $d\Phi \mapsto (2\pi C^{(i)})^{-1} \hat{h}^{(i)}(\Phi) d\Phi$ (see Remark 3).

777 In Figures 3a and 4a, we report a selected collection of data, extracted for “Figure 9a (ii)” of Mansfield
778 et al. [109] and replotted in radians for comparison with our numerical results, as shown in Figures
779 3b and 4b. In these figures, with the same convention adopted in [109], the directions identified by
780 $(\Theta, \Phi) = (\pi/2, 0)$ are parallel to the Cartesian unit vector \mathbf{E}_1 , along which the tissue is stretched. Note
781 that, in order to directly compare our numerical results with the experimental findings of Mansfield et
782 al. [109], we redefined $\hat{f}_{SR}^{(i)}$ so as to exploit the symmetry condition $\hat{f}_{SR}^{(i)}(\Theta, \Phi) = \hat{f}_{SR}^{(i)}(\pi - \Theta, \Phi + \pi)$
783 to restrict the plot of $\hat{f}_{SR}^{(i)}$ along Φ on the subdomain $[-\pi/2, \pi/2] \subset [-\pi, \pi[$. The agreement between
784 the experimental data and the probability densities of our model is particularly good for strains equal to,
785 or greater than, the 8% of the overall length L of the slice. However, for smaller strains, the probability
786 densities computed numerically differ quantitatively from the experimental ones in appreciable way,
787 although their trend is still in agreement with the experimental data.

788 A similar detachment of our numerical results from the experimental ones of Mansfield et al. [109]
789 occurs in correspondence to the “tails” of the bi-variate distribution in Figure 4b, i.e., for the values
790 attained by $\hat{f}_{SR}^{(2)}$ as Φ approaches both $-\pi/2$ and $\pi/2$. In fact, in the experiment the number of fibers
791 aligned in the direction perpendicular to the one along which the strain is applied decreases for small
792 strains (i.e., from $\varepsilon = 0.00$ to $\varepsilon = 0.04$) more markedly than predicted by our simulations. In our opinion,
793 this would suggest some form of self-interactions among the collagen fibers, which is not considered in
794 the present model, and that could improve the accuracy in the modeling of the fiber reorientation process.
795 With respect to the viewpoint expressed in [115], the behavior observed in Figure 4a, and, to a smaller

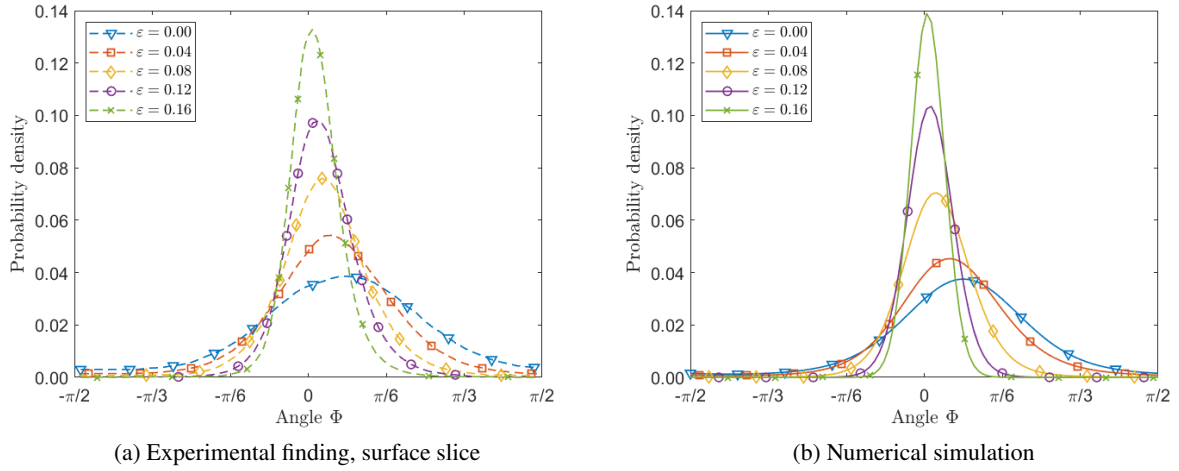


Figure 3: Comparison between the experimental findings of Mansfield et al. [109] (Figure 3a, adapted from “Figure 9a (ii)” [109]) and our numerically simulated curves for an imposed deformation $\varepsilon = 0.04n$, for $n = 0, 1, 2, 3, 4$ (Figure 3b). The experimental data points of Mansfield et al.[109] have been extracted from their “Figure 9a (ii)” by using the online software WebPlotDigitizer [114], and have been replotted vs radians (degrees are used in the original image) as shown in Figure 3a.

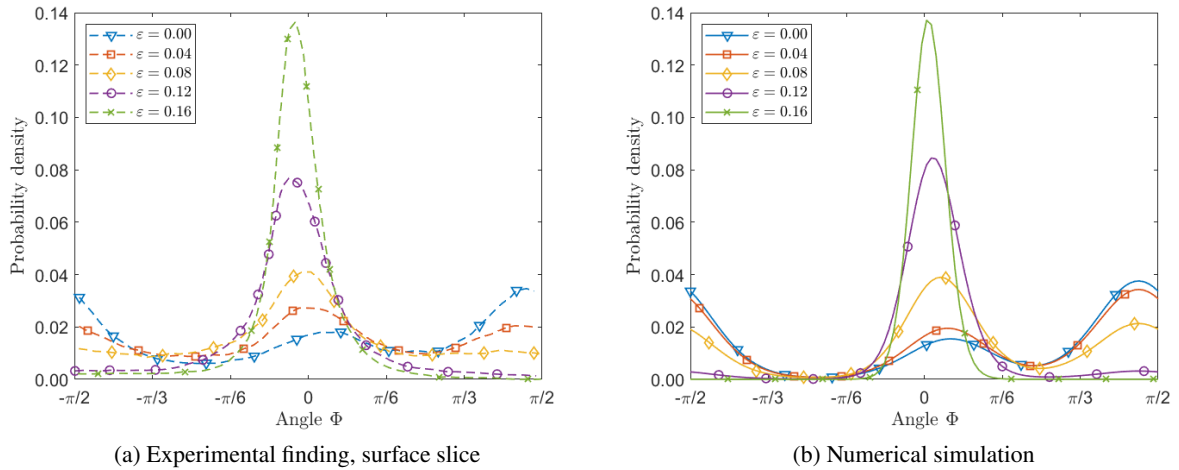


Figure 4: Comparison between the experimental findings of Mansfield et al. [109] (Figure 4a, adapted from “Figure 9b (ii)” [109]) and our numerically simulated curves for an imposed deformation $\varepsilon = 0.04n$, for $n = 0, 1, 2, 3, 4$ (Figure 4b). The experimental data points of Mansfield et al.[109] have been extracted from their “Figure 9b (ii)” by using the online software WebPlotDigitizer [114], and have been replotted vs radians (degrees are used in the original image) as shown in Figure 4a.

796 extent, in Figure 3a, could constitute a clue that there are cross-links between collagen fibers.

797 We remark that the hypothesis of transverse isotropy is not respected, since not only are the initial
 798 distributions of fibers nonuniform with respect to Φ , but, in addition, the subsequent mechanical action
 799 reorients the fibers significantly, even for moderate strains.

800 Finally, we observe that the fitting of the experimental curves returns very different numerical
 801 values for β and k_2 depending on the considered experiment (as indicated in Table 1, we take k_1 from
 802 the literature). This difference could be interpreted as a material heterogeneity of the cartilage under
 803 examination, or as a byproduct of a remodeling process that took place and altered irreversibly the
 804 mechanical behavior. In particular, from the fitting of Figure 3a we obtain $\beta = 2.71 \cdot 10^{-4} \text{ Pa}^{-1}$ and

805 $k_2 = 0.5$, while from the fitting of Figure 4a we obtain $\beta = 1.042 \cdot 10^{-4} \text{ Pa}^{-1}$ and $k_2 = 8$. We took
 806 the former values of β and k_2 as a reference for Table 1 since the initial distribution $\hat{f}_{\text{SR}}^{(1)}$ exhibits less
 807 deviation from a uniform distribution with respect to $\hat{f}_{\text{SR}}^{(2)}$.

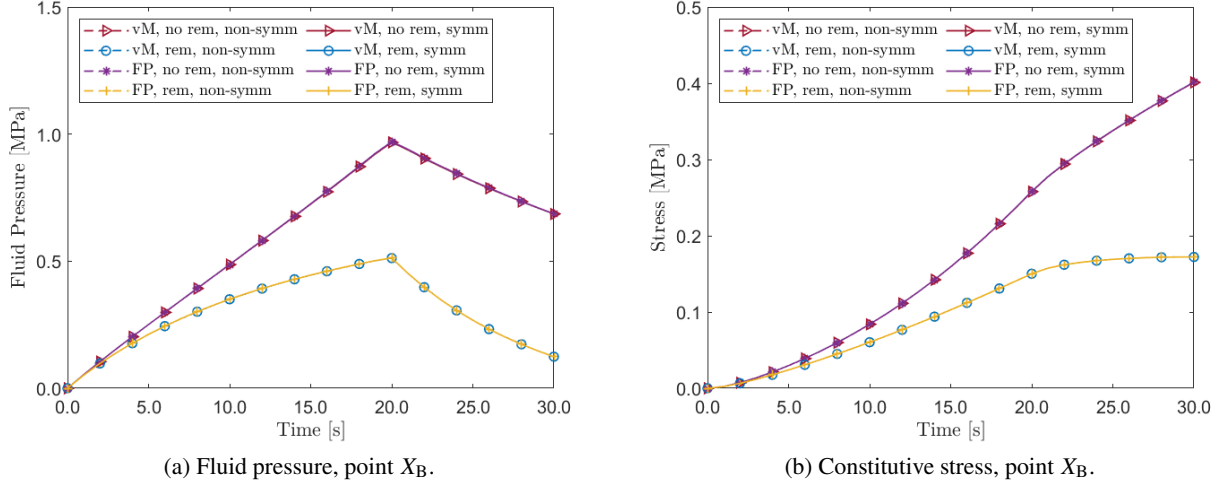


Figure 5: Comparison between the time evolution of pressure field (figure on the left) and of the constitutive normal stresses (figure on the right) under different remodeling processes, evaluated at the point X_B . The curves associated with the label “non-symm” refer to the simulations obtained with the initial probability density distribution given in Equation (71d), while the curves associated with the label “symm” adopt the symmetric probability density distribution discussed in the conclusions (cf. Equation (80)) as initial condition.

808 6.2 Compression of a cylindrical specimen

809 In this section, we report the results of the numerical simulations of the benchmark described in section
 810 5.2, and we discuss their possible physical interpretation. In particular, we address the relevance of the two
 811 types of remodeling considered in our work, i.e., the reorientation of the fibers and the isotropic structural
 812 reorganization of the matrix, in the characterization of the medium’s behavior under compressive loading.

813 We consider the following different simulations: (i) the one in which no remodeling is considered;
 814 (ii) the one in which both types of remodeling are present; (iii) and the two intermediate cases, with one
 815 active and the other switched off. To compare the data, we take measurements in three points of the
 816 specimen: one placed near the intersection between the upper surface and the lateral one, denominated
 817 X_U ; one placed at half of the height of the cylinder, near the symmetry axis, and denominated X_I ; the last
 818 one is placed in the center of the bottom surface, denominated X_B . For brevity, we refer to the anelastic
 819 distortions developed in the material as “remodeling” and we distinguish the case in which the anelastic
 820 distortions are deactivated (marked in the figures as “no remodeling”) from the one in which they are
 821 active (indicated by “remodeling”).

822 As expected, the fluid pressure and the overall constitutive stresses in X_B in direction E_3 (i.e., $[\mathbf{P}_s]_3^3$),
 823 shown in Figures 5a and 5b, respectively, are largely influenced by the onset of remodeling distortions,
 824 while the reorientation of the fibers does not alter significantly their values. In fact, since the fibers are
 825 aligned perpendicularly to the lower surface and, thus, are compressed by the loading, they do not provide
 826 any contribution, and the production of anelastic distortions is the dominant mechanism of remodeling.

827 Next, we examine the behavior of the porous medium at X_I and X_U , and we focus on the anisotropic
 828 contributions to stress and permeability. In particular, we want to relate the obtained values with the
 829 evolution at the mesoscale of the fibers’ probability density distributions. We remark that, since the
 830 points X_I and X_U have null X_1 -coordinate, they belong to the plane spanned by E_2 (oriented radially)

831 and E_3 (symmetry axis). Moreover, for this particular choice of coordinates the 22-components of
 832 \mathbf{K}_a and \mathbf{P}_{sa} evaluated at X_I and X_U are representative of the radial components of \mathbf{K}_a and \mathbf{P}_{sa} , since
 833 the problem describing this benchmark is axial-symmetric. As highlighted in Figures 6a and 6b, the
 834 reorientation of the fibers heavily impacts the anisotropic term in the hydraulic conductivity⁴, whereas the
 835 isotropic remodeling (i.e., the anelastic distortions) influences slightly less the anisotropic contribution
 836 to the hydraulic conductivity. Indeed, the increase or decrease in the hydraulic conductivity is due to the
 837 process of alignment of the fibers along the radial and circumferential directions, since the compression is
 838 unconfined and the solid matrix can spread radially and guide the fibers embedded in it. The reorientation
 839 of the fibers results in an increase of the radial permeability in the interior point X_I , whereas it results
 840 in a decrease of this quantity at X_U . However, since this quantity is already a correction to the isotropic
 841 hydraulic conductivity, it does not alter significantly the fluid efflux (data not shown).

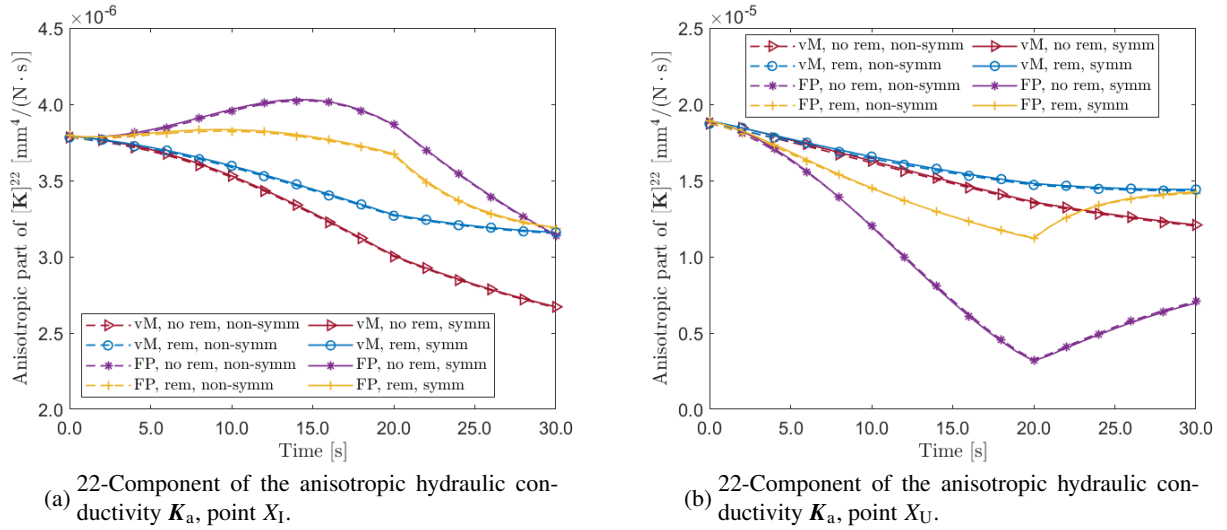
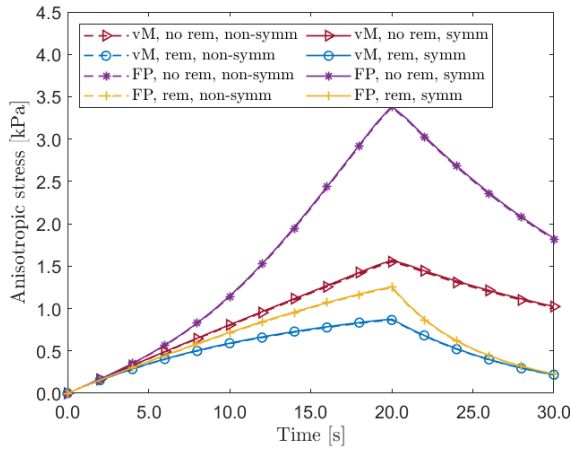


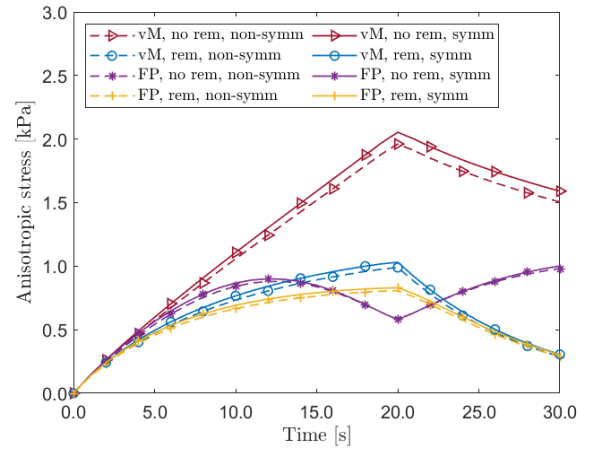
Figure 6: Comparison between the time evolution of the anisotropic contribution to the component $[\mathbf{K}_a]_{22}$ of the permeability tensor evaluated at the points X_I (figure on the left) and X_U (figure on the right). We remark that, at these points, the radial direction coincides with the Cartesian direction E_2 . The curves associated with the label “non-symm” refer to the simulations obtained with the initial probability density distribution given in Equation (71d), while the curves associated with the label “symm” adopt the symmetric probability density distribution discussed in the conclusions (cf. Equation (80)) as initial condition.

842 A much more nuanced situation appears when examining the 22-component of the anisotropic stress,
 843 which is shown in Figures 7a and 7b. We consider first the case in which the anelastic distortions are
 844 switched off. In this situation, the anisotropic stresses $[\mathbf{P}_{sa}]_{22}^2$ registered in X_I when the probability
 845 density distribution is the stationary solution of the Fokker–Planck equation, with the drift term featuring
 846 both Π and \mathcal{W}_{1a} , are higher than those obtained for the von Mises distribution, which considers only
 847 $\beta\Pi$ as drift term. This is because $[\mathbf{P}_{sa}]_{22}^2$, being a directional average, depends on the probability
 848 density distribution. This distribution, in turn, evolves in time under the guidance of \mathcal{W}_{1a} and deviates
 849 considerably from the von Mises distribution, taken as initial datum. In particular, the probability density
 850 distribution driven by \mathcal{W}_{1a} weighs the fibers in a way that depends on both angles Θ and Φ (see Figures 8a
 851 and 8b). Moreover, if no anelastic distortions are considered, the radial stress registered at X_I increases for
 852 $t \in [t_{in}, t_{ramp}[$ and decreases for $t > t_{ramp}$, i.e., when the imposed deformation is kept fixed. However, at
 853 X_U the value of the radial anisotropic contribution to the first Piola–Kirchhoff stress computed by solving

⁴When we speak of “hydraulic conductivity”, we mean here the ratio between the permeability of the medium, expressed in m², and the viscosity of the fluid, expressed in N·s/m². Note, however, that in the literature on porous media the wording “hydraulic conductivity” usually refers to the ratio $k\rho g/\mu$, where k is a constant referential value of permeability, ρ is the constant true density of water, and g the magnitude of the gravity acceleration vector.



(a) 22-Component of the anisotropic stress, point X_I .



(b) 22-Component of the anisotropic stress, point X_U .

Figure 7: Comparison between the time evolution of the 22-component of the anisotropic contribution of the first Piola–Kirchhoff stress tensor of the solid phase, evaluated at the points X_I (figure on the left) and X_U (figure on the right). At these points, the radial direction coincides with the Cartesian direction \mathbf{E}_2 . The curves associated with the label “non-symm” refer to the simulations obtained with the initial probability density distribution given in Equation (71d), while the curves associated with the label “symm” adopt the symmetric probability density distribution discussed in the conclusions (cf. Equation (80)) as initial condition.

854 the Fokker–Planck equation exhibits a different, non-monotonic behavior in $t \in [t_{in}, t_{ramp}]$. At first it
 855 increases, but it reaches the peak before the compressive ramp attains the maximum compression. The
 856 difference in the examined behaviors can be explained by looking at the evolution of the fiber probability
 857 density distributions (see in particular Figures 9a and 9b).

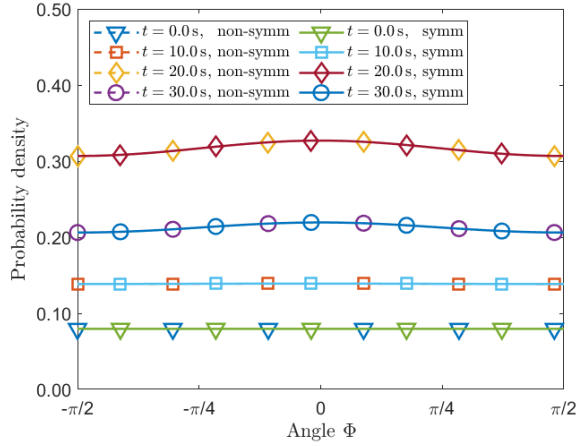
858 We report the evolution of the fiber probability density distributions at X_I in Figure 8, where Figures
 859 8a and 8b refer to the case of no anelastic distortions (“no remodeling”), and Figures 8c and 8d refer
 860 to the case in which anelastic distortions are switched on (“remodeling”). In Figure 9, we report the
 861 probability density distributions at X_U , with Figures 9a and 9b reporting the case of no remodeling, and
 862 Figures 9c and 9d the case in which remodeling is switched on.

863 In our model, in the absence of remodeling distortions, the fibers tend to align themselves along the
 864 direction of higher deformation. In X_I , the radial deformation, which coincides with the deformation along
 865 the Cartesian direction \mathbf{E}_2 , is lower than the circumferential deformation during the whole simulation.
 866 In fact, the probability density registered along the radial direction, individuated by $\Theta = \pi/2$ and
 867 $\Phi = \pm\pi/2$, increases with the application of the compressive ramp, i.e., up to 20 s (see e.g. Figure
 868 8a and 8b), which means that it is more likely to find fibers that have reoriented in parallel with the
 869 transversal plane and along the radial direction. However, at X_U , a similar trend takes place: the
 870 deformation along the circumferential direction is greater than the radial one, and the fibers tend to
 871 align in parallel with the transversal plane, but orthogonally to the radial deformation. Hence, at X_U the
 872 anisotropic contributions to permeability and to the stress computed by solving the stationary Fokker–
 873 Planck equation are lower than those computed with the von Mises distribution, since the fibers reorient
 874 mostly in the direction orthogonal to the radial displacement, which does not coincide with the direction
 875 of maximum deformation.

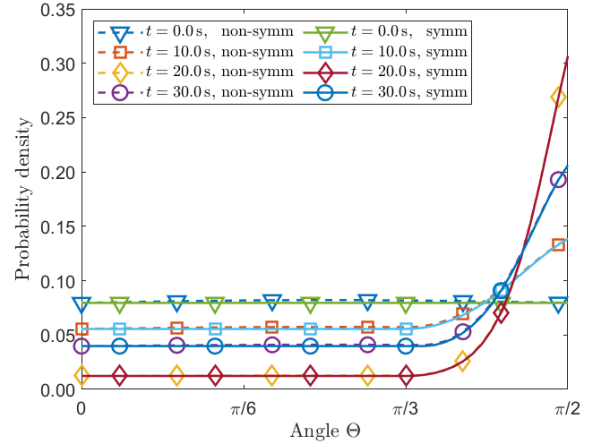
876 However, if the extracellular matrix undergoes isotropic remodeling, the radial anisotropic perme-
 877 abilities are lower in the case of no remodeling, as shown in Figure 6b, and, for the von Mises distribution,
 878 they decrease even after the compressive ramp reaches the maximum displacement, while, for the Fokker–
 879 Planck distribution, they increase for $t > t_{ramp}$. In fact, as can be seen in Figures 8c, 8d, 9c, and 9d,
 880 isotropic remodeling reduces the capacity of the fibers of reorienting for the considered benchmark,

881 thereby making them less susceptible to follow the mechanical stimuli.

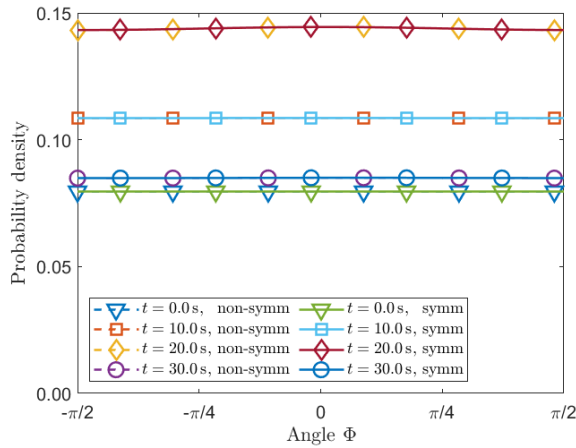
882 In our opinion, our results indicate that the anisotropic stresses and permeabilities predicted by our
 883 model should be viewed as phenomena related to two levels of descriptions. Indeed, the remodeling
 884 contributions associated with the reorientation of the fibers (resolved at the mesoscale through the Fokker–
 885 Planck equation) and those related to the anelastic distortions of the extracellular matrix (resolved at the
 886 scale of the tissue as a whole) affect significantly, but in different ways, the stress and the permeability
 887 distribution in the tissue.



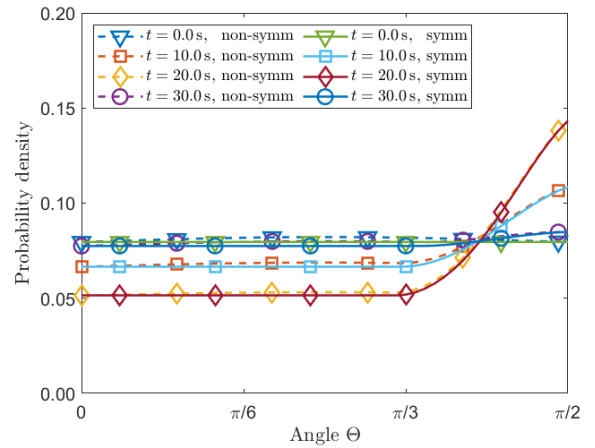
(a) Probability density distribution along Φ for $\Theta = \pi/2$, no remodeling, point X_1 .



(b) Probability density distribution along Θ for $\Phi = \pi/2$, no remodeling, point X_1 .



(c) Probability density distribution along Φ for $\Theta = \pi/2$, remodeling, point X_1 .



(d) Probability density distribution along Θ for $\Phi = \pi/2$, remodeling, point X_1 .

Figure 8: Comparison among fibers probability density distributions at the point X_1 (see Figure 2b for reference) obtained by solving the Fokker–Planck equation with the drift term $\beta[\Pi + \Phi_{1s}\mathcal{W}_{1a}]$. The curves associated with the label “non-symm” refer to the simulations obtained with the initial probability density distribution given in Equation (71d), while the curves associated with the label “symm” adopt the symmetric probability density distribution discussed in the conclusions (cf. Equation (80)) as initial condition.

888 7 Concluding remarks and future developments

889 In this work, we presented a model of a fiber-reinforced, soft, hydrated, biphasic porous medium under
 890 the explicit constraints of saturation, incompressibility of its constituents, and of shared kinematics

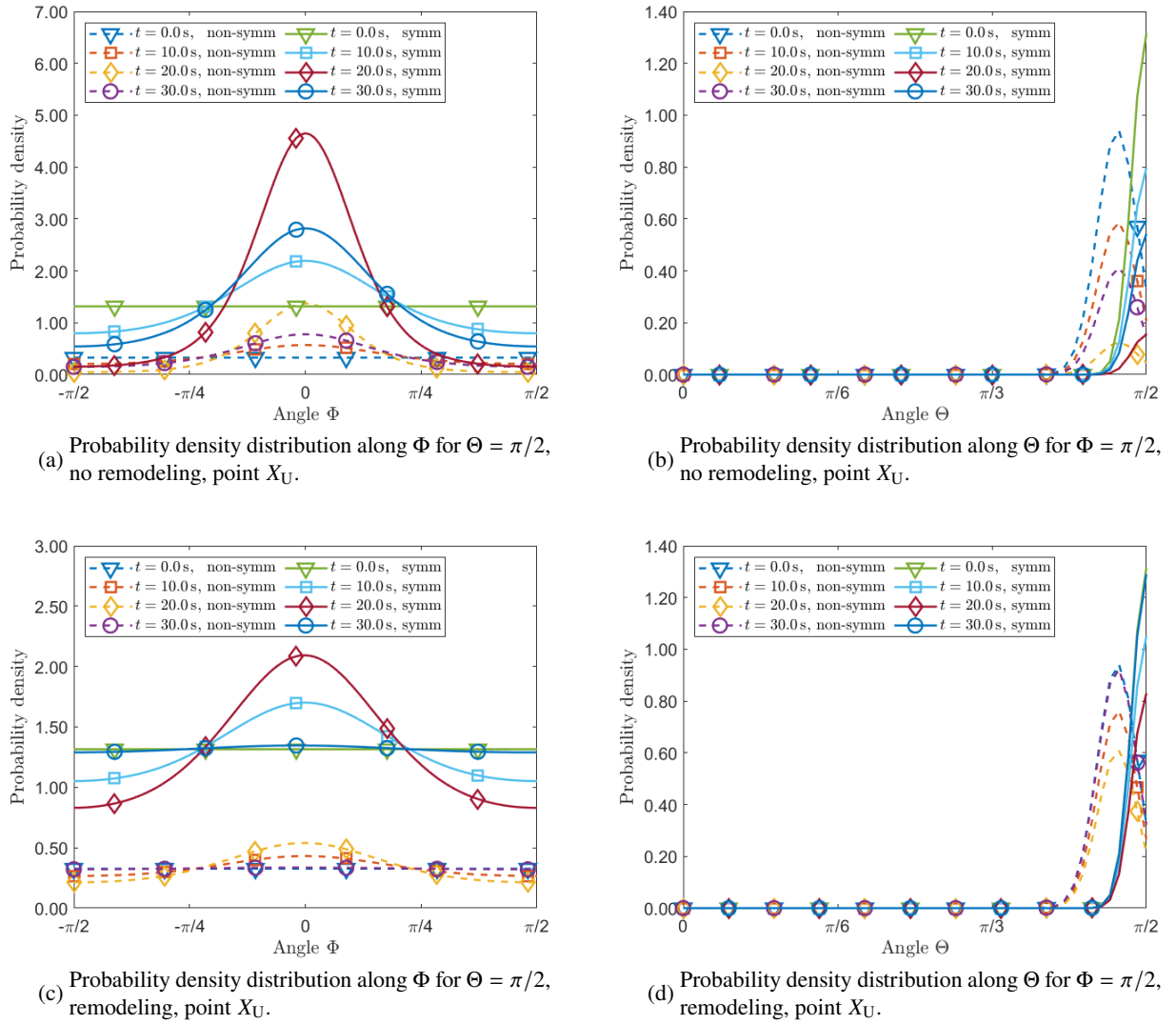


Figure 9: Comparison among fibers probability density distributions at the point X_U (see Figure 2b for reference) obtained by solving the Fokker-Planck equation with the drift term $\beta[\Pi + \Phi_{1s}\mathcal{W}_{1a}]$. The curves associated with the label “non-symm” refer to the simulations obtained with the initial probability density distribution given in Equation (71d), while the curves associated with the label “symm” adopt the symmetric probability density distribution discussed in the conclusions (cf. Equation (80)) as initial condition.

891 between extracellular matrix and fibers, whereas we considered the constraints of isochoric remodeling
892 and of incompressibility of the overall mixture through the Lagrange multiplier technique. In this regard,
893 we framed the model by recurring to the Principle of Virtual Power as used in [51, 52]. In addition,
894 the solid phase, which comprises both the isotropic extracellular matrix and the fibers, is subjected to
895 two processes of structural changes that, however, are modeled at different levels. In fact, we dealt with
896 two remodeling processes, both of configurational nature, one described at the scale of the tissue and
897 consisting of the production of anelastic distortions, while the other concerns the reorientation of the
898 fibers and is affected by interactions of statistical type that take place at the mesoscopic scale. While
899 both have been previously studied, e.g., in [32, 31, 61], the latter constitutes an enrichment of the
900 framework of fiber-reinforced, statistically oriented materials for two reasons. First, the remodeling of
901 the fibers, i.e., their reorientation, occurs through the evolution of their probability density distribution.
902 This constitutes a step forward with respect to the works by Grillo et al. [31] and Crevacore et al. [32],

903 in which the functional form of the probability density distribution was given once and for all, although
 904 it was parameterized by the evolution of the direction of the most probable orientation of the fibers. The
 905 second reason is that, the probability density distribution determined in the present work is shaped by the
 906 deformation occurring in the medium, thereby establishing a two-way-coupling between the deformation
 907 and the evolution of the fibers. Indeed, the deformation determines the anisotropic strain energy density
 908 $\hat{\mathcal{W}}_{1a}$, which, in turn, updates the probability density distribution \hat{f}_R (or \hat{f}_{SR}), which enters the directional
 909 averages of the macroscopic strain energy density itself and of the permeability.

910 We achieved the following results:

- 911 i) We derived a Fokker–Planck equation for the evolution of the probability density f_R associated
 912 with the Langevin-like process of the reorientation of the fibers, and we obtained the von Mises
 913 distribution as a particular case of stationary solution. We expanded the framework of Crevacore et
 914 al. [32] by introducing a target probability density distribution associated with a potential Π and,
 915 when specializing our model to articular cartilage, we formulated Π in order to identify the target
 916 probability density distribution in the absence of deformation with the one capable of recovering
 917 the histological pattern of the fibers.
- 918 ii) We characterized the mesoscopic properties of articular cartilage by fitting experimental curves,
 919 and we analyzed the uni-axial compression test of a hypothetical tissue undergoing remodeling
 920 with properties borrowed from articular cartilage. Our model predicts correctly the experimental
 921 curves showing the angular distribution of the collagen fibers under mechanical deformation in
 922 a slice of articular cartilage [109]. Moreover, the simulations of the uni-axial compression test
 923 showed that the two remodeling processes have a different influence on the evolution of the system
 924 under study: the anelastic distortions affect considerably the evolution of the overall stress fields,
 925 but the fiber reorientation alters significantly the anisotropic part of the permeability and stress
 926 tensors. These results are coherent with the ones of Tomic et al. [29] In particular, the magnitude
 927 of the remodeling contributions are comparable for the radial anisotropic stresses, even though the
 928 two processes are concerned with two different levels of description.

929 The results commented above emphasize how the introduction of Langevin-like processes to describe
 930 fiber reorientation could open many possibilities in a scientific scenario that has been widely investigated
 931 by researchers in the last decades. Since the aim of this work is to introduce a framework that combines
 932 configurational and statistical mechanics, based on the idea put forward in [6], we did not carry out a
 933 comparison between our results and the ones obtained with the models already present in the literature.
 934 However, a comprehensive review of the literature is well within our sight, and we believe that it would
 935 be of great benefit to the researchers that are active in the fields of fiber-reinforced media.

936 Moreover, there are three directions that we plan to explore in future works:

- 937 i) Modifying the constitutive framework adopted in this work to take into account more complex
 938 forms of self interactions or the formation of cross-links among the fibers;
- 939 ii) Studying the evolution of the material properties if the tissue due to the anelastic distortions is no
 940 more deemed to be isotropic, but follows an anisotropic evolutionary law.
- 941 iii) Modifying the probability density distribution by prescribing the potential $\hat{\Pi}$ to be

$$\begin{aligned}
 \hat{\Pi}(\Theta; \Theta_{hi}, \omega) &:= \frac{\Pi_c}{\omega^2} \{ [\cos(\Theta - \Theta_{hi})]^2 + [\cos(\Theta - (\pi - \Theta_{hi}))]^2 \} \\
 &= \frac{\Pi_c}{\omega^2} \{ [\cos(\Theta - \Theta_{hi})]^2 + [\cos(\Theta + \Theta_{hi})]^2 \} \\
 &= \frac{2\Pi_c [\sin \Theta_{hi}]^2}{\omega^2} + \frac{2\Pi_c \cos(2\Theta_{hi})}{\omega^2} [\cos \Theta]^2,
 \end{aligned} \tag{76}$$

942 with $\Theta_{hi} \in [0, \pi/2]$, and, thus, $\cos(2\Theta_{hi}) \in [-1, 1]$. This, indeed, introduces the symmetry
 943 $\hat{f}_R(\Theta, \Phi) = \hat{f}_R(\pi - \Theta, \Phi)$, for all $\Phi \in [0, 2\pi]$. However, since the first summand on the right-hand

944
945
946

side of Equation (76) is independent of Θ and Φ , it does not contribute to the calculation of the normalizing factor associated with the probability density distribution generated by $\hat{\Pi}$. Thus, we can focus on the *effective potential*

$$\hat{\Pi}_{\text{eff}}(\Theta; \Theta_{\text{hi}}, \omega) := \frac{2\Pi_c \cos(2\Theta_{\text{hi}})}{\omega^2} [\cos \Theta]^2. \quad (77)$$

947
948

In this case, by recalling the presence of the factor $\beta = (D\gamma)^{-1} > 0$ stemming from the Fokker–Planck Equation (40), we introduce the parameter

$$b_{\text{hi}} := \frac{\beta\Pi_c \cos(2\Theta_{\text{hi}})}{\omega^2}, \quad (78)$$

949
950
951
952

which can be positive, null, or negative, depending on the values taken by $\cos(2\Theta_{\text{hi}})$. To account for this variability in view of the calculation of the von Mises probability density distribution generated by $\hat{\Pi}_{\text{eff}}$, which requires the determination of the square root of b_{hi} (to be understood in complex sense, when $b_{\text{hi}} < 0$), we formally rewrite b_{hi} as the complex number

$$\mathfrak{b}_{\text{hi}} = |b_{\text{hi}}| \exp\left(i\pi \frac{1 - \text{sign}(b_{\text{hi}})}{2}\right), \quad \text{with } |b_{\text{hi}}| = \frac{\beta\Pi_c |\cos(2\Theta_{\text{hi}})|}{\omega^2}, \quad (79)$$

953
954

where $\text{sign}(\cdot)$ is the sign function ($\text{sign}(\kappa) = \pm 1$ for $\kappa \gtrless 0$, and $\text{sign}(0) = 0$). Thus, we write the probability density distribution as

$$\hat{f}_{\text{SVM}}(\Theta; \Theta_{\text{hi}}, \omega) = \begin{cases} \frac{1}{\mathcal{Z}_0} \exp(2b_{\text{hi}} [\cos \Theta]^2), & \text{for } b_{\text{hi}} \neq 0, \\ \frac{1}{4\pi}, & \text{for } b_{\text{hi}} = 0 \ (\Rightarrow \Theta_{\text{hi}} = \pi/4), \end{cases} \quad (80)$$

955

and the normalization factor \mathcal{Z}_0 can be computed by direct integration and is equal to

$$\mathcal{Z}_0 = \frac{2\pi\sqrt{\pi}}{\sqrt{2\mathfrak{b}_{\text{hi}}}} \text{erfi}(\sqrt{2\mathfrak{b}_{\text{hi}}}) = \begin{cases} \frac{2\pi\sqrt{\pi}}{\sqrt{2b_{\text{hi}}}} \text{erfi}(\sqrt{2b_{\text{hi}}}), & b_{\text{hi}} > 0 \ (\Rightarrow \Theta_{\text{hi}} \in [0, \pi/4[), \\ \frac{2\pi\sqrt{\pi}}{\sqrt{2|b_{\text{hi}}|}} \text{erf}(\sqrt{2|b_{\text{hi}}|}), & b_{\text{hi}} < 0 \ (\Rightarrow \Theta_{\text{hi}} \in]\pi/4, \pi/2]). \end{cases} \quad (81)$$

956

with $\lim_{b_{\text{hi}} \rightarrow 0} \mathcal{Z}_0 = \lim_{\Theta_{\text{hi}} \rightarrow \pi/4} \mathcal{Z}_0 = 4\pi$.

957
958

With the aid of Equations (80) and (81), the models referred to as “Model A” and “Model B” by Federico and Gasser [27] are condensed in one model, parameterized by Θ_{hi} .

959

Conflict of Interests

960

The Authors declare that they have no conflict of interests.

961

Authors’ contributions

962

All authors have equally contributed to this work.

963

Acknowledgment

964
965

We thank Dr. Marco Coco and Dr. Salvatore Di Stefano for various fruitful discussions in the preliminary stages of this work. A. Grillo is partially supported by MIUR (Italian Ministry of Education,

966 University and Research) through the PRIN project n. 2017KL4EF3 on “*Mathematics of active materi-*
967 *als: From mechanobiology to smart devices*”, the PRIN project n. 2020F3NCPX on “*Mathematics for*
968 *industry 4.0 (Math4I4)*”. A. Grillo’s research group is funded by the European Union - Next Generation
969 EU. A. Grillo, A. Giammarini and A. Pastore have been supported by the Research Project Prin2022
970 PNRR of National Relevance P2022KHFNB on “*Innovative multiscale approaches, possibly based on*
971 *Fractional Calculus, for the effective constitutive modeling of cell mechanics, engineered tissues, and*
972 *metamaterials in Biomedicine and related fields*” granted by the Italian MUR. This study was carried out
973 within the MICS (Made in Italy – Circular and Sustainable) Extended Partnership and A. Giammarini
974 received funding from the European Union Next-GenerationEU (PIANO NAZIONALE DI RIPRESA E
975 RESILIENZA (PNRR) – MISSIONE 4 COMPONENTE 2, INVESTIMENTO 1.3 – D.D. 1551.11-10-
976 2022, PE00000004). This manuscript reflects only the authors’ views and opinions, neither the European
977 Union nor the European Commission can be considered responsible for them.

978 **References**

- 979 [1] Gunda S, Natarajan S and Barrera O. On the fractional transversely isotropic functionally graded
980 nature of soft biological tissues: Application to the meniscal tissue. *Journal of the Mechanical*
981 *Behavior of Biomedical Materials* 2023; 143: 105855.
- 982 [2] Ateshian G. On the theory of reactive mixtures for modeling biological growth. *Biomechanics*
983 *and Modeling in Mechanobiology* 2007; 6(6): 423–445. DOI:10.1007/s10237-006-0070-x.
- 984 [3] Holmes M and Mow V. The nonlinear characteristics of soft gels and hydrated connective tissues
985 in ultrafiltration. *Journal of biomechanics* 1990; 23: 1145–1156. DOI:10.1016/0021-9290(90)
986 90007-P.
- 987 [4] Loret B and Simões F. A framework for deformation, generalized diffusion, mass transfer and
988 growth in multi-species multi-phase biological tissues. *Eur J Mech A* 2005; 24: 757–781. DOI:
989 10.1016/j.euromechsol.2005.05.005.
- 990 [5] Ambrosi D, Preziosi L and Vitale G. The insight of mixtures theory for growth and remodeling.
991 *Z Angew Math Phys* 2010; 61: 177–191. DOI:10.1007/s00033-009-0037-8.
- 992 [6] Grillo A, Federico S and Wittum G. Growth, mass transfer, and remodeling in fiber-reinforced,
993 multi-constituent materials. *Int J Nonlinear Mech* 2012; 47: 388–401. DOI:10.1016/j.ijnonlinmec.
994 2011.09.026.
- 995 [7] Ateshian G and Weiss J. Anisotropic hydraulic permeability under finite deformation. *J Biomech*
996 *Engng* 2010; 132: 111004–1–111004–7. DOI:10.1115/1.4002588.
- 997 [8] Holzapfel G, Gasser T and Ogden R. A new constitutive framework for arterial wall mechanics
998 and a comparative study of material models. *J Elast* 2000; 61(1-3): 1–48.
- 999 [9] Pandolfi A and Manganiello F. A model for the human cornea: constitutive formulation and
1000 numerical analysis. *Biomechanics and Modeling in Mechanobiology* 2006; 5(4): 237–246. DOI:
1001 10.1007/s10237-005-0014-x.
- 1002 [10] Pandolfi A and Holzapfel GA. Three-dimensional modeling and computational analysis of the
1003 human cornea considering distributed collagen fibril orientations. *Journal of Biomechanical*
1004 *Engineering* 2008; 130(6). DOI:10.1115/1.2982251.
- 1005 [11] Gentleman E, Lay AN, Dickerson DA et al. Mechanical characterization of collagen fibers
1006 and scaffolds for tissue engineering. *Biomaterials* 2003; 24(21): 3805–3813. DOI:10.1016/
1007 s0142-9612(03)00206-0.

- 1008 [12] Merodio J and Ogden R. Mechanical response of fiber-reinforced incompressible non-linearly
1009 elastic solids. *Int J Nonlinear Mech* 2005; 40(2-3): 213–227. DOI:10.1016/j.ijnonlinmec.2004.
1010 05.003.
- 1011 [13] Gasser T, Ogden R and Holzapfel G. Hyperelastic modelling of arterial layers with distributed
1012 collagen fibre orientations. *J R Soc Interface* 2006; 3: 15–35. DOI:10.1098/rsif.2005.0073.
- 1013 [14] Federico S, Grillo A, La Rosa G et al. A transversely isotropic, transversely homogeneous
1014 microstructural-statistical model of articular cartilage. *J Biomech* 2005; 38: 2008–2018. DOI:
1015 10.1016/j.jbiomech.2004.09.020.
- 1016 [15] deBotton G, Hariton I and Socolsky E. Neo-hookean fiber-reinforced composites in finite elasticity.
1017 *Journal of the Mechanics and Physics of Solids* 2006; 54(3): 533–559. DOI:10.1016/j.jmps.2005.
1018 10.001.
- 1019 [16] Spencer A and Soldatos K. Finite deformations of fibre-reinforced elastic solids with fibre
1020 bending stiffness. *International Journal of Non-Linear Mechanics* 2007; 42(2): 355–368. DOI:
1021 10.1016/j.ijnonlinmec.2007.02.015.
- 1022 [17] Hariton I, deBotton G, Gasser T et al. Stress-driven collagen fiber remodeling in arterial walls.
1023 *Biomech Model Mechanobiol* 2007; 6(3): 163–175. DOI:10.1007/s10237-006-0049-7.
- 1024 [18] Holzapfel GA and Ogden RW. Constitutive modelling of arteries. *Proceedings of the Royal*
1025 *Society A: Mathematical, Physical and Engineering Sciences* 2010; 466(2118): 1551–1597.
1026 DOI:10.1098/rspa.2010.0058.
- 1027 [19] Holzapfel GA, Niestrawska JA, Ogden RW et al. Modelling non-symmetric collagen fibre dis-
1028 persion in arterial walls. *Journal of The Royal Society Interface* 2015; 12(106): 20150188.
1029 DOI:10.1098/rsif.2015.0188.
- 1030 [20] Holzapfel G and Ogden R. On fiber dispersion models: Exclusion of compressed fibers and
1031 spurious model comparisons. *J Elast* 2017; 129(1-2): 49–68. DOI:10.1007/s10659-016-9605-2.
- 1032 [21] Melnik A, HB Da Rocha and Goriely A. On the modeling of fiber dispersion in fiber-reinforced
1033 elastic materials. *Int J Nonlinear Mech* 2015; 75: 92–106. DOI:http://dx.doi.org/10.1016/j.
1034 ijnonlinmec.2014.10.006.
- 1035 [22] Itskov M and Aksel N. A class of orthotropic and transversely isotropic hyperelastic constitu-
1036 tive models based on a polyconvex strain energy function. *International Journal of Solids and*
1037 *Structures* 2004; 41(14): 3833–3848. DOI:10.1016/j.ijsolstr.2004.02.027.
- 1038 [23] Nolan D, Gower A, Destrade M et al. A robust anisotropic hyperelastic formulation for the
1039 modelling of soft tissue. *Journal of the Mechanical Behavior of Biomedical Materials* 2014; 39:
1040 48–60. DOI:10.1016/j.jmbbm.2014.06.016.
- 1041 [24] Lanir Y. Constitutive equations for fibrous connective tissues. *J Biomech* 1983; 16: 1–12.
- 1042 [25] Federico S and Herzog W. On the anisotropy and inhomogeneity of permeability in articular
1043 cartilage. *Biomech Model Mechanobiol* 2008; 7: 367–378. DOI:10.1007/s10237-007-0091-0.
- 1044 [26] Federico S and Herzog W. Towards an analytical model of soft biological tissues. *J Biomech*
1045 2008; 41: 3309–3313. DOI:https://doi.org/10.1016/j.jbiomech.2008.05.039.
- 1046 [27] Federico S and Gasser T. Non-linear elasticity of biological tissues with statistical fibre orientation.
1047 *J R Soc Interface* 2010; 7: 955–966. DOI:10.1098/rsif.2009.0502.
- 1048 [28] Federico S and Grillo A. Elasticity and permeability of porous fibre-reinforced materials under
1049 large deformations. *Mech Mater* 2012; 44: 58–71. DOI:10.1016/j.mechmat.2011.07.010.

- 1050 [29] Tomic A, Grillo A and Federico S. Poroelastic materials reinforced by statistically oriented fibres
1051 — numerical implementation and application to articular cartilage. *IMA J Appl Math* 2014; 79:
1052 1027–1059. DOI:10.1093/imamat/hxu039.
- 1053 [30] Gizzi A, Pandolfi A and Vasta M. A generalized statistical approach for modeling fiber-
1054 reinforced materials. *Journal of Engineering Mathematics* 2017; 109(1): 211–226. DOI:
1055 10.1007/s10665-017-9943-5.
- 1056 [31] Grillo A, Carfagna M and Federico S. An Allen-Cahn approach to the remodelling of
1057 fibre-reinforced anisotropic materials. *J Eng Math* 2018; 109(1): 139–172. DOI:10.1007/
1058 s10665-017-9940-8.
- 1059 [32] Crevacore E, Di Stefano S and Grillo A. Coupling among deformation, fluid flow, structural
1060 reorganisation and fibre reorientation in fibre-reinforced, transversely isotropic biological tissues.
1061 *International Journal of Nonlinear Mechanics* 2019; 111: 1–13. DOI:https://doi.org/10.1016/j.
1062 ijnonlinmec.2018.08.022.
- 1063 [33] Maleki M, Hashlamoun K, Herzog W et al. Effect of structural distortions on articular cartilage
1064 permeability under large deformations. *Biomechanics and Modeling in Mechanobiology* 2019;
1065 19(1): 317–334. DOI:10.1007/s10237-019-01213-6.
- 1066 [34] Vasta M, Gizzi A and Pandolfi A. On three- and two-dimensional fiber distributed models of
1067 biological tissues. *Probabilist Eng Mech* 2014; 37: 170–179. DOI:http://dx.doi.org/10.1016/j.
1068 probengmech.2014.05.003.
- 1069 [35] Holzapfel G, Ogden R and Sherifova S. On fibre dispersion modelling of soft biological tissues:
1070 a review. *Proc R Soc A* 2019; 475(2224): 1–22. DOI:https://doi.org/10.1098/rspa.2018.0736.
- 1071 [36] Quinn T, Dierickx P and Grodzinsky A. Glycosaminoglycan network geometry may contribute
1072 to anisotropic hydraulic permeability in cartilage under compression. *Journal of Biomechanics*
1073 2001; 34(11): 1483–1490. DOI:10.1016/s0021-9290(01)00103-8.
- 1074 [37] Pierce DM, Ricken T and Holzapfel GA. A hyperelastic biphasic fibre-reinforced model of articular
1075 cartilage considering distributed collagen fibre orientations: continuum basis, computational
1076 aspects and applications. *Computer Methods in Biomechanics and Biomedical Engineering* 2013;
1077 16(12): 1344–1361. DOI:10.1080/10255842.2012.670854.
- 1078 [38] Hashlamoun K, Grillo A and Federico S. Efficient evaluation of the material response of tissues
1079 reinforced by statistically oriented fibres. *Z Angew Math Phys* 2016; 67: 113–145. DOI:10.1007/
1080 s10237-006-0049-7.
- 1081 [39] MAROUDAS A and BULLOUGH P. Permeability of articular cartilage. *Nature* 1968; 219(5160):
1082 1260–1261. DOI:10.1038/2191260a0.
- 1083 [40] Epstein M and Maugin G. Thermomechanics of volumetric growth in uniform bodies. *Interna-
1084 tional Journal of Plasticity* 2000; 16(7-8): 951–978. DOI:10.1016/s0749-6419(99)00081-9.
- 1085 [41] Garikipati K, Arruda E, Grosh K et al. A continuum treatment of growth in biological tissue:
1086 the coupling of mass transport and mechanics. *J Mech Phys Solids* 2004; 52: 1595–1625.
1087 DOI:10.1016/j.jmps.2004.01.004.
- 1088 [42] Wilson W, Driessen N, CC van Donkelaar et al. Prediction of collagen orientation in articular
1089 cartilage by a collagen remodeling algorithm. *Osteoarthr Cartil* 2006; 14: 1196–1202. DOI:
1090 10.1016/j.joca.2006.05.006.
- 1091 [43] Ambrosi D, Ateshian G, Arruda E et al. Perspectives on biological growth and remodeling. *Journal
1092 of the Mechanics and Physics of Solids* 2011; 59(4): 863–883. DOI:10.1016/j.jmps.2010.12.011.

- 1093 [44] Lin WJ, Iafrati MD, Peattie RA et al. Growth and remodeling with application to abdominal
1094 aortic aneurysms. *Journal of Engineering Mathematics* 2017; 109(1): 113–137. DOI:10.1007/
1095 s10665-017-9915-9.
- 1096 [45] Soldatos KP. Foundation of polar linear elasticity for fibre-reinforced materials. *Journal of*
1097 *Elasticity* 2013; 114(2): 155–178. DOI:10.1007/s10659-013-9433-6.
- 1098 [46] Soldatos KP, Shariff MHBM and Merodio J. On the constitution of polar fiber-reinforced materials.
1099 *Mechanics of Advanced Materials and Structures* 2020; 28(21): 2255–2266. DOI:10.1080/
1100 15376494.2020.1729449.
- 1101 [47] Driessen N, Wilson W, Bouten C et al. A computational model for collagen fibre remodelling in
1102 the arterial wall. *J Theor Biol* 2004; 226: 53–64. DOI:10.1016/j.jtbi.2003.08.004.
- 1103 [48] Menzel A. Modelling of anisotropic growth in biological tissues — a new approach and
1104 computational aspects. *Biomechan Model Mechanobiol* 2005; 3: 147–171. DOI:10.1007/
1105 s10237-004-0047-6.
- 1106 [49] Menzel A. A fibre reorientation model for orthotropic multiplicative growth, configurational
1107 driving stresses, kinematics-based reorientation and algorithmic aspects. *Biomechan Model*
1108 *Mechanobiol* 2007; 6(5): 303–320. DOI:10.1007/s10237-006-0061-y.
- 1109 [50] Gizzi A, Cyron CJ, Falcinelli C et al. Evolution of fiber distributions in homogenized constrained
1110 mixture models of soft tissue growth and remodeling: Uniaxial loading. *Journal of the Mechanics*
1111 *and Physics of Solids* 2024; 183: 105491. DOI:10.1016/j.jmps.2023.105491.
- 1112 [51] Grillo A and Di Stefano S. A formulation of volumetric growth as a mechanical problem subjected
1113 to non-holonomic and rheonomic constraint. *Mathematics and Mechanics of Solids* 2023; : 1–
1114 10 DOI:10.1177/10812865231152228.
- 1115 [52] Grillo A and Di Stefano S. Addendum to “a formulation of volumetric growth as a mechanical
1116 problem subjected to non-holonomic and rheonomic constraint”. *Mathematics and Mechanics of*
1117 *Solids* 2023; 29(1): 62–70. DOI:10.1177/10812865231178291.
- 1118 [53] Martins J, Pires E, Salvado R et al. A numerical model of passive and active behavior of skeletal
1119 muscles. *Computer Methods in Applied Mechanics and Engineering* 1998; 151(3–4): 419–433.
1120 DOI:10.1016/s0045-7825(97)00162-x.
- 1121 [54] Blemker SS, Pinsky PM and Delp SL. A 3d model of muscle reveals the causes of nonuniform
1122 strains in the biceps brachii. *Journal of Biomechanics* 2005; 38(4): 657–665. DOI:10.1016/j.
1123 jbiomech.2004.04.009.
- 1124 [55] Giamberini G, Muscati A and Riccobelli D. A comparison between active strain and active stress
1125 in transversely isotropic hyperelastic materials. *Journal of Elasticity* 2018; 137(1): 63–82. DOI:
1126 10.1007/s10659-018-9708-z.
- 1127 [56] Olsson T and Klarbring A. Residual stresses in soft tissue as a consequence of growth and
1128 remodeling: application to an arterial geometry. *Eur J Mech A* 2008; 27(6): 959–974. DOI:
1129 10.1016/j.euromechsol.2007.12.006.
- 1130 [57] Wilson W, Huyghe J and CC van Donkelaar. A composition-based cartilage model for the
1131 assessment of compositional changes during cartilage damage and adaptation. *Osteoarthr Cartil*
1132 2006; 14: 554–560. DOI:10.1016/j.joca.2005.12.006.
- 1133 [58] Pierce DM, Ricken T and Holzapfel GA. A hyperelastic biphasic fibre-reinforced model of articular
1134 cartilage considering distributed collagen fibre orientations: continuum basis, computational
1135 aspects and applications. *Computer Methods in Biomechanics and Biomedical Engineering* 2013;
1136 16(12): 1344–1361. DOI:10.1080/10255842.2012.670854.

- 1137 [59] Li K, Ogden R and Holzapfel G. Computational method for excluding fibers under compression
1138 in modeling soft fibrous solids. *Eur J Mech A/Solids* 2016; 57: 178–193. DOI:10.1016/j.
1139 euromechsol.2015.11.003.
- 1140 [60] Garcia D, Zysset P, Charlebois M et al. A three-dimensional elastic plastic damage con-
1141 stitutive law for bone tissue. *Biomech Model Mechanobiol* 2009; 8(2): 149–165. DOI:
1142 10.1007/s10237-008-0125-2.
- 1143 [61] Di Stefano S, Carfagna M, Knodel MM et al. Anelastic reorganisation of fibre-reinforced
1144 biological tissues. *Computing and Visualization in Science* 2019; 20(3-6): 95–109. DOI:
1145 10.1007/s00791-019-00313-1.
- 1146 [62] Mićunović M. *Thermomechanics of Viscoplasticity*. Springer New York, 2009. DOI:10.1007/
1147 978-0-387-89490-4.
- 1148 [63] DiCarlo A and Quiligotti S. Growth and balance. *Mechanics Research Communications* 2002;
1149 29(6): 449–456. DOI:10.1016/s0093-6413(02)00297-5.
- 1150 [64] Di Stefano S, Ramírez-Torres A, Penta R et al. Self-influenced growth through evolving material
1151 inhomogeneities. *International Journal of Non-Linear Mechanics* 2018; 106: 174–187. DOI:
1152 10.1016/j.ijnonlinmec.2018.08.003.
- 1153 [65] Ciancio V, Dolfin M, Francaviglia M et al. Uniform materials and the multiplicative decomposition
1154 of the deformation gradient in finite elasto-plasticity. *J Non-Equilib Thermodyn* 2008; 33(3): 199–
1155 234. DOI:10.1515/JNETDY.2008.009.
- 1156 [66] Marsden J and Hughes T. *Mathematical Foundations of Elasticity*. Dover Publications, Inc.,
1157 Mineola, New York, 1983.
- 1158 [67] Quiligotti S, Maugin G and F dell’Isola. An eshelbian approach to the nonlinear mechanics of
1159 constrained solid-fluid mixtures. *Acta Mech* 2003; 160: 45–60. DOI:10.1007/s00707-002-0968-z.
- 1160 [68] Cermelli P, Fried E and Sellers S. Configurational stress, yield and flow in rate-independent
1161 plasticity. *Proc R Soc Lond A* 2001; 457: 1447–1467. DOI:10.1098/rspa.2001.0786.
- 1162 [69] Giorgio I, dell’Isola F, Andreus U et al. An orthotropic continuum model with substructure
1163 evolution for describing bone remodeling: an interpretation of the primary mechanism behind
1164 wolff’s law. *Biomechanics and Modeling in Mechanobiology* 2023; 22(6): 2135–2152. DOI:
1165 10.1007/s10237-023-01755-w.
- 1166 [70] Gantmacher F. *Lectures in Analytical Mechanics*. MIR Publishers, 1975.
- 1167 [71] Llibre J, Ramírez R and Sadovskaia N. Nonlinear dynamics. *A new approach to the vakonomic*
1168 *mechanics* 2014; 78: 2219–2247. DOI:10.1007/s11071-014-1554-3.
- 1169 [72] Pars L. *A treatise on Analytical Dynamics*. Heinemann, London, 1965.
- 1170 [73] Hassanizadeh SM. Derivation of basic equations of mass transport in porous media, part 1.
1171 macroscopic balance laws. *Advances in Water Resources* 1986; 9(4): 196–206. DOI:10.1016/
1172 0309-1708(86)90024-2.
- 1173 [74] Hassanizadeh S. Derivation of basic equations of mass transp. porous med., part 2. generalized
1174 Darcy’s and Fick’s laws. *Adv Water Resour* 1986; 9: 207–222.
- 1175 [75] Bear J and Bachmat Y. *Introduction to Modeling of Transport Phenomena in Porous Media*.
1176 Kluwer, Dordrecht, 1990.

- 1177 [76] Bennethum L, Murad M and Cushman J. Macroscale thermodynamics and the chemical potential
1178 for swelling porous media. *Transport in Porous Media* 2000; 39(2): 187–225. DOI:10.1023/a:
1179 1006661330427.
- 1180 [77] Ateshian G and Humphrey J. Continuum mixture models of biological growth and remodeling:
1181 Past successes and future opportunities. *Annual Review of Biomedical Engineering* 2012; 14(1):
1182 97–111. DOI:10.1146/annurev-bioeng-071910-124726.
- 1183 [78] Holzapfel GA and Ogden RW. An arterial constitutive model accounting for collagen content
1184 and cross-linking. *Journal of the Mechanics and Physics of Solids* 2020; 136: 103682. DOI:
1185 10.1016/j.jmps.2019.103682.
- 1186 [79] Moo EK, Tanska P, Federico S et al. Collagen fibres determine the crack morphology in articular
1187 cartilage. *Acta Biomaterialia* 2021; 126: 301–314. DOI:10.1016/j.actbio.2021.03.031.
- 1188 [80] Maugin GA and Metrikine AV. *Mechanics of Generalized Continua: One Hundred Years After the*
1189 *Cosserats*. Springer New York, 2010. ISBN 9781441956958. DOI:10.1007/978-1-4419-5695-8.
- 1190 [81] Baaijens F, Bouten C and Driessen N. Modeling cartilage remodeling. *J Biomech* 2010; 43:
1191 166–175. DOI:10.1016/j.jbiomech.2009.09.022.
- 1192 [82] Grillo A, Wittum G, Tomic A et al. Remodelling in statistically oriented fibre-reinforced
1193 materials and biological tissues. *Math Mech Solids* 2015; 20(9): 1107–1129. DOI:
1194 10.1177/1081286513515265.
- 1195 [83] Loy N and Preziosi L. A statistical mechanics approach to describe cell reorientation under stretch.
1196 *Bulletin of Mathematical Biology* 2023; 85(7). DOI:10.1007/s11538-023-01161-4.
- 1197 [84] Federico S and Herzog W. On the permeability of fibre-reinforced porous materials. *Int J Solids*
1198 *Struct* 2008; 45: 2160–2172. DOI:https://doi.org/10.1016/j.ijsolstr.2007.11.014.
- 1199 [85] Federico S and Grillo A. *Linear Elastic Composites with Statistically Oriented Spheroidal In-*
1200 *clusions*. Springer International Publishing. ISBN 9783319527949, 2017. pp. 307–346. DOI:
1201 10.1007/978-3-319-52794-9_11.
- 1202 [86] Grillo A, Carfagna M and Federico S. Non-Darcian flow in fibre-reinforced biological tissues.
1203 *Meccanica* 2017; 52: 3299–3320. DOI:10.1007/s11012-017-0679-0.
- 1204 [87] Carfagna M and Grillo A. The spherical design algorithm in the numerical simulation of biological
1205 tissues with statistical fibre-reinforcement. *Comput Vis Sci* 2017; 18: 157–184. DOI:10.1007/
1206 s00791-017-0278-6.
- 1207 [88] Grillo A, Di Stefano S, Ramírez-Torres A et al. A study of growth and remodeling in isotropic
1208 tissues, based on the anand-aslan-chester theory of strain-gradient plasticity. *GAMM-Mitteilungen*
1209 2019; 42(4). DOI:10.1002/gamm.201900015.
- 1210 [89] Destrade M, Donald BM, Murphy JG et al. At least three invariants are necessary to model
1211 the mechanical response of incompressible, transversely isotropic materials. *Computational*
1212 *Mechanics* 2013; 52(4): 959–969. DOI:10.1007/s00466-013-0857-4.
- 1213 [90] Hamdaoui ME, Merodio J, Ogden RW et al. Finite elastic deformations of transversely isotropic
1214 circular cylindrical tubes. *International Journal of Solids and Structures* 2014; 51(5): 1188–1196.
1215 DOI:10.1016/j.ijsolstr.2013.12.019.
- 1216 [91] Simo J. A framework for finite strain elastoplasticity based on maximum plastic dissipation and
1217 the multiplicative decomposition: Part i. continuum formulation. *Computer Methods in Applied*
1218 *Mechanics and Engineering* 1988; 66(2): 199–219. DOI:10.1016/0045-7825(88)90076-x.

- 1219 [92] Green AE and Naghdi PM. A general theory of an elastic-plastic continuum. *Archive for Rational*
1220 *Mechanics and Analysis* 1965; 18(4): 251–281. DOI:10.1007/bf00251666.
- 1221 [93] Wu JZ and Herzog W. Finite element simulation of location- and time-dependent mechanical
1222 behavior of chondrocytes in unconfined compression tests. *Annals of Biomedical Engineering*
1223 2000; 28(3): 318–330. DOI:10.1114/1.271.
- 1224 [94] Athanasiou KA, Darling EM and Hu JC. *Articular Cartilage Tissue Engineering*. Springer
1225 International Publishing, 2010. DOI:10.1007/978-3-031-02578-5.
- 1226 [95] Grillo A and Di Stefano S. An a posteriori approach to the mechanics of volumetric growth.
1227 *Mathematics and Mechanics of Complex Systems* 2023; 11(1): 57–86. DOI:10.2140/memocs.
1228 2023.11.57.
- 1229 [96] Pericak-Spector KA and Spector SJ. On the representation theorem for linear, isotropic tensor
1230 functions. *Journal of Elasticity* 1995; 39(2): 181–185.
- 1231 [97] Holzapfel GA and Ogden RW. Constitutive modelling of passive myocardium: a structurally
1232 based framework for material characterization. *Philosophical Transactions of the Royal Society A:*
1233 *Mathematical, Physical and Engineering Sciences* 2009; 367(1902): 3445–3475. DOI:10.1098/
1234 rsta.2009.0091.
- 1235 [98] Risken H. *The Fokker-Planck Equation: Methods of Solution and Applications*. Springer Berlin
1236 Heidelberg, 1996. ISBN 9783642615443. DOI:10.1007/978-3-642-61544-3.
- 1237 [99] Jordan R, Kinderlehrer D and Otto F. The variational formulation of the fokker–planck equation.
1238 *SIAM Journal on Mathematical Analysis* 1998; 29(1): 1–17. DOI:10.1137/s0036141096303359.
- 1239 [100] Aspden RM and Hukins DW. Collagen organization in articular cartilage, determined by x-ray
1240 diffraction, and its relationship to tissue function. *Proceedings of the Royal Society of London*
1241 *Series B Biological Sciences* 1981; 212(1188): 299–304. DOI:10.1098/rspb.1981.0040.
- 1242 [101] Clark A, Barclay L, Matyas J et al. In situ chondrocyte deformation with physiological compression
1243 of the feline patellofemoral joint. *Journal of Biomechanics* 2003; 36(4): 553–568. DOI:10.1016/
1244 s0021-9290(02)00424-4.
- 1245 [102] Mollenhauer J, Aurich M, Muehleman C et al. X-ray diffraction of the molecular substructure
1246 of human articular cartilage. *Connective Tissue Research* 2003; 44(5): 201–207. DOI:10.1080/
1247 03008200390244005.
- 1248 [103] Mansour J. *Biomechanics of cartilage*, chapter 5. 2013. pp. 69–83.
- 1249 [104] Hedlund H, Mengarelli-Widholm S, Reinholt FP et al. Stereologic studies on collagen in bovine
1250 articular cartilage. *APMIS* 1993; 101(1–6): 133–140. DOI:10.1111/j.1699-0463.1993.tb00092.x.
- 1251 [105] Chen S, Falcovitz Y, Schneiderman R et al. Depth-dependent compressive properties of normal
1252 aged human femoral head articular cartilage: relationship to fixed charge density. *Osteoarthritis*
1253 *and Cartilage* 2001; 9(6): 561–569. DOI:10.1053/joca.2001.0424.
- 1254 [106] Rodriguez E, Hoger A and McCulloch A. Stress-dependent finite growth in soft elastic tissues. *J*
1255 *Biomech* 1994; 27: 455–467. DOI:10.1016/0021-9290(94)90021-3.
- 1256 [107] Hardin R and Sloane N. McLaren’s improved snub cube and other new spherical designs in three
1257 dimensions. *Discrete Comput Geom* 1996; 15: 429–441.
- 1258 [108] Markowich P and Villani C. On the trend to equilibrium for the Fokker-Planck equation: an
1259 interplay between physics and functional analysis. *Mat Contemp* 2000; .

- 1260 [109] Mansfield JC, Mandalia V, Toms A et al. Collagen reorganization in cartilage under strain probed
1261 by polarization sensitive second harmonic generation microscopy. *Journal of The Royal Society*
1262 *Interface* 2019; 16(150): 20180611. DOI:10.1098/rsif.2018.0611.
- 1263 [110] Givero C, Stefano SD, Grillo A et al. A three dimensional model of multicellular aggregate
1264 compression. *Soft Matter* 2019; 15(48): 10005–10019. DOI:10.1039/c9sm01628g.
- 1265 [111] Grillo A, Carfagna M and Federico S. The Darcy-Forchheimer law for modelling fluid flow in
1266 biological tissues. *Theoretical and Applied Mechanics (TEOPM7)* 2014; 41(4): 283–322.
- 1267 [112] Pins GD, Huang EK, Christiansen DL et al. Effects of static axial strain on the tensile properties and
1268 failure mechanisms of self-assembled collagen fibers. *J Appl Polym Sci* 1997; 63(11): 1429–1440.
- 1269 [113] Holmes MH. Finite deformation of soft tissue: Analysis of a mixture model in uni-axial compres-
1270 sion. *Journal of Biomechanical Engineering* 1986; 108(4): 372–381. DOI:10.1115/1.3138633.
- 1271 [114] Rohatgi A. Webplotdigitizer. URL <https://automeris.io>.
- 1272 [115] Holzapfel GA and Ogden RW. A damage model for collagen fibres with an application to collage-
1273 nous soft tissues. *Proceedings of the Royal Society A: Mathematical, Physical and Engineering*
1274 *Sciences* 2020; 476(2236). DOI:10.1098/rspa.2019.0821.